DISSERTATION

Experimental Study of the Neutron Induced Fission Cross-Section of ^{234}U, ^{237}Np and ^{243}Am with Time-of-Flight Spectrometry Technics

Ausgeführt zum Zwecke der Erlangung des akademischen Grades eines Doktors der technischen Wissenschaften unter der Leitung von

Ao. Univ. Prof. Dipl. Ing. Dr. Helmut Leeb
E141
Atominstitut Wien

eingereicht an der Technischen Universität Wien

Fakultät der Physik

von

Vitaly Konovalov
0726913

A-1190 Raimund-Zoder-Gasse 15/4 Wien

Wien, am_____ _____

Table of Contents

Abstract

The current work concentrates on the measurements of the nuclear data needed for solving the problem of transmutation of radiotoxic waste. It includes fission cross-section of ^{234}U in the energy range from thermal to 1 MeV, ^{237}Np and ^{243}Am in the resonance region and average group capture cross-section of ^{234}U and ^{236}U. Almost all of these data are recommended by IAEA as a first priority needs for transmutation problem.

Another objective is to obtain the high resolution data of the fission cross-section of the ^{234}U on the fission barrier to confirm the existence of the fine structure, attributed to the vibrational resonances in the third well of the fission barrier.

The Dissertation summarizes more, than 10 years of the experiments, performed on the pulsed neutron sources IBR-2 and IBR-30 of Frank Laboratory of Neutron Physics of the Joint Institute for Nuclear Research (FLNP JINR) in Dubna, Russia; "Fakel" of Russian Scientific Center "Kurchatov's Institute" and n_TOF of CERN. The TOF technique was used for neutron energy spectrometry and various kinds of detectors to mark the fission events.

The independent measurements of the same isotopes done on different neutron sources and sometimes with different techniques gives strong, self-consistent set of data.

The dissertation has the following structure.

Chapter 1 is the introduction.

In the Chapter 2 the measurements of the nuclear data for ADS is described. The first Section is about the methodic of cross-section measurement. The measurements carried out in 1995-1998 in Dubna, on the pulsed fast reactor IBR-30, are described there. The measurements of the average cross-sections of $^{234, 236}$U, carried out in RSC "Kurchatov's Institute" by γ-quanta multiplicity spectrometry technique, are also described in Section 2.1. Methodic of the measurements and data processing for neutron multiplicity and its dependence of the incident neutron energy are described in Section 2.2. Third Section of this Chapter is dedicated to results discussion.

In the Chapter 3 the measurements of fission cross-section with high resolution on n_TOF installation in CERN are described. The data on ^{232}Th, ^{234}U and ^{237}Np are necessary for solving the problem of radiotoxic waste transmutation and Thorium cycle development. Besides that, since the achieved resolution is very high, the new information on fission barrier structure is obtained. This data are very important for "Thorium anomaly" understanding. The n_TOF installation, detector design and methodics of experiment and data processing are described in this Chapter.

Final Chapter is dedicated to discussion of the obtained results.

Abstrakt

Die vorliegende Arbeit konzentriert sich auf Messungen von nuklearen Daten die notwendig sind, um das Problem der Transmutation von nuklearem Abfall zu lösen. Sie beinhaltet den Spaltwirkungsquerschnitt von ^{234}U im Energiebereich von thermischer Energie bis zu 1 MeV, ^{237}Np und ^{243}Am in der Resonanzregion und durchscnittlichen Gruppeneinfangsquerschnitt von ^{234}U und ^{236}U. Fast alle dieser Daten sind von der IAEA vorrangig empfohlenen Daten, um das Problem der Transmutation zu lösen.

Weiteres Ziel ist es eine hohe Auflösung der Spaltwirkungsquerschnittsdaten von ^{234}U auf der Spaltbarriere zu erreichen, um die Existenz der Feinstruktur zu bestätigen, die auf die Vibrationsresonanzen im dritten Minimum der Spaltbarriere zurückzuführen ist.

Die vorliegende Dissertation fasst die mehr als zehnjährigen Experimente zusammen, die an Pulsneutronenquellen IBR-2 und IBR-30 des Frank Laboratoriums für Neutronenphysik des Gemeinschaftsinstituts für nukleare Forschung in Dubna, Russland, „Fakel“ des russischen wissenschaftlichen Zentrums „Kurchatov Institut“ und dem n_TOF von CERN durchgeführt wurden. Die TOF Technik wurde für die Neutronenenergiespektrometrie genutzt sowie verschiedene Arten von Detektoren, um die Spaltereignisse zu kennzeichnen.

Die voneinander unabhängigen Messungen desselben Isotops an unterschiedlichen Neutronenquellen und manchmal mit unterschiedlichen Techniken liefern ein starkes, konsistentes Datenset.

Die Dissertation ist wie folgt strukturiert.

Kapitel 1 beinhaltet die Einleitung.

Kapitel 2 beschreibt die Messungen von nuklearen Daten für ADS. Der erste Abschnitt beschreibt die Methodic der Wirkungsquerschnittmessung. Die Messungen, die von 1995-1998 in Dubna am schnellen Pulsreaktor IBR-30 durchgeführt wurden, sind hier beschrieben. Die Messungen von durchscnittlichen Spaltwirkungsquerschnitten von ^{234}U und ^{236}U, die am RSC „Kurchatov Institut“ mittels Gammaquantenmultiplikationsspektrometrietechnik durchgeführt wurden, sind im Abschnitt 2.1 beschrieben. Die Methodik der Messungen und Datenverarbeitung für Neutronenmultiplikation und ihrer Abhängigkeit von der dazugehörigen Neutronenenergie sind im Abschnitt 2.2 beschrieben.

Kapitel 3 beschreibt die Messungen von Spaltwirkungsquerschnitten mit hoher Auflösung an der n_TOF Installation in CERN. Die Daten von ^{232}Th, ^{234}U und ^{237}Np sind erforderlich, um das Problem der radiotoxischen Abfallumwandlung und die Entwicklung des Thoriumkreislaufes zu lösen. Außerdem, weil die erreichte Auflösung sehr hoch ist, werden die neuen Informationen der Struktur der Spaltbarriere erhalten. Diese Daten sind sehr wichtig für das Verständnis von „Thoriumanomalien“. Die n-TOF installation, Detektordesign und Methoden der Experiment- und Datenverarbeitung sind in diesem Kapitel beschrieben.

Das letzte Kapitel ist der Datendiskussion sowie den erzielten Ergebnissen gewidmet.

Chapter 1. Introduction

1.1. Motivation of the Current Work

Creation of ecologically pure and wasteless nuclear energy is one of the most acute problems of today. One of the serious approaches towards the solution of this problem is the design of a facility, with corresponding technology, for incineration of weapon plutonium, some minor actinides and transmutation of some fission products. Less studied among the materials, needed to develop such a facility, are the so called minor actinides (MA), such as Np, Pu, Am and Cm are built up as a result of multiple neutron captures and radioactive decays in the presently operating nuclear reactors based on the U/Pu nuclear fuel cycle. Some highly active isotopes of these elements constitute the most important hazard for nuclear waste management. Recently, several proposals have been made to reduce the radiotoxicity of nuclear waste containing transuranium elements (TRU). They all rely on neutron induced capture and fission of the MA, in particular of ^{237}Np, ^{241,243}Am, and ^{244,245}Cm. It is clear that any kind of waste burner system, critical or sub-critical, thermal or fast, will need to be loaded with fuel containing a large fraction of TRU. The response of these systems (e.g. criticality conditions) to the presence of TRU is directly linked to the fission and capture cross sections of the mentioned TRU isotopes. The fission cross sections of TRU are therefore fundamental elements in assessing the strategy to be followed in detailed feasibility studies of nuclear waste transmutation.

The current work concentrates on the measurements of the nuclear data needed for solving the problem of transmutation of radiotoxic waste. It includes fission cross-section of ^{234}U in the energy range from thermal to 1 MeV, ^{236}U, ^{237}Np and ^{243}Am in the resonance region and average group capture cross-section of ^{234}U.

The fission cross section of isotopes ^{234}U and ^{232}Th, in addition to their interest to the present nuclear technology, bears important information on Nuclear Structure due to their specific nucleonic composition, giving very complicated and pronounced fine structure of the potential surface energy around the fission barrier. The neutron induced fission process can be understood [12] by introducing a double-humped fission barrier (DHB), in good agreement between experimental data and theoretical predictions for the light and heavy actinides. However, the fission of the thorium nuclei departs from this general behavior, giving rise to the notion of the “Th-anomaly” [13]. In particular, experimental results on the nuclei ^{230}Th and ^{232}Th indicate a dominant additional barrier, resulting in the creation of a shallow third well [14] roughly 1 MeV deep, just deep enough to accommodate some very deformed metastable states. This effect suggests the existence of the so-called triple-humped fission barrier (THB), predicted by A. Bohr already in 1955 [15, 16].

Thermal fission cross-section of ^{234}U, besides its importance for transmutation problem, is also interesting for the results interpretation of the experiment of parity-non-conservation (PNC) effect measurement, performed in 2001 on PF1 beam of high-flux reactor of Institute of Laue-Langevin, Grenoble, France with about 75mg highly enriched ^{234}U isotope (the isotope

admixture of ^{235}U does not exceed 0.078%) in the form U_3O_8. The only about 50% of fission registered events belongs to the ^{234}U fission, so, very good accuracy the thermal fission cross-section of the ^{234}U is needed. However, the data available is contradictory.

1.2. Current Status of the Nuclear Data of Interest and Needs for Measurements

1.2.1. Nuclear Data for Transmutation of Radiotoxic Waste in Accelerator-Driving Systems

The present concern about a sustainable energy supply [1] is characterised by a considerable uncertainty: the greenhouse effect and foreseeable limits in fossil fuel resources on the one hand, the concern about the environmental impact of nuclear fission energy and the long term fusion research on the other hand, have led to the consideration of a variety of advanced strategies for the nuclear fuel cycle and related nuclear energy systems. The present research directories concern such strategies as the extension of the life span of presently operating reactors, the increase of the fuel burn-up, the plutonium recycling, and in particular the incineration of actinides and long-lived fission products, the accelerator driven systems (ADS), like the "Energy Amplifier" (EA) concept [2,3] of C. Rubbia, and the possible use of the Thorium fuel cycle [4].

The Long Lived Heavy Element component of the radioactive waste comes from parasitic reactions on the different constituents of the fuel. For the Th-cycle the parasitic reactions are $^{233}U(n,2n)^{232}U$, $^{232}Th(n,2n)^{231}Th(\beta^-)^{231}Pa$ and $^{231}Pa(n,\gamma)^{232}Pa(\beta^-)^{232}U$ leading to the production of ^{232}U, which is responsible for a large part of the short term (few centuries) radiotoxicity, and ^{231}Pa responsible for the long term radiotoxicity.

Such a facility project represents a combination of the most complicated physical and technical problems that are different from the known problems of atomic and accelerator technique. The essential issue of solving these tasks are strongly related with precise knowledge of the nuclear constants of the materials used. Such data determine the choice between different conceptual variants of the project and the design of the target, blanket and outward contour.

The summary report of the INDC/IAEA consultant's meeting [5] concluded that:

- There is a growing wide interest for advanced nuclear power technologies of the future involving new types of nuclear fuel, providing inherent safety, being resistant to nuclear proliferation, reduction of weapon grade plutonium and solving the problems of radioactive wastes.
- The Th-U cycle is the most prospective one, which meets the above goals

- The nuclear data for nuclides of the Th-U fuel cycle have been evaluated in the early seventies and middle of the eighties and do not fulfil the current accuracy requirements. Similar efforts to the U-Pu cycle need to be undertaken for the Th-U cycle.

The IAEA recommendations [5] included ^{232}Th, ^{231,233}Pa and ^{232,233,234,236}U as first priority isotopes. ^{236}U was added because of its build-up in the equilibrium fuel composition. For the fast reactors and ADS systems the neutron spectra are rather similar and the corresponding data are required with the following accuracy [5, 6] for both concepts: ^{232}Th(n,f) with 5%, ^{231}Pa with 20%, ^{233}Pa(n,f) with 20%, ^{232}U(n,f) with 20%, ^{233}U(n,f) with 1%, ^{234}U with 3% and ^{236}U with 5%.

^{230}Th: In the fast energy region it has about twice the fission cross section of ^{232}Th. For instance, the fission spectrum averaged neutron induced fission cross section is 163 mb as compared to 78.5 mb for ^{232}Th. This leads to a slight increase of the power production coming from thorium fission and also helps in breeding $_{233}$U fuel by its contribution to the neutron balance.

^{231}Pa: This is the main actinide produced in the Th cycle, primarily through the (n, 2n) reaction on the main element ^{232}Th and subsequent beta decay of ^{231}U. The neutron fission cross section is expected to be measured with a precision of 20% at least.

^{232}Th: In an ADS or equivalent fast reactor it accounts for 3% of the fissions, and at least for 8% in a gas cooled reactor. Indeed, near the fission threshold, ^{232}Th has an important contribution of 2% to delayed neutrons as compared to 0.25% for ^{233}U. So the knowledge of the neutron induced fission is requested with good accuracy, of the order of 5%.

^{233}U: The cross section of this main fissile element is to be known with an accuracy of 1%.

^{234}U: Formed by neutron capture in ^{233}U, it decays by alpha emission with a half-life of 2.5×10^5 years. In thorium reactors, the formation of ^{235}U by neutron capture in ^{234}U helps to reduce the burn-up swing in long lived cores. Since ^{234}U also gets formed by (n,2n) reactions in ^{235}U, the ^{234}U isotope is common to both uranium and thorium fuel cycles. The ^{234}U isotope plays a role in thorium fuel cycle similar to the ^{240}Pu isotope in the Pu fuel cycle.

^{236}U: In the Th fuel cycle this isotope plays a similar role as ^{242}Pu in the U/Pu fuel cycle.

It is of interest because of its build-up in the equilibrium fuel composition, so its fission cross section is expected to be measured with 5% precision.

A brief description of the present situation, also from [5], of nuclear data on fission cross section of the other nuclei relevant for the present work is given here below.

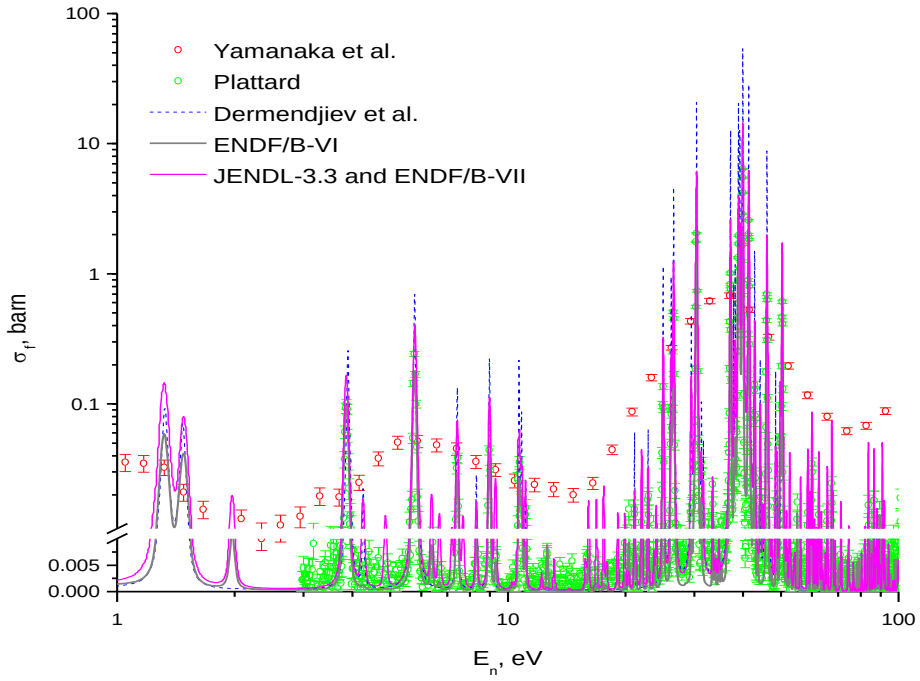

Figure 1.1. The ^{237}Np Fission cross-section. Data taken from [7] (red dots), [8] (green dots), [30] and [53] (blue dashed line) and from evaluated data libraries.

^{237}Np. Several measurements of the fission cross section of ^{237}Np have been made previously, below and above threshold. However, the quality of the data is not always acceptable, in accuracy as well as concerning the energy range covered. In particular, in the sub-threshold resonance energy region, ^{237}Np has a small fission cross section which is important for transmutation studies in Pb or Pb-Bi cooled systems, where the epithermal neutron flux is not negligible in the periphery of the fuel core, and where some proposal to perform heterogeneous transmutation of minor actinides has been made. Recent measurements by Yamanaka *et al*. [7] carried out at the Kyoto University Lead Slowing-down Spectrometer (KULS) and used in JENDL-3.3 are a factor of three higher than those measured by Plattard *et al*. [8] on which the ENDF/B-VI evaluated file is based. Newer library ENDF/B-VII for Np-237 coincides with JENDL-3.3 below 10 keV.

^{243}Am: there exist a very limited number of experimental data in the EXFOR data base in the lower energy region [8,9,10]. Seeger *et al*. [8] measured the fission cross section above 50 eV using a nuclear explosion experiment, and Wisshak *et al.* [9] determined the neutron capture and fission cross sections in the energy range from 5 to 250 keV with a Van de Graaff accelerator. Knitter *et al*.[10] measured the resonance parameters between 1 and 100 eV and the fission cross sections above 100 eV with an electron linear accelerator.

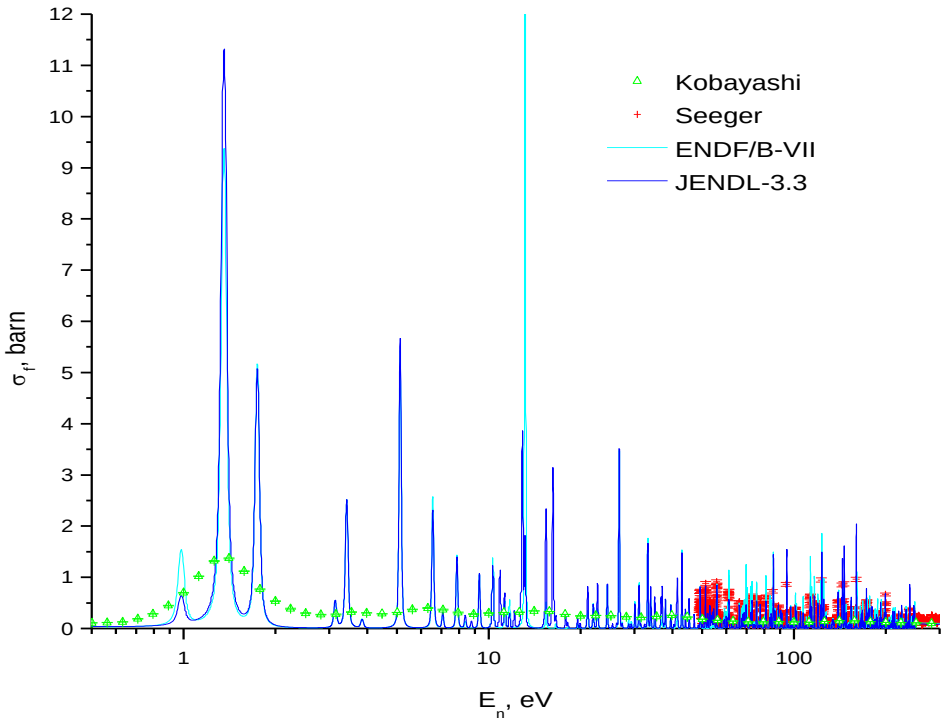

Figure 1.2. The ^{243}Am fission cross-section. Data taken from [8] (red cross), [11] (green triangles) and from evaluated data libraries

The comparison between the latest measurements by Kobayashi *et al.* [11] with the evaluated cross sections in ENDF/B-VI and JENDL-3.2 shows some discrepancies between both evaluated data in the energy regions below 0.3 eV and above 15 eV.

Although the ENDF/B-VI data are in agreement with the measurements, they are lower at energies between 15 and 60 eV. The JENDL-3.2 data seem to be lower than the measurements above 100 eV. When comparing the latest measurements with existing experimental data, it appears that the data by Wisshak *et al.* [9] and Knitter *et al.* [10] are in agreement, however, the results by Seeger *et al.* [8] are considerably higher above several hundred eV. The data measured in the MeV energy region show good agreement amongst each other. In this work the detailed structure of the cross section is studied, in the fission threshold region as well as above. An improved determination of the resonance parameters in the very low energy region was attempted in case of ^{243}Am.

1.2.2. Study of the Fine Structure of the Fission Cross-section for Isotopes ^{232}Th and ^{234}U on the Fission Barrier

A simple representation of one-dimensional fission barrier is shown in Figure 1.1. The deformation axis β_2 corresponds to an elongation of the fissile system through the fission direction. The population of states inside the intermediate well leads to the known effect of *shape isomerism* [17]. Resonance penetration of the potential barrier below the saddle points will give narrow resonance-like structures, observable if the energy resolution is good enough.

From the experimental point of view, the use of neutrons in the energy range below 2 MeV for the Thorium cycle isotopes is required. For the Th, Pa and U nuclei very pronounced vibrational resonances have been observed between 0.1 and 2 MeV. These resonanses were studied at CERN Neutron Source with an energy resolution better than 2 keV..

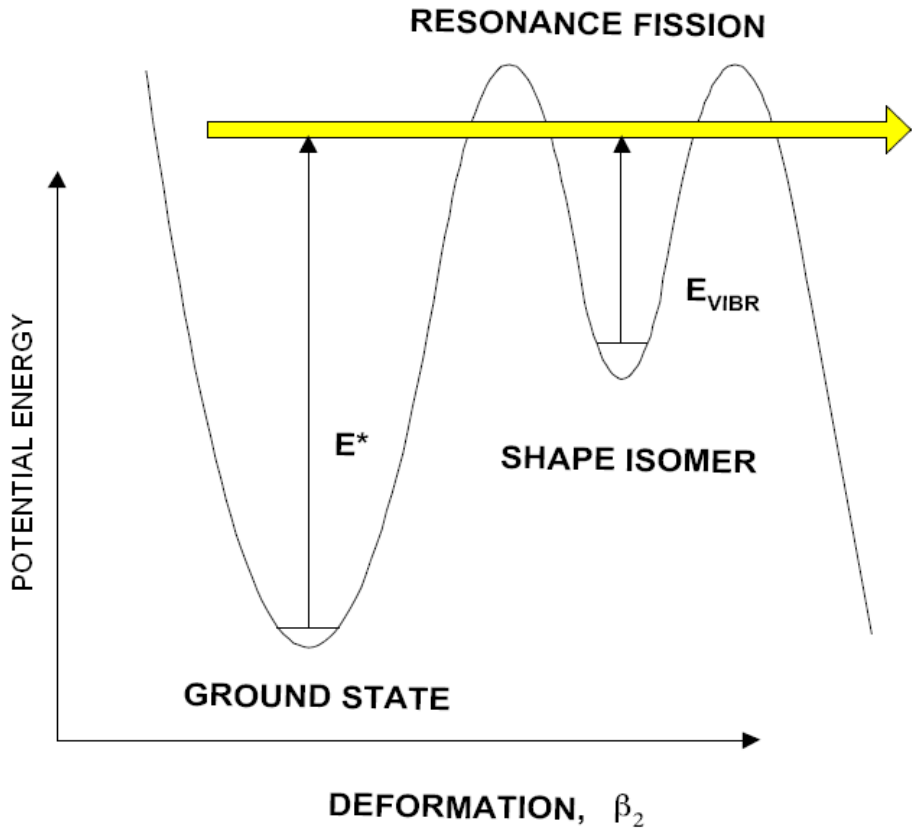

Figure 1.1. Fission barrier

The theory of Strutinsky [12], introducing multi-humped fission barrier of the actinide nuclei, allows to explain [12] many resonance-like structures in fission cross-sections for fast neutrons. The weakly damped beta-vibrational states in the secondary well of the potential barrier are responsible for those resonances and should be associated with a few-phonon states populating the secondary or third barrier well. The weak damping, due to the combination of

the low excitation energy in the second well and the inhibition provided by the first or intermediate barrier hump was observed in an experiment.

The best studied example of a classical damped vibrational resonance was found in the compound nucleus of uranium-235 in the ^{234}U(n,f) reaction [18]. The basic resonance-like feature at approximately 300 keV neutron energy, was long believed to be understood as a competition between opening of the fission and the inelastic neutron scattering channels, as assumed already in the sixties [19]. High-resolution studies were performed first by James [18] to investigate the so-called class-II (associated with compound levels in the second well of fission barrier) intermediate structure within separate vibrational resonance. Due to relatively poor energy resolution of this measurement, the class-II structures could not be observed. Nevertheless, very considerable fluctuations of the data points at the vibrational resonance were observed and were attributed to five different class-II states.

Careful analysis of the James data [18] can lead to the conclusions, that the ^{234}U(n,f) reaction should be accurately remeasured. Indeed the data on the "classical" damping of vibration resonance should be confirmed, because resonance-like fluctuations in these data [18] appear over the whole energy range and they are equally visible both inside and outside of the vibrational resonances. The energy spacing of these fluctuations is approximately constant over the whole range and could be attributed to the instabilities of the detection system, probably influenced by the accelerator driven neutron source. Another motivation to repeat the measurement of the ^{234}U(n,f) reaction is the lack of the pronounced resonance around the neutron energy of 780 keV in the data by James when these data are compared with the results of the experiment by Meadows [20] performed with a Van-de-Graaff accelerator.

Investigations for confirming this possible sub-structure of the vibrational resonances around 330 keV, 550 keV and 780 keV are also needed for the adequate explanation of the fission barrier properties in the uranium region, where the data from charged particle induced fission give a completely different characteristic of the barrier shape.

The designed features of the n_TOF neutron source are very attractive for the study of such quantum effects in fission due to the high resolution. These features permit to reveal structures of vibration resonances, directly confirming the existence of the THB for these anomalous elements in the vicinity of and above the barrier. The measurement of the fission cross-section for the ^{232}Th and ^{234}U with an accuracy 1-3% on the barrier is needed to confirm the existence of the fine structure, caused by vibrational resonances. At the CERN Neutron Source the resolution at 189 m flight path is approximately 1 keV which is not sufficiently good to observe separate class-II states for ^{234}U. However, fine structure can be observed.

1.2.4. Thermal Fission Cross-section of ^{234}U

The ^{234}U, like other even isotopes of the uranium, have a threshold-type energy dependence of the fission cross-section, and therefore, small cross-section at the thermal point.

The data available for the fission cross-section of ^{234}U in the vicinity of the thermal point is contradictory.

Measurements described in the paper [27] were carried out on the ILL high-flux reactor on the neutron beam having Maxwellian spectrum with average energy 11 meV and gives the value of σ_{th}=300±20 mb, then was also published as [28]. Few years later the same authors had published another value, σ_{th}=67±14 mb [29].

1.3. Objective of the Current Work and Goals Achieved

The first objective of the current work is to measure fission cross-section of ^{234}U in the energy range from thermal to 1 MeV, ^{236}U, ^{237}Np and ^{243}Am in the resonance region. Almost all of these data are recommended by IAEA [5] as a first priority needs for transmutation problem.

Another objective is to obtain the high resolution data of the fission cross-section of the ^{234}U on the fission barrier to confirm the existence of the fine structure, attributed to the vibrational resonances in the third well of the fission barrier.

The Dissertation summarizes more, than 10 years of the experiments, performed on the pulsed neutron sources IBR-2 and IBR-30 of Frank Laboratory of Neutron Physics of the Joint Institute for Nuclear Research (FLNP JINR) in Dubna, Russia; "Fakel" of RSC "Kurchatov's Institute" and n_TOF of CERN. The TOF technique was used for neutron energy spectrometry and various kinds of detectors to mark the fission events.

The independent measurements of the same isotopes done on different neutron sources and sometimes with different techniques gives strong, self-consistent set of data.

Our data on fission cross-section of ^{237}Np allows one to resolve contradiction between two main libraries of nuclear data, JENDL-3.2 and ENDF-B/VI, which are based on results of [7] and [8], respectively and differs in a factor of three. Our data coincide with [7].

High-resolution data for ^{234}U obtained on n_TOF neutron source confirms the results of [18] for the fine structure connected with vibrational resonances and a third well. Despite the resolution which is lower than expected fine structure period, the observed structure of the cross-section is in good agreement with results of the modeling.

The results of the independent measurements of ^{234}U fission cross-section near the thermal point, carried out with time-of-flight (TOF) technique on the pulsed neutron sources, described in the current dissertation [30, 31], are in good agreement with each other.

1.4. Structure of the Dissertation

In the Chapter 2 the measurements of the nuclear data for ADS is described. The first Section is about the methodic of cross-section measurement. The measurements carried out in 1995-1998 in Dubna, on the pulsed fast reactor IBR-30, are described there. The measurements of the average cross-sections of $^{234, 236}$U, carried out in RSC "Kurchatov's Institute" by γ-quanta

multiplicity spectrometry technique, are also described in Section 1. Methodic of the measurements and data processing for neutron multiplicity and its dependence of the incident neutron energy is described in Section 2. Third Section is dedicated to results discussion.

In the Chapter 3 the measurements of fission cross-section with high resolution on n_TOF installation in CERN are described. The data on ^{232}Th, ^{234}U and ^{237}Np are necessary for solving the problem of radiotoxic waste transmutation and Thorium cycle development. Besides that, since the achieved resolution is very high, the new information on fission barrier structure is obtained. This data are very important for "Thorium anomaly" understanding. The n_TOF installation, detector design and methodics of experiment and data processing are described in this Chapter.

Final Chapter is dedicated to discussion of the obtained results.

Chapter 2. Measurements of the Minor Actinides Nuclear Data in the Incoming Neutron Energy Range from 1 to 1000 eV.

2.1. Techniques of the Cross-section Measurements

This chapter describes the measurement of the energy dependence of the fission cross-sections of the ^{234}U and ^{243}Am, group constants for fission and capture cross-sections of ^{234,236}U. The measurements were performed using several independent techniques in the partially overlapping intervals of the incident neutron energy, that gives possibility to perform a cross-check and a correct normalization and decrease the systematical errors of the whole set of obtained data.

An energy dependence of the fission cross-sections and group constants was measured using time-of-flight (TOF) technique on the three pulsed neutron sources: FAKEL (RSC 'KI') and IBR-30 (JINR). Parameters of these sources are given in the Table 2.1 (See also [32, 33]).

Table 2.1. Parameters of pulse neutron sources

	Neutron source	
	IBR-30	FAKEL
maximal energy of electrons, MeV	40	100
electron pulse duration at half-height, ns	1800	60
pulse repetition rate, Hz	100	400
neutron producing target	W+^{239}Pu, gas flow cooling	natural uranium, water cooling
neutron pulse duration after moderation (at E_n=100 eV), ns	4500	210
4π neutron flux, neutrons per second	$5 \cdot 10^{14}$	$3 \cdot 10^{12}$

Derailed description of the experiments is given below.

2.1.1. Studying of the Neutron Induced Fission Cross-section of ^{234}U and ^{243}Am.

Fission cross-section of ^{234}U with resonance neutrons were measured on the pulsed booster IBR-30 of Joint Institute for Nuclear Research in Dubna [30]. TOF technique was used. Neutron flight path is 58.4 m, neutron pulse with is about 4 μs, so, achieved resolution is ~70 ns/m. Such a resolution allows to resolve almost all of the neutron resonances in the energy region below 200 eV.

The fast multisectional ionisation chamber is used in experiment for fission fragment registration and identification. The construction of the chamber permits to use up to 12 sections. Each section includes two separate parallel plate chambers with common cathode and thin two-sided target of ^{234}U in the form of U_3O_8. Chamber contain 10 layers of ^{234}U (total mass is 98.8 mg, admixture of ^{235}U 0.082±0.0052%, surface density 140 μg/cm^2) and calibration target of ^{233}U (25.2 mg, surface density 2,3 μg/cm^2). The schematic of the chamber is shown on the Figure 2.1.The parameters of the detectors are shown in Table 2.2.

Table 2.2. Properties of the fission fragments detectors

	^{234}U	^{243}Am
number of layers	8	1
sample mass (total)	98 mg	2 mg
Target diameter	60 mm	50 mm
distance between electrodes	6 mm	50 mm
working gas	90%Ar+10%CH_4	90%Ar+10%CH_4
gas pressure	400 mm Hg	400 mm Hg
target purity	99.84%	99.3%
admixtures	^{235}U — 0.08%	^{241}Am — 0.7%, ^{244}Cm — 0.05%, ^{245}Cm — 0.005%

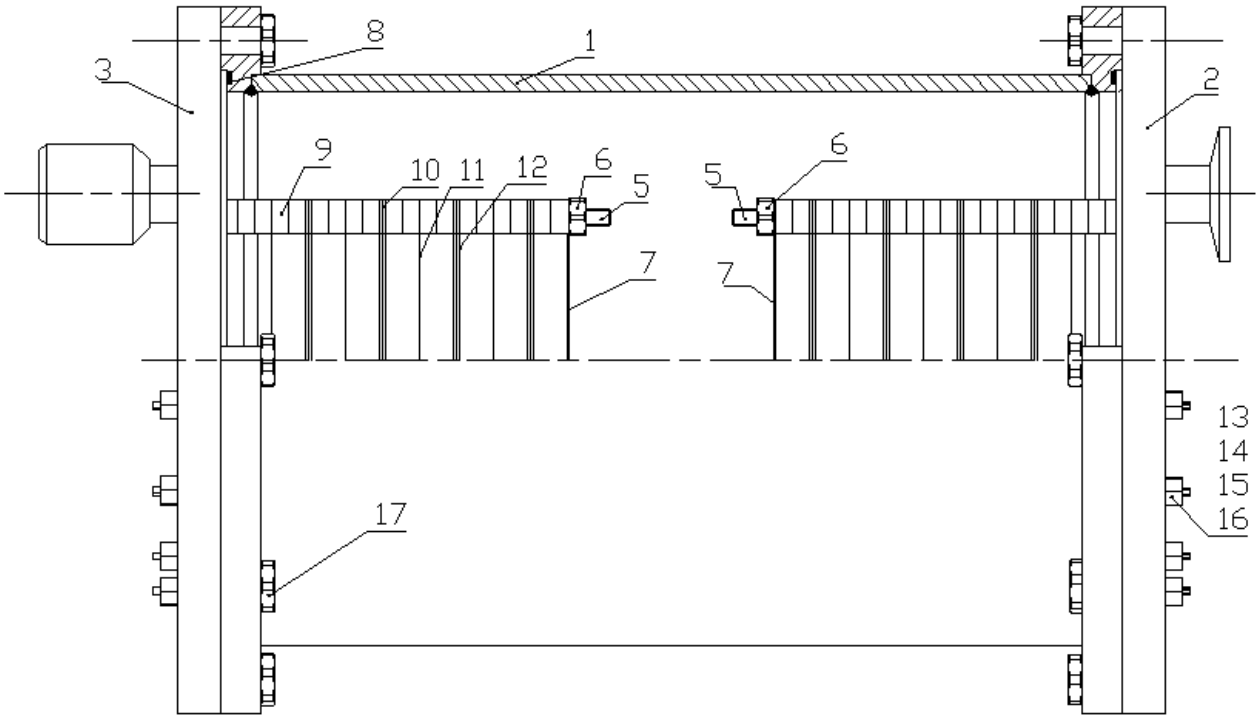

Figure 2.1. Detector schematics

Relative behaviour of the cross-section was determined from TOF spectra, which were collected during 600 hours.

Despite the low ^{235}U admixture, most pronounced resonances (9, 12, 19 and 35 eV) are clearly seen on the TOF spectrum and for determination cross-section $\sigma_f(E_n)$ a correction have to be introduced. For that the layer of ^{235}U (25.2 g) was placed inside the fission fragment detector and its fission TOF spectra are measured in parallel with ^{234}U. Measured spectra were subtracted from ^{234}U spectrum after background (BG) correction and normalization on strongest resonances' total count ratio.

Besides that, there were calibration measurements with very well-known amount of ^{235}U (2.5±0.8 mg) and ^{234}U (63.3±1.8 mg) in the energy region from 2.5 to 10 eV conducted on flight path 10 m. It gives the possibility to determine $\sigma_0\Gamma_f$ of the 5.16 eV resonance of ^{234}U.

The measurements with ^{243}Am were conducted by the time-of-flight method at the 14.5 m flight distance from active core of the IBR-30 pulsed booster in FLNP JINR [30]. The pulse repetition rate was 100 s^{-1}, the neutron pulse width at half maximum is 4 μs for the mean thermal power 10 kW. The back-to-back ionization chamber containing 2.2 mg of the investigated isotope and 0.88 mg of ^{235}U used for measuring the flux and calibration in energy were employed. A TOF spectrum is shown on Figure 2.2.

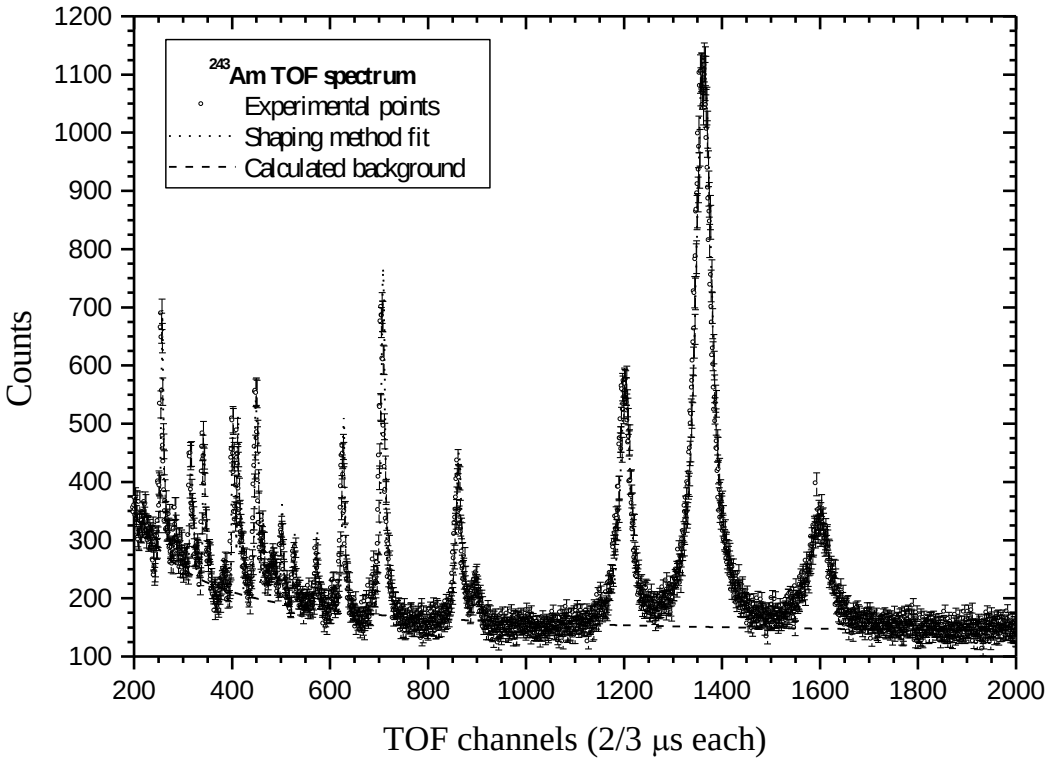

Figure 2.2. TOF spectrum (Raw data) of ^{243}Am with fit results

The energy behaviour of the neutron flux $\Phi(E)$ was determined over several intervals of the time-of-flight spectrum containing from one to seven ^{235}U resonances with known energy E_0 and area $\sigma_0\Gamma_f$. The number of counts N_λ in the resonance λ in the time-of-flight spectrum is:

$$N_\lambda = \frac{\pi}{2}(\sigma_0 \Gamma_f)^\lambda \varepsilon \Phi(E_0^\lambda) nt, \qquad (2.1)$$

where ε — efficiency of the fission fragment registration calculated from pulse-height spectra [34],

$\Phi(E_0^\lambda)$ — neutron flux,

n — number of nuclei in the sample,

t — time of measurement.

Writing $\Phi(E_0^\lambda)$ for each λ in Equation (2.1) we obtain the dependence $\Phi(E)$ which can be approximated as $\Phi(E) = \Phi_0 E^x$. The parameters Φ_0 and x are found by the least square method. The best fit results $\Phi_0=(6.946\pm0.002)\cdot10^2$ and $x=-0.94921\pm0.00013$ were used in the calculations of cross-sections. Resulting flux behaviour is shown on Figure 2.3.

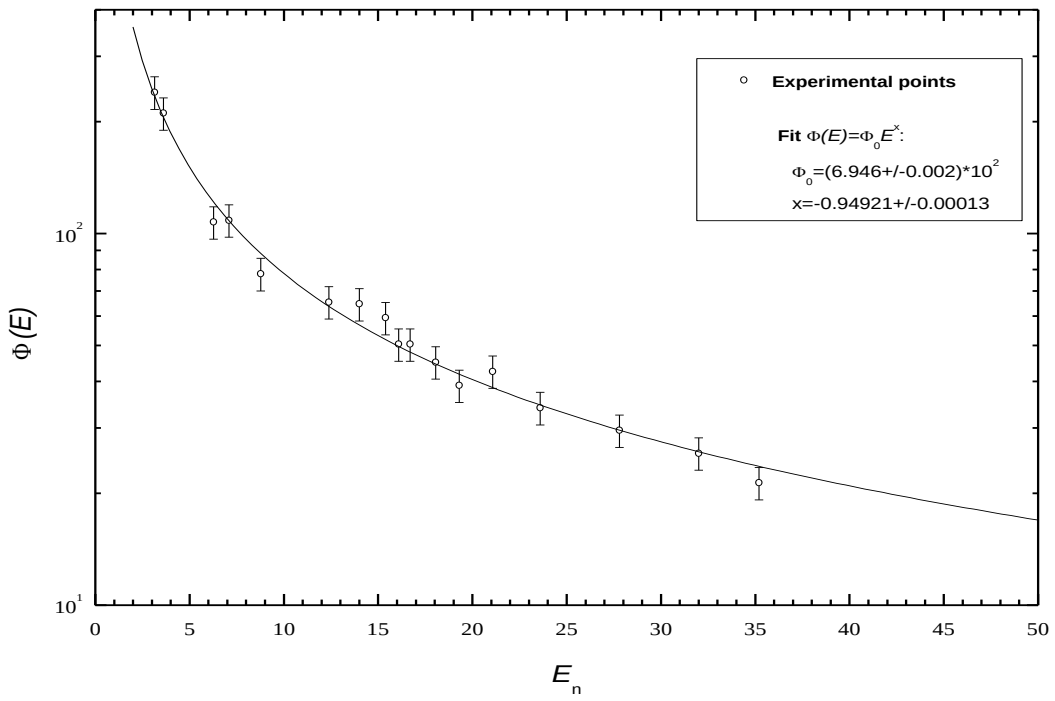

Figure 2.3. Neutron flux

Due to the design property of the IBR-30 booster, there is high neutron background in between the pulses. This is why direct measurement of interresonance cross-section is not possible and it was reconstructed using fission widths, extracted from TOF spectrum.

The fact that is interresonance cross-section is statistically zero, was used to determine the background. It was fitted using MINUIT program with the polynomial function

$$N_i^{BG} = At^2 + Bt + C + D/t, \tag{2.2}$$

where t is a time-of-flight.

For the ^{234}U the values of $\sigma_0 \Gamma_f$ was calculated by the method of areas, using formula (2.1) for the measured numbers of counts of the resonances of ^{234}U. The fission widths were found by the formula

$$\Gamma_f^{\lambda} = \frac{(\sigma_0 \Gamma_f)^{\lambda}}{4\pi\lambda^2} \frac{\Gamma_t^{\lambda}}{g\Gamma_n} \tag{2.3}$$

where $g\Gamma_n$, the neutron width of the λth resonance was taken from [18],

Γ_t^{λ} the total width of the λth resonance was calculated as the sum of the neutron and radiation widths, which is approximately a constant,

Γ_γ=25 meV [35].

The details of the calculation are given in Appendix I.

Measurements had been done in the energy interval of the incident neutrons from 1 to 1000 eV. Resonance parameters were calculated in the energy region below 200 eV.

Since achieved resolution is not enough to separate all the resonances of ^{243}Am, to calculate fission widths, the method of shaping described below is used.

The number of counts in each ith channel is determined by the function

$$f_i = \Phi(E_i) \Delta E n \sigma_f'(E_i) + N_i^{BG}, \tag{2.4}$$

where E_i is the energy corresponding to the ith channel,

ΔE is the channel width,

σ_f' is the "observed" fission cross section,

n is the number of nuclei in the target,

N_i^{BG} is the number of "background" counts.

The "observed" cross section is the convolution of the real cross section $\sigma_f(E')$ with the resolution function $R(t,t')$ and the function $D(E-E')$ describing the Doppler broadening of the resonance

$$\sigma_f'(E') = \int_0^\infty R(t,t') \left(\int_{-\infty}^{\infty} \sigma_f(E') D(E-E') dE \right) dt . \quad (2.5)$$

In the simplest case,

$$D(E-E') = \frac{1}{\sqrt{\pi}\Delta_D} \exp\left(-\frac{(E-E')^2}{\Delta_D^2} \right), \quad (2.6)$$

where $\Delta_D = 2\sqrt{\frac{k_B T E}{m_A + 1}}$ is the Doppler width,

k_B is the Boltzmann constant,

T is the temperature of the sample.

The resolution function of the IBR-30 booster is determined by the width of the electron accelerator pulse t_L and the parameter τ=4.2μs connected with the multiplication of neutrons in the active zone of the booster:

$$R(t,t') = \begin{cases} 0, & t < 0 \\ 1 - \exp\left(-\frac{t-t'}{\tau} \right), & 0 < t < t_L \\ \left(1 - \exp(-t_L/\tau)\right) \exp\left(-\frac{t-t'}{\tau} \right), & t > t_L . \end{cases} \quad (2.7)$$

In this formula t is the neutron time-of-flight.

To describe fission cross sections, the single-level approximation is used

$$\sigma_f(E) = \sum_\lambda 4\pi\lambda^2 \left(\frac{g\Gamma_n \Gamma_f}{(E-E_0)^2 + \frac{\Gamma_t^2}{4}} \right)_\lambda , \quad (2.8)$$

where $g\Gamma_n$, Γ_f, Γ_t and E_0, the neutron, fission, total widths and the energy of the resonance λ, are taken from [35] and [36].

After substitution of (2.7) to (2.6), (2.6) and (2.8) into (2.5) and, finally, (2.5) into (2.4), the parameters Γ_f and E_0 were found by the maximum likelihood method. Number of background counts, N_i^{BG} was determined separately as (2.1). Resulting fit together with TOF spectra shown on Figure 2.2. Obtained resonance parameters of ^{234}U and ^{243}Am are shown in Tables 2.3 and 2.4 (paragraph 2.4.1), respectively. Measured and calculated cross-sections for

these isotopes shown on Figures 2.8 and 2.9 in the same paragraph. These results were published in [30, 37].

2.1.3. Measurement of the Fission and Capture Cross-section of ^{234}U and ^{236}U

To measure capture, fission and scattering cross sections, there was proposed and realised an universal method of the multiplicity spectrometry [38]. This method allows the events of different reactions to be identified through measurement of the multiplicity spectrum of emitted gamma-quanta. The measurements had been done on the FAKEL neutron source at 5.2 m flight path. The multiplicity spectrum was measured by the multisectional 4π–detector with a gamma-quanta detection efficiency of ~100%. The samples under investigation were placed in the channel going along the detector axis that coincides with neutron beam direction.

Various collimating systems, detector shielding and multisectional 4π–detectors have been constructed and tested. It has been found that the compact 8-sectional and 16-sectional detectors were optimal for capture and fission cross sections measurements, respectively. The total volume of NaI(Tl) crystals was 72 litres for 8-section detector and 94 litres for 16-section one. To shield crystals against scattered neutrons, the (n,γ)-converter of ^{10}B layer was placed between scintillator and sample.

Two identical metallic disks of 20 mm in diameter, $9.443 \cdot 10^{-4}$ atoms/b of overall thickness and 99.845% of enrichment were used as ^{236}U sample.

The ^{234}U sample consisted of 5 identical layers of U_3O_8 on 0.03 mm aluminium foil backing. For each layer, the diameter was 10 mm; the uranium density was 88 mg/cm^2. The sample contains 99.84% of ^{234}U and 0.082% of ^{235}U. The background from γ-activity of the sample was ~10^4 counts per second with the energy release in any detector section more than 0.8 MeV.

For each event detected, the electronics allowed accumulation of the flight time, time of detection and energy release in each detector section. They constitute a set of 17 parameters for 16-section detector. Up to ~10^7 events were accumulated in each experimental run.

A variety of supplementary measurements has been performed in addition to experiments with ^{234}U and ^{236}U samples.

1. Measurements “without a sample” were made to find the background which was not caused by a sample. During such experiments the ^{234}U sample was placed inside of the detector channel, but outside of a neutron beam in order to keep identical the detector capacity.

2. Measurements with a carbon sample were carried out to find the multiplicity spectrum of neutrons scattered on the uranium samples.

3. A similar measurement was performed with a lead sample to evaluate the background caused by gamma-quanta in a neutron beam.

4. To find the energy spectrum of incident neutrons, measurements with ^{10}B sample were made. In this case, the lead only shielded the detectors. Background were measured under the same conditions.

5. Transmission of ^{10}B sample was measured to find the probability of $(n,\alpha\gamma)$-reaction as function of neutron energy.

6. A measurement with ^{238}U sample was performed to find detector response function for neutron capture.

7. A measurement with ^{235}U sample was made to find a shape of fission multiplicity spectrum.

The combination of two last measurements allows choosing the interval of multiplicity spectrum for fission cross-section determination.

The results of all measurements were corrected to compensate miscounts. The constant background component was subtracted from all time-of-flight spectra. This component was found within time-of-flight spectra interval which was placed before the linac pulse. The background obtained in corresponding "without a sample" measurement was subtracted from all time-of-flight spectra (if such a background needed to be taken into account). The background of scattered neutrons was subtracted from the results of measurements performed with ^{234}U and ^{236}U samples.

Since the uranium samples were rather thick (especially the ^{236}U sample), it was necessary to take into account the "self-shielding" and multiple neutron interaction in the sample. It was also necessary to keep in mind the finite energy resolution of the neutron spectrometer in order to calculate correctly the cross sections within a given energy interval (for example, with incident neutron energy spectrum normalising in the vicinity of ~5 eV resonance).

The time-of-flight spectra have been simulated to consider factors mentioned. First, the total, capture and scattering cross sections were calculated on the basis of resonance parameters with the Doppler effect taking into account. Using these cross sections, the capture probability was calculated:

$$W_\gamma = \left(1 - e^{-n\sigma_t}\right)\frac{\sigma_\gamma}{\sigma_t} + W_{s\gamma} \qquad (2.9)$$

where $W_{s\gamma}$ is the probability of radiative capture after neutron scattering.

The value $W_{s\gamma}$ was calculated by integration over sample thickness and scattering angles taking into account the energy losses at neutron scattering. As the neutron energy rises, $W_{s\gamma}$ decreases quickly.

The calculated number of counts in the i-th time-of-flight channel is

$$N_\gamma^0(E_i) = \int P(E) \cdot W_\gamma(E) \cdot R(E_i, E) dE\,, \tag{2.10}$$

where $R(E_i,E)$ is the resolution function of the neutron spectrometer and $P(E)$ is the incident neutron spectrum.

So the factor for correction of the measured data to obtain the capture cross section averaged in the Å$_1$÷Å$_2$ energy interval could be calculated by the formula:

$$\beta(E_1, E_2) = \frac{\sum_{i(E_1)}^{i(E_2)} \frac{N_\gamma^0(E_i)}{P(E_i)}}{\int_{E_1}^{E_2} n\sigma_\gamma(E) dE} \tag{2.11}$$

Using β ratios, the capture cross section weighted group constant could be obtained as:

$$< \sigma_\gamma >= \frac{\int_{E_1}^{E_2} \frac{\sigma_\gamma(E)}{E} dE}{\int_{E_1}^{E_2} \frac{dE}{E}}\,, \tag{2.12}$$

where

$$\int_{E_1}^{E_2} \frac{\sigma_\gamma(E)}{E} dE = \frac{\sum_{i(E_1)}^{i(E_2)} \frac{N_\gamma(E_i)}{P(E_i)E_i}}{n \cdot \beta(E_1, E_2)} \tag{2.13}$$

In a similar way, the group constant for fission cross section could be obtained. The calculation is given in Appendix II.

The count rate was too small to measure real energy dependence of studied cross-sections nevertheless rather short flight path. So group constants for investigated isotopes can only be obtained.

Respective results for capture and fission cross-section for ^{234}U and ^{236}U are presented in the Tables 2.5–2.8, Section 2.4.2. In the Table 2.6 also shown the group constants for ^{234}U fission cross-section, calculated on the basis of resonance parameters, obtained on the IBR-30 pulse booster (See Sect. 2.1.1. and 2.4.1) For more details see [39].

2.2. Measurements of Thermal Neutron Induced Fission Cross-section of ^{234}U

2.2.1. Measurements on IBR-30 Pulsed Reactor

Measurements were carried out by the time-of-flight (TOF) technique on the IBR-30 booster in Dubna. Flight path was 15.2 m. For the pulse repetition rate 100 s^{-1}, the lower boundary of neutron energy is 0.0146 eV at such distance. Fission fragments were detected by multisectional ionization chamber containing 98.8 mg of ^{234}U and 25.2 mg of ^{235}U used for neutron flux determination and energy calibration. Background was measured with 0.5 mm thick cadmium filter in the neutron beam. Measurement time for each spectra (effect and background) was 15 h. These spectra are shown in the Figure 4.2.

In spite of a low ^{235}U content in the ^{234}U sample, the fission of nuclei of ^{235}U supplies at least the half of the fission events in the vicinity of the thermal point. The contribution of ^{235}U was calculated using simultaneously measured ^{235}U spectra that were normalised on samples mass ratio and content of ^{235}U in the ^{234}U sample (4.2).

$$N_{\text{adm}} = \frac{N^{235} m^{234} C^{235}}{m^{235}}, \qquad (2.14.)$$

where N_{adm} — number of admixture counts , N^{235} — Number of ^{235}U sample counts, C^{235} — ^{235}U concentration in ^{234}U sample, m^{234} and m^{235} — masses of ^{234}U and ^{235}U samples, respectively.

The content of ^{235}U in the ^{234}U sample should be determined as accurate, as possible. The value C^{235}=0.082±0.008% obtained by α-spectrometry method was not satisfactory because the 10% uncertainty of this value leads to 20–100% error in determination of ^{234}U cross-section.

The ^{235}U concentration was calculated on the basis of the TOF spectrum of fission measured with the same sample on the flight path 58.4 m during 600 h. This spectrum was fitted using resonance parameters of ^{234}U and ^{235}U and concentration was set as free parameter. Obtained value C^{235}=0.078±0.001% have much smaller error and gives us possibility to determine energy dependence of the ^{234}U fission cross-section with reliable accuracy.

An excess of the number of fission events over the ^{235}U contribution is related to ^{234}U fission, thus, the cross-section at thermal point is:

$$\sigma_{\text{f}}^{\text{th}} = \frac{\sigma_{\text{f}}^{235}(0.025\,\text{eV}) C^{235} N^{234}}{N^{235}}, \qquad (2.15.)$$

The obtained value [30] of the thermal fission cross section of ^{234}U is $\sigma_f^{\text{th}} = 180 \pm 50$ mbarn.

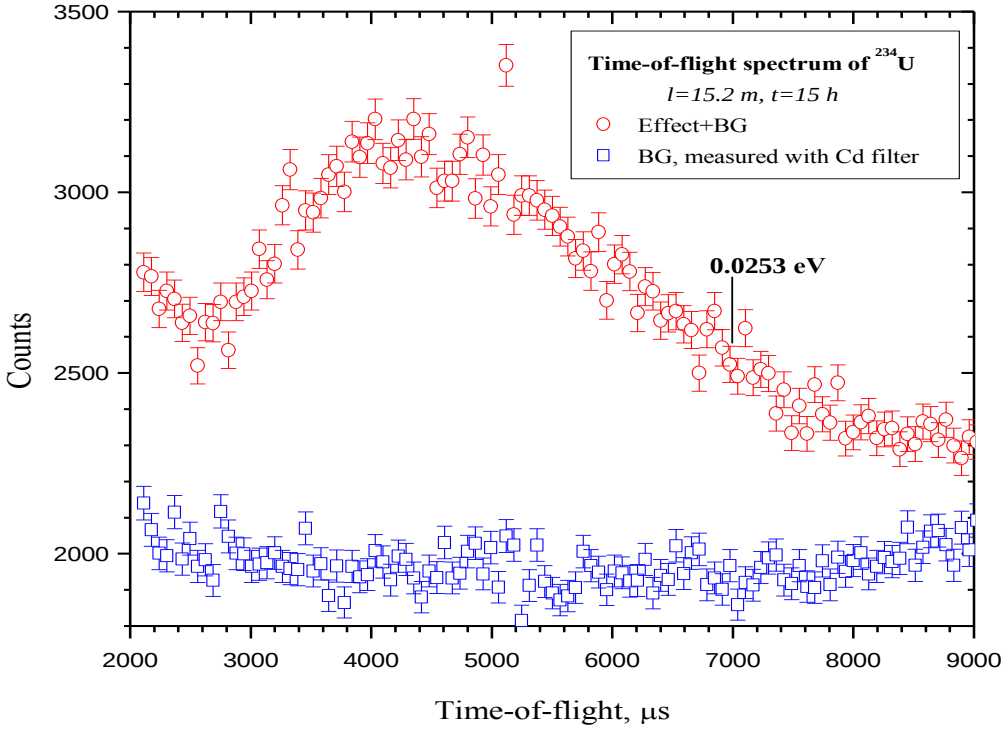

Figure 2.4. TOF spectrum

2.2.2. Measurements on IBR-2 Pulsed Reactor

Measurements were carried out by the TOF technique on the IBR-2 pulsed reactor in Dubna. Tangential neutron beam was chosen to diminish the background caused by the fast neutrons. Resulting effect/background ratio was 100 times better than in our previous measurement [30, 31]. Fission fragments were detected by multisectional ionisation chamber containing 12.5 mg of ^{234}U and 0.84 mg of ^{235}U used for neutron flux determination and energy calibration. Background was measured with 0.5 mm thick cadmium filter in the neutron beam. Measurement time for spectrum without filter was 33 h, and background one — 13 h.

Procedure, described in the previous paragraph, was conducted for 19 intervals on TOF spectra. Width of each interval was 0.005 eV. Cross-section in each interval:

$$\sigma_f(< E_n >) = \frac{\sigma_f^{235}(< E_n >) C^{235} N^{234}}{N^{235}}, \qquad (2.16)$$

где $<E_n>$ — average energy of the interval, σ_f^{235} —^{235}U fission cross-section.

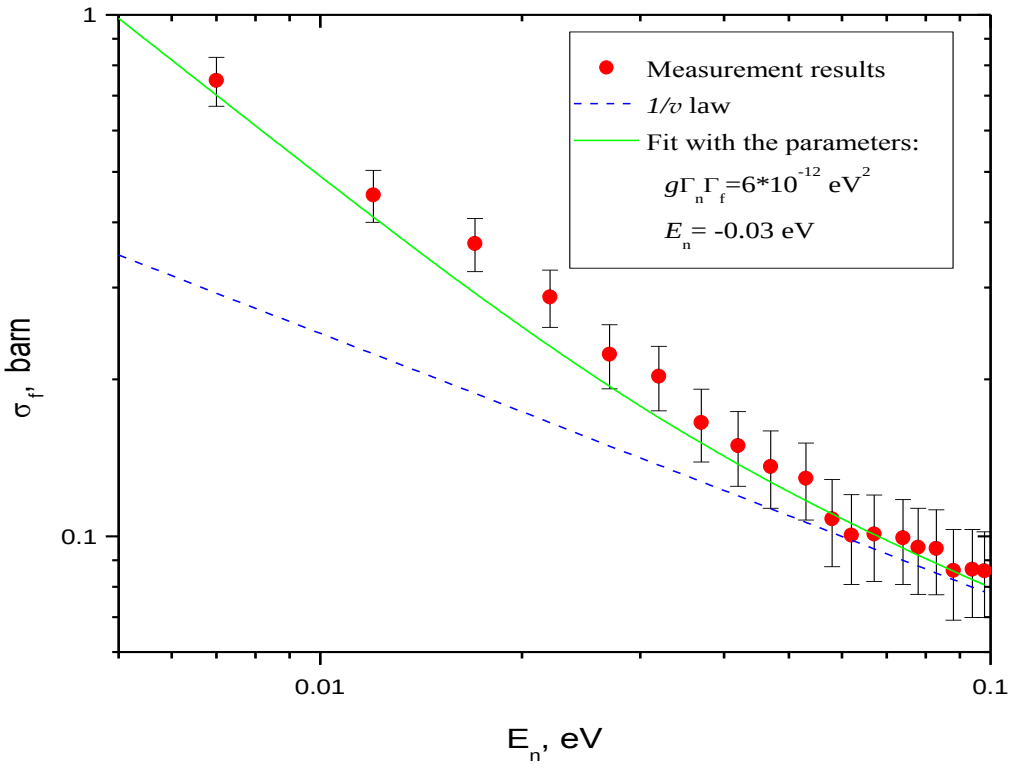

Figure 2.5. The energy dependence of ^{234}U fission cross-section in the vicinity of thermal point

The obtained energy dependence of ^{234}U fission cross-section is shown on Figure 2.5. One could see that this dependence do not follow the 1/*v* law that is plotted by dashed line.

The experimental points were fitted by Breit-Wigner formula in order to estimate the parameters of the negative resonance that caused deviation from 1/*v* law. The energy of the negative level E_n and product of the multiplication of the neutron and the fission widths of the resonance $g\Gamma_n\Gamma_f$ were the free parameters of the fit. Upper estimation of these parameters are given on the Figure 2 together with the result of the fit. Using average fission width for ^{234}U resonance $<\Gamma_f>\sim 10$ μeV one could obtain the neutron width of the negative resonance $\Gamma_n \sim 10^{-7}$–10^{-8} eV. It could be *p*-wave resonance.

2.3. Prompt Fission Neutron Multiplicity Measurements

2.3.1. Measurement Technique and Detector Design

This section is written on base of [40], describing the technique.

Measurements were carried out on channel #3 (60 m flight path) of pulsed reactor IBR-30. Energy of incident neutrons was measured by TOF method. As a ‘stop” for TOF measurement the signal from the fission fragment detector was used. As a detector the parallel plate pulsed ionization chamber was used. The design of the chamber is drawn on the Figure 2.6. Anodes were made of aluminium foils 50 μm thick fixed on stainless steel support rings. Layers of isotope under investigation, as well as ^{235}U (for neutron flux measurements) and ^{244}Cm (for neutron detector efficiency measurements) were placed on cathodes.

There was a flow through the chamber of pure methane (about 2 l/hour) with atmospheric pressure.

Signals from the chamber were amplified by current sensitive preamplifier and were sent to a fast discriminator. Logical signal from the discriminator gave the time stamp for TOF, ‘start’ for neutron detector and opens the gate for amplitude analysis of the signals from the camera. That latest was used to control the stability of the camera regime.

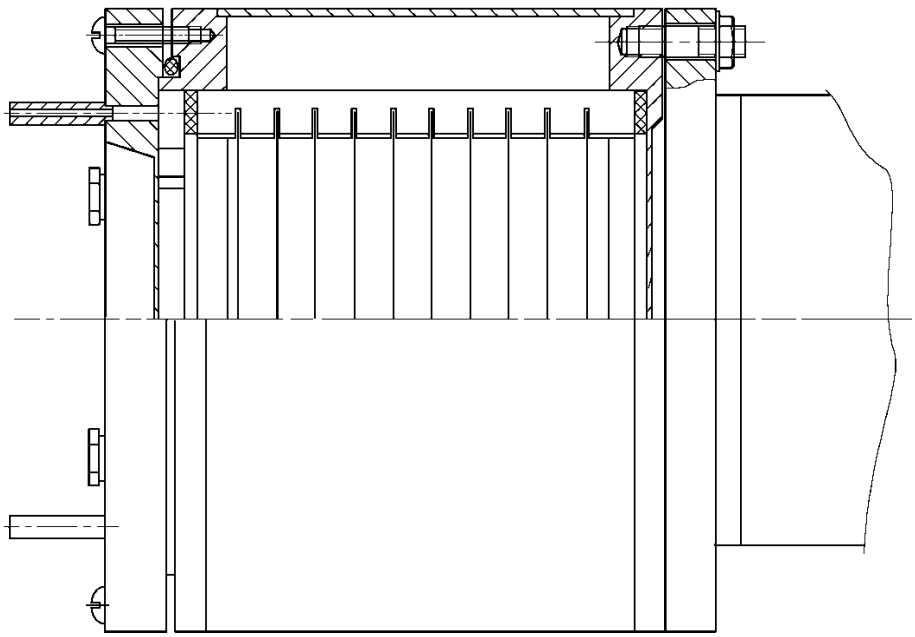

Figure. 2.6. Ionisation chamber used as a fission fragment detector

The ionization chamber was placed in the central channel of the neutron detector (Figure 2.7). The detector was made of 72 polyethylene blocks of the shape of hexagonal prism. Along the axis of every prism there was a ^{3}He neutron counter. The detector was surrounded by borated polyethylene shielding with thickness from 5 to 10 cm. A central channel of the neutron detector was layered with 0.5 mm of Cadmium. After receiving the 'start' signal from the chamber, 128 μs long gate was opened. During this time, all the signals from neutron counters were counted and stored in the list mode. One record contained number of registered neutrons, identification numbers of counters, time of registration of every neutron relative to 'start', time of flight and ionization chamber pulse amplitude.

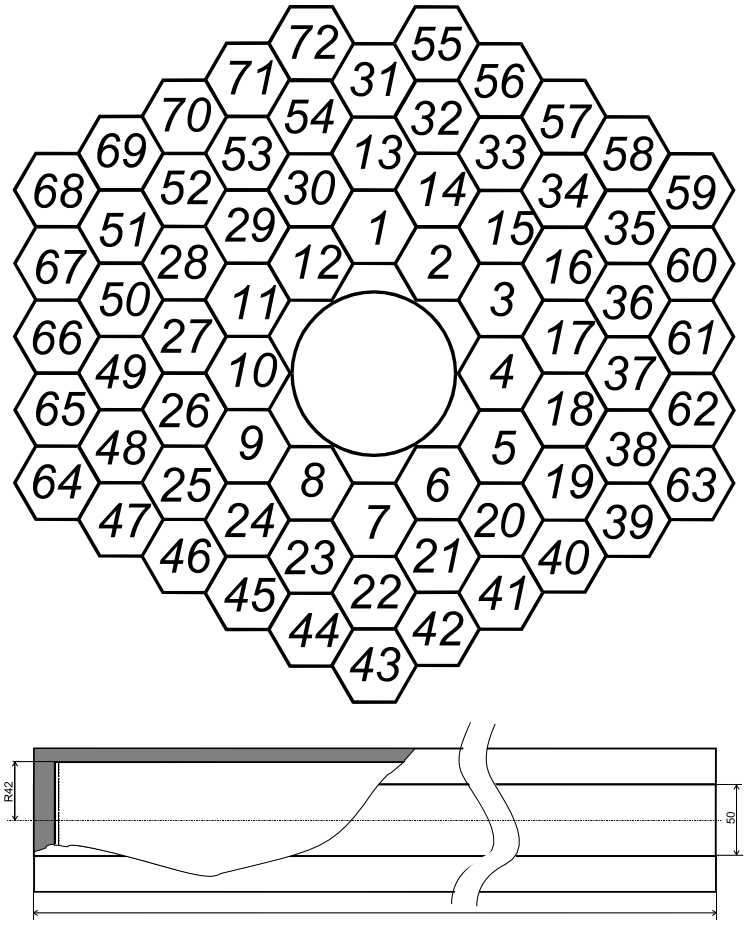

Figure 2.7. Neutron detector and moderator block with neutron counter

Efficiency of the neutron detector was determined by two methods. First one (integral): 'start' pulses came from the Curium fission fragments (chamber with Curium layer placed inside the neutron detector central channel). Background from cosmic radiation, spontaneous fission, delayed neutrons and neutrons from (α, n) reaction was measured by random signals from chamber outside the detector. As a result,

$$\varepsilon = \frac{N_n - N_\Phi}{N_f \overline{\nu}_p}, \tag{2.17}$$

where N_n - number of neutron pulses

N_ϕ - number of BG pulses

N_f - number of registered fissions

$\bar{\nu}_p$ - average neutron multiplicity for ^{244}Cm spontaneous fission.

Second method is based on counting the neutron multiplicity distribution from the ^{244}Cm spontaneous fission. The probability to register several neutrons are determined by probability of emitting ν neutrons $P(\nu)$ and probability to register each neutron ε, e.g., neutron detector efficiency. The efficiency can be found from the relation

$$\frac{M_2}{M_3} = f(\varepsilon), \tag{2.18}$$

where $M_k = \sum_{i=k} \mathbf{C_k^i} P(i)\varepsilon^k (1-\varepsilon)^{i-k}$,

$i = k,\ k+1,\ k+2,\ \ldots$

$\mathbf{C_k^i}$ — binomial coefficient

Practically it is better to calculate a table $f(\varepsilon)$ and find a solution from the table. Efficiency, determined by two methods, coincides within the error limits. Average value, used in the calculations, was 39±2%.

2.3.2. Distribution of the Neutron Registration Time

Time intervals between two independent events are described by Poisson distribution with zero degree of freedom [41]

$$p(t)dt = re^{-rt}dt\,, \tag{2.19}$$

where $p(t)dt$ - probability that in interval $[0;t]$ there will be no event and in interval $[t, t+dt]$ there will be only one event.

From other hand, the intervals between detections of two neutrons which appear simultaneously inside the neutron detector volume are correlated. They are connected by neutron life-time in the detector and distributed, as a first approximation, on the exponential decay law.

$$I_{2n}(t)dt = Ae^{-t/\tau}dt, \tag{2.20}$$

where τ - average neutron life-time

$A = \frac{1}{\tau}$ - normalising coefficient

The equation 2.17 is as well valid for probability $p_1(t_1)dt$ to register first neutron in the interval $[t_1, t_1+dt_1]$ after 'start' from the fission event.

The probability $p_2(t_2)dt$ of second neutron detection in the interval $[t_2, t_2+dt_2]$ after 'start' can be obtained as follows:

The probability $p_{21}(t_{21})dt$ to detect second neutron in the interval $[t_{21}, t_{21}+dt]$ after first one can be found by equation 2.17.

Then, $p_2(t_2)dt = \int_0^{t_2} p_1(t_1)dt_1 p_{21}(t_{21})dt$

Taking into account that $t_{21}=t_2-t_1$ one get after integration

$$p_2(t_2) = \frac{1}{\tau^2} t_2 \exp\left(-\frac{t_2}{\tau}\right)dt, \tag{2.21}$$

In the same way one can get $p_3(t_3)dt = \frac{t_3^2}{2\tau^3}\exp\left(-\frac{t_3}{\tau}\right)dt$, $p_4(t_4)dt = \frac{t_4^3}{6\tau^4}\exp\left(-\frac{t_4}{\tau}\right)dt$ etc..

In a general way,

$$p_i(t) = \frac{t^{i-1}}{(i-1)!\tau^i}\exp\left(-\frac{t}{\tau}\right)dt, \tag{2.22}$$

Analogously one can get equation for the single neutron background in multiple events:

$$p_i^{\mathrm{BG}}(t) = Ct^{i-1}\exp(-rt)dt, \tag{2.23}$$

For the BG measurements additional ionization chamber contained layer of ^{244}Cm was used. It was placed far away from the detector under additional shielding and gave random 'start' signal. Neutrons, emitted from the fission, occurred in this chamber, cannot be registered by neutron detector. 'Main' chamber at that time was still in the neutron beam in the central channel of the detector. The acquisition system works as usual. Such a procedure gives the possibility to measure time distribution of the BG neutrons and get a distribution of the neutron background over the TOF spectra, which is essential for TOF measurements.

The distributions of the detection time of first, second, … fifth and all of the neutrons are shown on the Figures 2.8–2.10 for three cases:

1. Spontaneous fission ^{244}Cm: 'start' from fission chamber in the centre of ND, no neutron beam

2. Same as previous, but with neutron beam

3. BG measurement: ‘start’ from chamber outside the detector, in the centre of the detector there are ‘main’ chamber in the neutron beam.

Two-dimensional distributions of the neutron multiplicity over time-of-flight for ^{234}U fission and for BG are shown on Figure 2.11. There are very well pronounced resonance 5.16 eV.

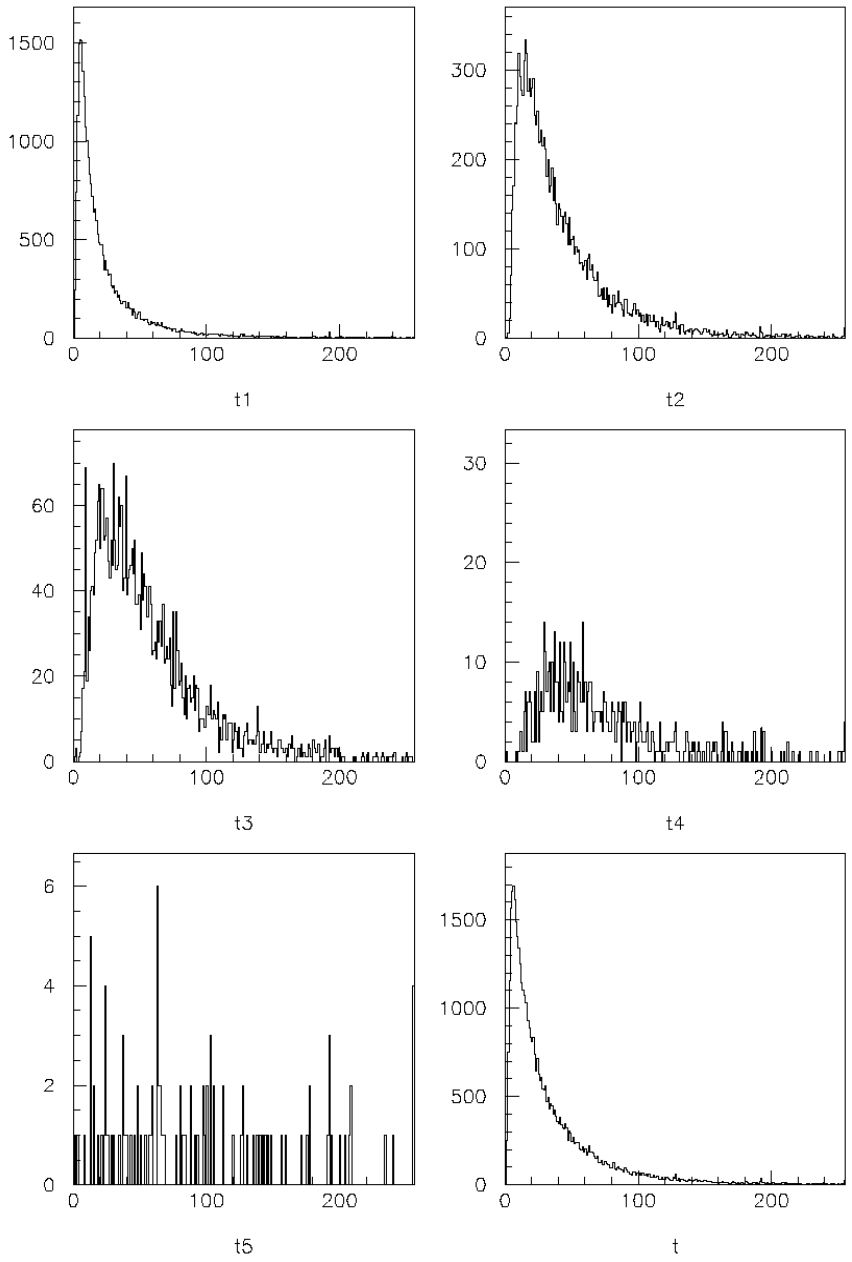

Figure 2.8. The distribution of detection time for ^{244}Cm spontaneous fission

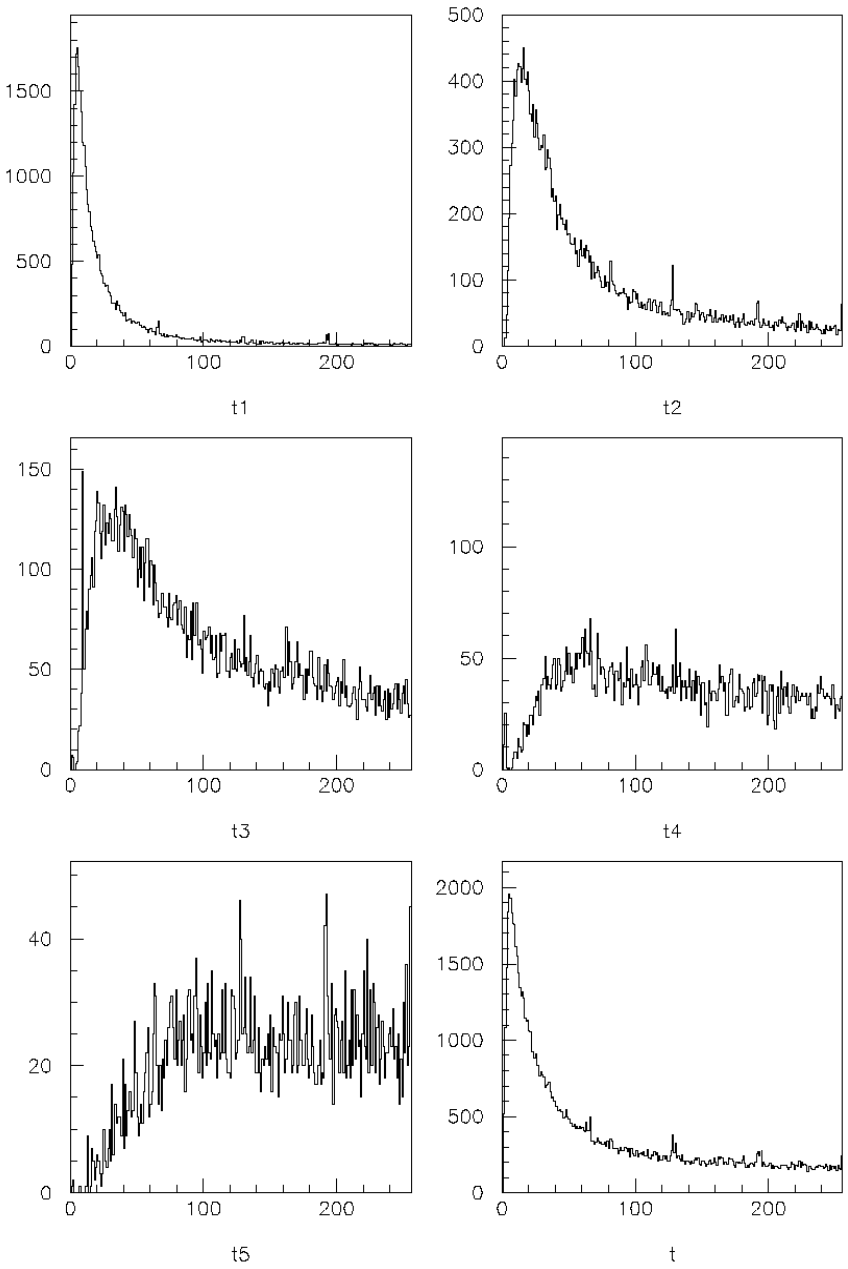

Figure 2.9. The distribution of detection time for ^{244}Cm spontaneous fission with background from neutron beam

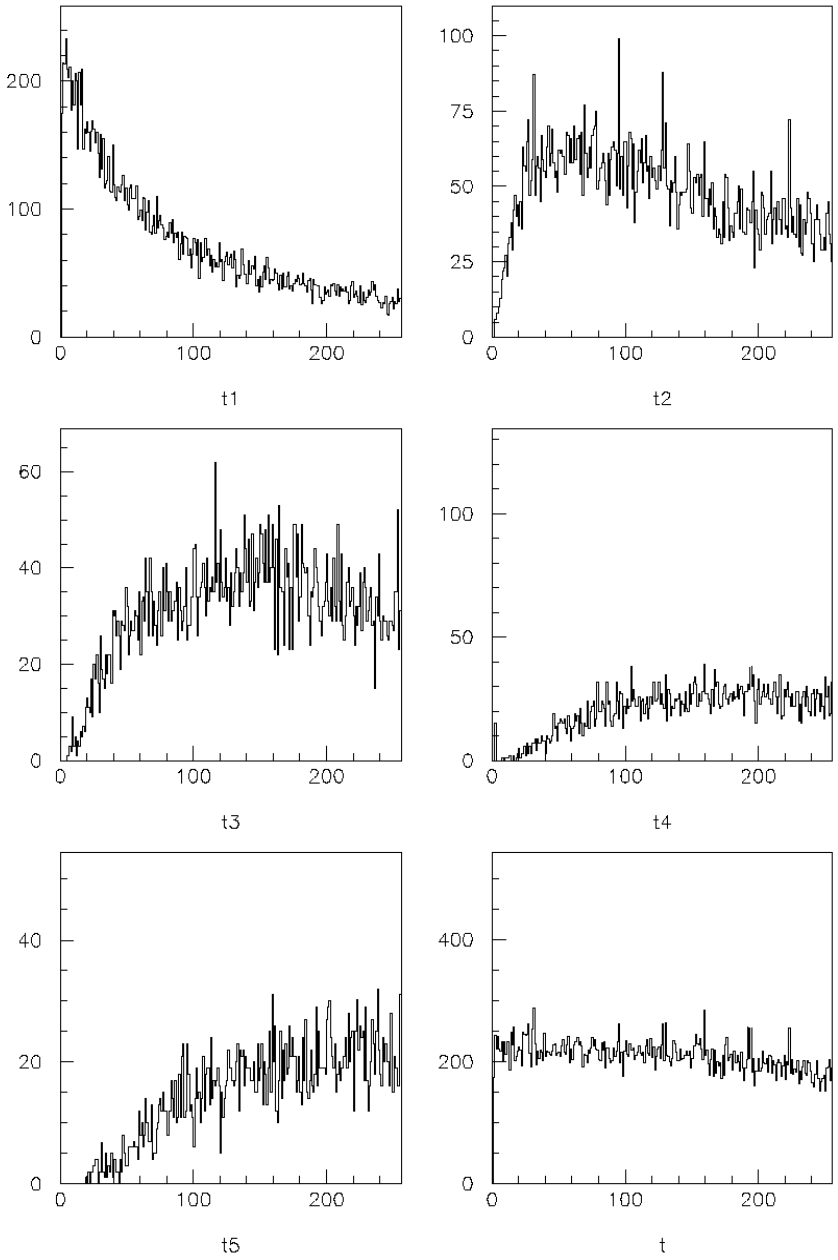

Figure 2.10. The distribution of detection time for background neutrons

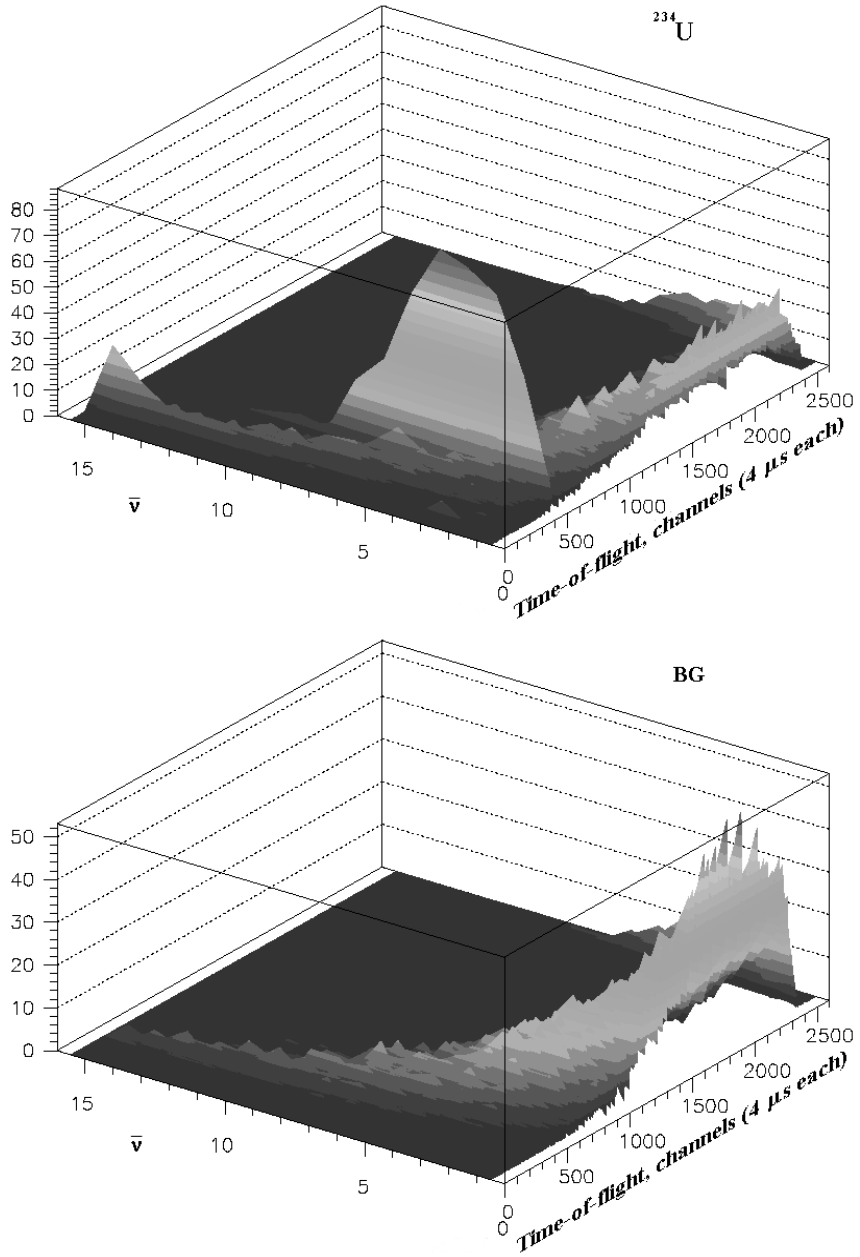

Figure 2.11. Two-dimensional distribution of registered multiplicity versus time-of-flight for ^{234}U.

2.4. Experimental results

The data, described in this chapter, is obtained in Dubna in years 1994-2000. Main achievement of this period is development of the methods of fission cross-section measurement of the highly α-radioactive nuclides using parallel plate ionization chambers as a detector. This technique was later used in CERN on n_TOF neutron source.

Data on fission cross-section of ^{234}U and ^{243}Am are in good agreement with existing data and was cross-checked with another methods, i.e. gamma-multiplicity detection. This makes the data reliable and it is used for evaluated data libraries.

2.4.1. Neutron Induced Fission Cross-section of ^{234}U and ^{243}Am.

Measured and calculated fission cross-section for ^{234}U and ^{243}Am are shown on Figures 2.8 and 2.9, respectively. Calculated cross-sections are obtained using one-level approximation from fission widths, shown in Tables 2.3 and 2.4 together with data from [10], [18] and [36]. Relative cross-section behaviour is determined with accuracy better, than 1% in the resonances. In between the resonances accuracy is lower, due to BG-effect ratio.

Systematical uncertainties in absolute cross-sections are connected mainly with sample mass errors. They are 4.5% for ^{234}U and 7% for ^{243}Am. Fission width errors appears from neutron and total widths uncertainties and from systematical errors mentioned above.

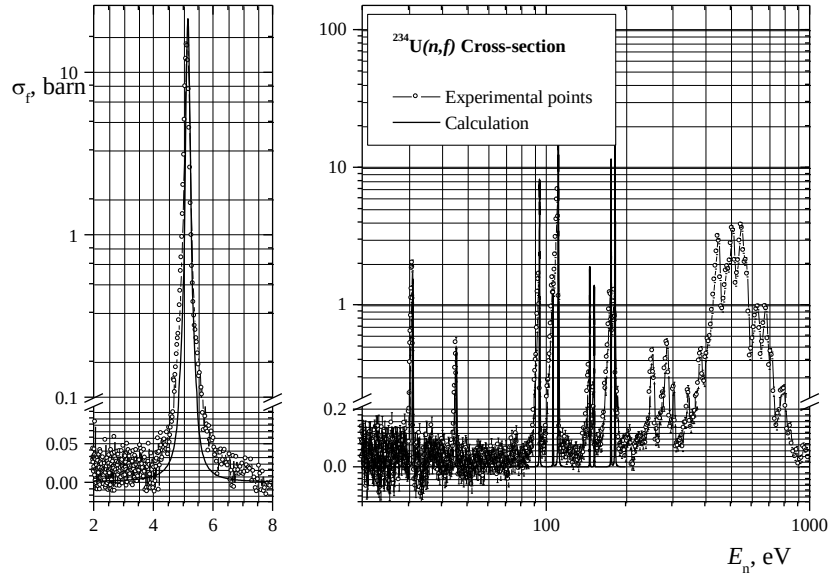

Figure 2.8. The cross-section of the neutron induced fission of ^{234}U

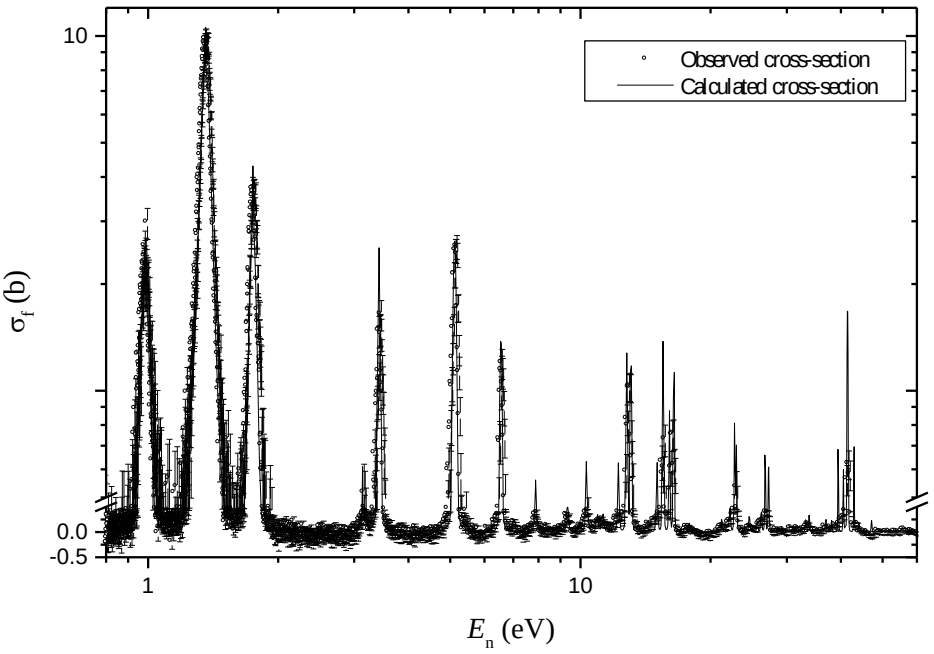

Figure 2.9. ^{243}Am fission cross-section

Table 2.3. ^{234}U Resonance Parameters

E_n, eV	$\sigma_0\Gamma_f$, b·eV	$\Delta\sigma_0\Gamma_f$, b·eV	Γ_f, meV	$\Delta\Gamma_f$, meV	Γ_f, meV [18]	$\Delta\Gamma_f$, meV [18]
5.16	1.38	0.06	0.0201	0.0008	0.0182	0.0009
31.13	0.17	0.01	0.009	0.001	0.008	0.001
45.61	0.08	0.01	0.08	0.01	0.067	0.007
94.29	0.66	0.05	0.038	0.004	0.033	0.003
106.13	0.23	0.03	0.07	0.01	0.091	0.008
111.06	3.2	0.2	0.33	0.03	0.31	0.03
146.25	0.29	0.04	0.047	0.007	0.028	0.002
152.16	0.19	0.04	0.027	0.005	0.022	0.002
176.18	0.98	0.09	0.11	0.01	0.09	0.006
182.49	1.37	0.07	0.146	0.009	0.114	0.007

Obtained fission widths shown in the Table 2.4 together with data from [10] and [36] are in the reasonable agreement with data [10] for the energy region up to 10 eV with the exception of a two resonances: 7.8 and 9.9 eV. In the paper [10] for energy region above 20 eV the Γ_f values are given only for few resonances. The area $\sigma_0\Gamma_f$ of them are much higher then our one, probably, due to neibouring unresolved resonances. For some groups of resonances that could not be resolved, only total area given in this table.

Our spectrum contain resonance with energy about 9.9 eV that is absent in [35] and [36]. Origin of this level is not clear.

Table 2.4. ^{243}Am resonance parameters

E_n	$\sigma_0\Gamma_f$, barn·eV	Γ_f, meV	Γ_f, meV [36]	Γ_f, meV [10]
0.983	0.094 ± 0.002	0.189 ± 0.004	0.060	
1.359	0.584 ± 0.005	0.038 ± 0.001	0.030	0.020 ± 0.001
1.750	0.180 ± 0.003	0.048 ± 0.003	0.074	0.079 ± 0.003
3.134	0.029 ± 0.002	0.264 ± 0.022	0.226	0.269 ± 0.049
3.424	0.114 ± 0.002	0.052 ± 0.003	0.065	0.052 ± 0.006
5.12	0.260 ± 0.004	0.258 ± 0.011	0.212	0.254 ± 0.017
6.551	0.131 ± 0.005	0.042 ± 0.002	0.063	0.037 ± 0.003
7.021	0.021 ± 0.005	0.064 ± 0.016	0.064	0.064 ± 0.019
7.878	0.050 ± 0.006	0.007 ± 0.001	0.032	0.029 ± 0.002
8.412	0.011 ± 0.006	0.322 ± 0.184	0.492	0.315 ± 0.222
8.858	0.012 ± 0.007	0.031 ± 0.017	0.022	
9.335	0.050 ± 0.007	0.125 ± 0.019	0.193	0.226 ± 0.045
9.971	0.019 ± 0.008			
10.344	0.073 ± 0.008	0.085 ± 0.009	0.106	0.133 ± 0.014
10.933	0.036 ± 0.008	0.666 ± 0.159	1.846	0.111 ± 0.031
11.259	0.042 ± 0.009	0.066 ± 0.014	0.094	0.075 ± 0.030
11.706	0.024 ± 0.009	0.053 ± 0.021	0.027	
12.241	0.067 ± 0.009	0.186 ± 0.027	0.019	
12.796	0.141 ± 0.010	0.028 ± 0.008	0.098	0.059 ± 0.011
13.083	0.158 ± 0.010	0.066 ± 0.005	0.030	0.037 ± 0.006
15.026	0.076 ± 0.012	0.484 ± 0.081	0.089	
15.521	0.161 ± 0.013	0.199 ± 0.016	0.126	0.139 ± 0.029
16.065	0.106 ± 0.013	0.106 ± 0.014	0.386	0.367 ± 0.082
16.448	0.140 ± 0.013	0.293 ± 0.032	0.028	
17.846	0.021 ± 0.015	0.049 ± 0.034	0.023	
21.233	0.034 ± 0.018	0.024 ± 0.013	0.007	
21.837+22.163	0.088 ± 0.030			
22.726+22.976	0.202 ± 0.030			
24.593	0.047 ± 0.022	0.047 ± 0.022	0.095	0.113 ± 0.015
26.206+26.749	0.166 ± 0.034			
27.244	0.095 ± 0.025	0.156 ± 0.041	0.015	
33.211+33.803	0.101 ± 0.046			
36.962	0.044 ± 0.036	0.031 ± 0.025	0.009	
38.109	0.041 ± 0.037	0.114 ± 0.103	0.177	0.153 ± 0.036
39.459	0.112 ± 0.039	0.182 ± 0.064	0.123	0.179 ± 0.030
40.572	0.102 ± 0.040	1.930 ± 0.760	0.166	
41.401+41.559	0.426 ± 0.057			
42.938	0.127 ± 0.043	0.071 ± 0.024	0.148	0.115 ± 0.021

2.4.2. Neutron Fission and Capture Cross-section of ^{234}U and ^{236}U

The ^{236}U capture cross section weighted over a $1/E$ spectrum within energy intervals adopted in the BNAB library [42] along with estimated data of ENDF/B-VI [43], JENDL [44] and BNAB-LIP [42] is presented in Table 2.7.

The weighted capture and fission cross sections of ^{234}U are given in Table 2.5 and Table 2.6, respectively. In Table 2.6 the values of group constant, calculated on the basis on the resonance parameters, obtained in JINR (See sections 2.1.2 and 3.1.2) is also presented. In capture cross section measurements, the time allotted for the present experiments allowed us to obtain a statistical accuracy better than 5% within each energy interval excluding No.20 in which the cross section value is too small. In fission cross section measurements, the statistical accuracy is twice lower. But errors provided by cross-section normalisation are difficult to estimate. The impurity of ^{235}U in the ^{234}U sample under investigation has been taken into account in analysis of the respective fission cross section.

Table 2.5. The capture cross section $<\sigma_\gamma>$ in barns for ^{234}U.

Group number	Energy interval, eV		Present work	Estimated		
	E_1	E_2		ENDF/B-VI	JENDL	BNAB-LIP
21	4.65	10.0	676	708,2	674,8	677,6
20	10.0	21.5	0,25	0,318	0,240	0,224
19	21.5	46.5	33,3	36,75	42,94	33,7
18	46.5	100	31,8	35,95	35,95	30,76
17	100	215	20,1	23,74	21,93	19,45
16	215	465	7,30	7,16	6,96	6,11
15	465	1000	5,70	5,72	5,02	4,42
14	1000	2150	3,70	3,46	3,05	1,58

Table 2.6. The fission cross section $<\sigma_f>$ in barns for ^{234}U.

Group number	Energy interval, eV		Present work		Estimated		
	E_1	E_2	JINR	KI	ENDF/B-VI	JENDL	BNAB-LIP
23	1	2.15	0.0014				
22	2.15	4.65	0.0058				
21	4.65	10.0	0.51	0,496	0,324	0,521	0,496
20	10.0	21.5	0.00012	> 0	0,0005	0,0002	0,0006
19	21.5	46.5	0.015	0,03	0,0094	0,0173	0,0139
18	46.5	100	0.014	0,01	0,0112	0,0151	0,0145
17	100	215	0.11	0,1	0,0693	0,0997	0,0917
16	215	465		0,06	0,0624	0,0915	0,0858
15	465	1000		0,17	0,1638	0,2237	0,2162

Table 2.7. The capture cross section $<\sigma_\gamma>$ in barns for ^{236}U.

Group number	Energy interval eV		Present work	Estimated		
	E_1	E_2		ENDF/B-VI	JENDL	BNAB-LIP
21	4.65	10.0	365.1	364.8	352.8	353.6
20	10.0	21.5	0.101	0.099	0.104	0.104
19	21.5	46.5	38.28	27.88	38.50	37.00
18	46.5	100	21.46	18.46	21.28	19.30
17	100	215	16.14	12.94	15.02	14.35
16	215	465	6.14	4.86	5.66	6.24
15	465	1000	5.28	4.35	4.93	4.73
14	1000	2150	2.56	2.16	2.43	2.12

Table 2.8. The fission cross section $<\sigma_f>$ in barns for ^{236}U.

Group number	Energy interval eV		Present work	Estimated		
	E_1	E_2		ENDF/B-VI	JENDL	BNAB-LIP
21	4.65	10.0	4.21	4.32	4.18	4.19
20	10.0	21.5	>0.001	0.0012	0.0013	0.0013
19	21.5	46.5	0.56	0.716	0.673	0.532
18	46.5	100	0.37	0.297	0.298	0.262
17	100	215	0.28	0.168	0.244	0.202
16	215	465	0.094	0.102	0.099	0.097
15	465	1000	0.085	0.077	0.077	0.074

2.4.3. Prompt Fission Neutron Multiplicity

Due to limited measurement time and low fission cross-section of ^{234}U it was not possible to measure neutron multiplicity distribution, but average neutron multiplicity of the prompt neutrons for fission of ^{234}U with neutrons having energy 5.16 eV was obtained and appeared to be $\bar{\nu} = 2{,}13 \pm 0{,}34$.

Chapter 3. Investigation of the Neutron Induced Fission Cross-section of the Thorium Cycle Isotopes on the n_TOF Neutron Source at CERN, Geneva, Switzerland

3.1. Experimental Technique

3.1.1 n_TOF Neutron Source

The n_TOF facility of CERN (Conseille Européenne de Recherche Nucléaire) is a high energy and high fluence spallation neutron source, using a pulsed proton beam impinging on a Pb target, followed by a 185 m flight path, which leads to the measuring station.

The concept of the n_TOF neutron beam makes use of the high neutron flux from spallation reactions of 20 GeV protons on an extended lead target and the high beam density of the CERN Proton Synchrotron (PS), which provides up to 7×10^{12} protons per pulse, high enough to produce the vast number of 2×10^{15} neutrons per pulse, in the form of short (6 ns width) pulses with a repetition time varying from 2.4 s to 16.7 s. These features make the n_TOF facility an extremely luminous neutron source with an excellent time resolution [45]. Neutron production is accompanied by an intense flash of γ-rays and ultra-relativistic particles from the impact of the 20 GeV proton pulses on the neutron spallation target, which is nevertheless weaker than the specific γ-flash at electron machines. This γ-flash is reduced by appropriate shielding, a sweeping magnet, and two collimators. The n_TOF facility allows to study systematically and with excellent energy resolution, neutron induced cross-sections in the interval from thermal to hundreds of MeV, of almost any element using targets of very modest mass, a necessary requirement for unstable or expensive rare isotopes.

The parameters of the neutron source are shown in Table 3.1.

Neutron guide schematic is shown on Figure 3.1.

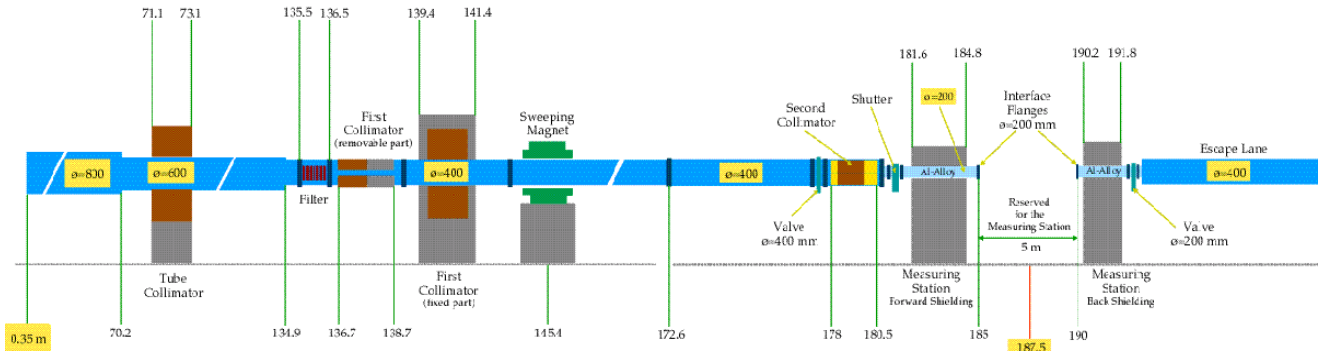

Figure 3.1. The schematics of the n_TOF neutron guide

Table 3.1. Parameters of n_TOF neutron source

Accelerator beam:		
Proton Energy:		20 GeV
Beam size on the target:		
σ (horizontal)		7.8 mm
σ (vertical)		5.6 mm
Intensity	TOF	7×10^{12}
[protons per pulse]	EASTC	4.5×10^{12}
Repetition rate:		$0.0625 – 0.71\ s^{-1}$
Pulse width		6 ns
Number of neutrons per proton		300

Lead target:	
Size:	80x80x60 [cm^3]
Beam cavity	55x20x20 [cm^3]
The proton beam is bended on 10 degrees in vertical direction relative to neutron guide axis to decrease the background of light charged particles in a neutron beam	

Window for neutrons:	
Material	Aluminium
Diameter	80 cm
Thickness	1.6 mm
Support grid thickness	40 mm
Average thickness	6.17 mm

Cooling and moderating:	
Cooler/Moderator	H_2O
Thickness	5 cm

Design of the neutron source is described in detail in [45].

The neutron flux and resolution was analysed during data processing and will be discussed below.

3.1.2. Fission Fragment Detector

The measurements were performed at n_TOF during the 2003 campaign with a Fast Ionization Chamber (FIC) [45, 46]. FIC was developed by the Institute of Physics and Power Engineering, Obninsk, in collaboration with the Joint Institute of Nuclear research (JINR),

Dubna, and the EET group at CERN. The FIC is composed of 17 ionization chambers, with a total of 16 targets and 18 electrodes, mounted together in a chamber 50 cm in length, thus allowing a simultaneous measurement of the fission cross-sections of several isotopes. Distance between electrodes was 5 mm. Detector was filled with mixture of Argon and Carbon Hexafluoride (90%Ar + 10%CF_4) with pressure 700 mbar. High voltage 400 V was applied on targets (cathodes), anodes, made of Aluminium, were grounded. The past experience, acquired in JINR, in use of analogous chambers (see Chapter 2) showed time resolution of 2-3 ns with minimal overlapping of FF-α-particles signals. It's completely enough for n_TOF timing and neutron flux. The detector was designed and manufactured according to standard ISO 2919 (sealed radioactive sources) [47]. That was required by safety authorities. Maximal number of targets that can be installed into the chamber was 16, so, different isotopes can be measured simultaneously. Besides that, inside the chamber targets made of ^{235}U and ^{238}U were installed. They were used as a reference for flux determination and energy calibration. A drawing of the detector design is shown on Figure 3.2.

The innovative feature of the detector, proposed by the Author of this Dissertation, is three off beam positions, occupied by targets of isotopes under investigation. These targets were connected to separate channel of Data Acquisition System and have been used to measure the background caused by alpha pile-ups, along with a dummy (empty) target mounted in-beam to record background events.

3.1.3. Targets

.

30 targets were made especially for these measurements. Every target consists of stainless steel support ring, on which aluminum foil was welded. The layers of the ceramics based on isotope under investigation were placed on the aluminum substrate using thermal baking process. Thicknesses of the layers were from 1 to 300 μg/sm^2, diameters of the spot 50 or 80 mm. Masses and isotope compositions of each target were determined using alpha-spectrometry. The procedure of target production is described in [48]. Targets' parameters are shown in Table 3.2.

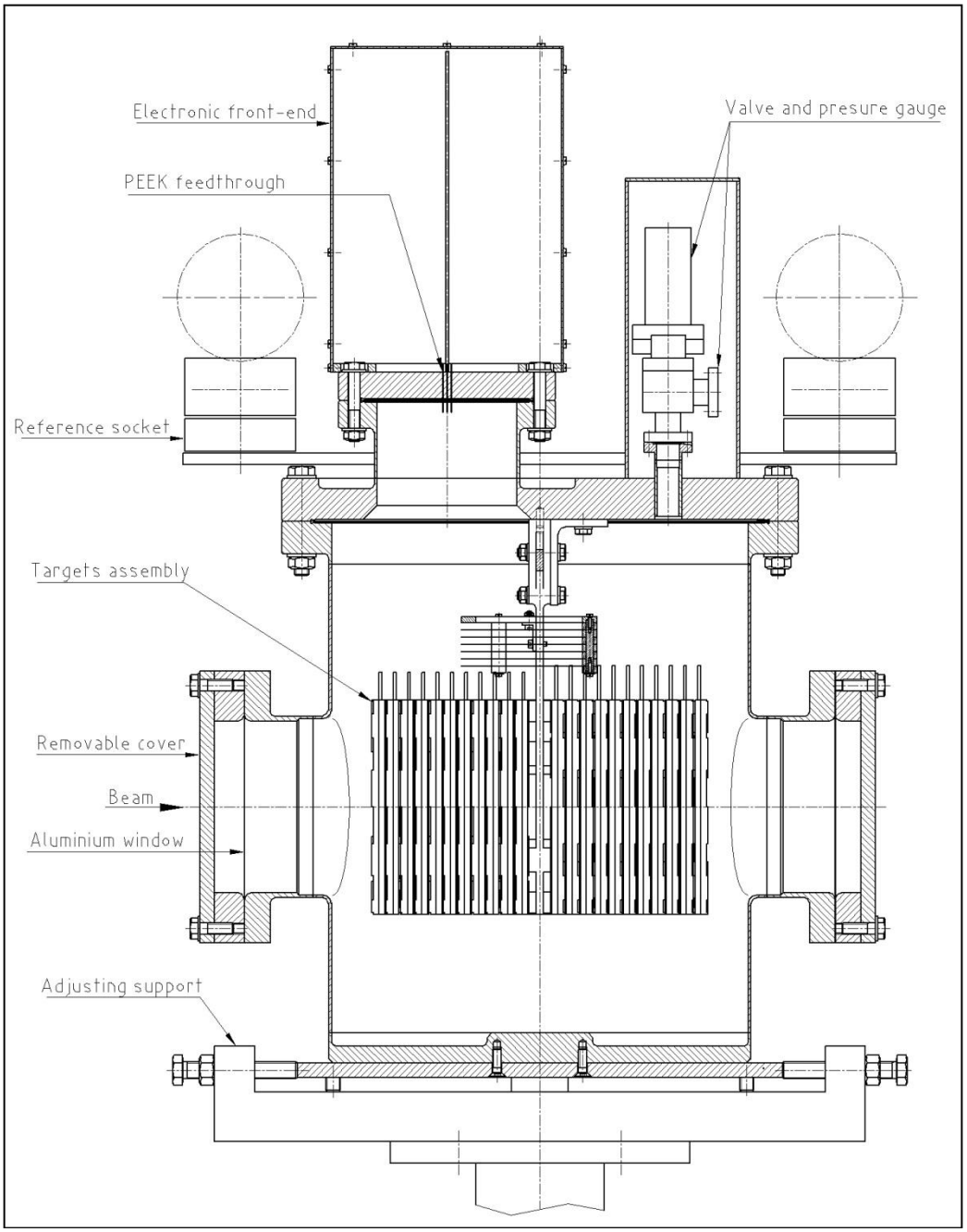

Figure 3.2. FIC detector set-up.

Table 3.2. Targets.

Isotope	Label	Mass, μg	Uncertainty of mass determination, %	Isotope	Label	Mass, μg	Uncertainty of mass determination, %
Th-232	1	1,92E+04	1,4	U-236	15		
	2	1,90E+04	1,2		16	5,82E+03	1,3
	3	1,94E+04	1,4		17	5,33E+03	1,4
	4	1,82E+04	1,3		18	5,25E+03	1,4
U-233	5	8,04E+03	1,2		19	4,95E+03	1,4
	6	7,45E+03	1,2	U-234	8	5.46E+03	5
	7	7,49E+03	1,3		7	5.00E+03	5
	8	5,86E+03	1,1		6	5.17E+03	5
U-235	9	1,67E+04	1,1		5	5.17E+03	5
	10	1,89E+04	1,1		4	5.46E+03	5
	11	1,52E+04	1,4		3	5.28E+03	5
	12	1,66E+04	1,3		2	5.40E+03	5
	13	6,47E+03	1,1		1	5.41E+03	5
	14	6,32E+03	1,1	U-238	209	10E+03	10
U-238	20	1,18E+04	1,3	U-238	210	10E+03	10
	21	1,15E+04	1,4	U-238	211	10E+03	10
	22	1,28E+04	1,4	U-235	78	5E+03	10
	23	1,26E+04	1,4	Am-243	38	5,56E+02	1,2
	24	1,34E+04	1,2	(Am-241)	39	5,85E+02 (1,48E+01)	1,3 (1,2)
	25	1,37E+04	1,4		40	6,13E+02	1,3
	26	1,28E+04	1,4		41	6,31E+02	1,3
	27	1,24E+04	1,4		42	5,37E+02	1,2
Am-241	30	2,34E+02	1,1		43	5,58E+02	1,2
	31	2,30E+02	1,2		44	5,95E+02	1,3
	32	2,80E+02	1,2		45	7,10E+02	1,2
	33	2,79E+02	1,2	Cm-245 (Cm-244)	46	3,67E+02 (2,43E+01)	1,3 (1,1)
	34	3,04E+02	1,2		47	5,38E+02	1,2
	35	3,36E+02	1,2		48	4,07E+02	1,3
	36	3,21E+02	1,2		49	3,99E+02	1,3
	37	2,77E+02	1,2	Np-237	28	6,34E+03	1,0
	37 (1)	2,82E+02	1,2		29	6,48E+03	1,1
	37 (2)	2,46E+02	1,2				

3.1.4. Data Acquisition System

Block diagram of the data acquisition system (DAQ) are shown on Figure 3.3. Detail description of the DAQ is published as [49].

Since experiment control room was situated approximately in 100 m from measurement station, signals from the chamber were amplified by preamplifiers and converted to the twisted pair signal. That was done by one 16-channels block, which was made on one printed circuit board and was connected to the camera flange through specially designed air-tide connector. In the control room signal was converted again to one relative to ground, amplified and split into two parallel signals (see Figure 3.3). One signal, after discrimination by constant-fraction

discriminator, was used as a time-stamp, which was registered by time-to-digit converter (TDC). Working range of TDC was from few μs to 100 ms (from 0.01 eV to 1 MeV on used TOF base) with time resolution about 0.8 ns.

Another signal was digitized by flash analogue-to-digit converter (FADC) with sampling frequency 40 MHz, 10-bit word for signal coding and 4096 words of internal memory. That give a full information about the signal from the detector for the time up to 100 μs, which correspond to a neutron energy 20 keV on a flight path 185 m.

All signal parameters were stored in list mode, which gives a possibility of complete reconstruction of the experiment off-line.

So, data from FADC and TDC were overlapped in the energy range from 20 keV to 1 MeV. Data, obtained by these two methods, were processed independently for cross-checks and normalization.

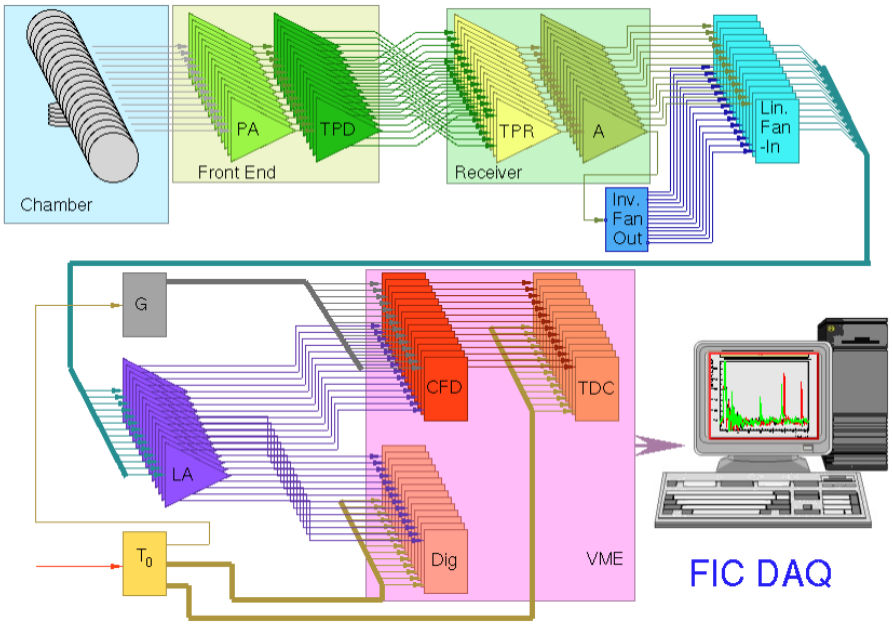

Figure 3.3. FIC electronics set-up.

3.2. Data Analysis

Processing of the data was done in the several steps. First step was done for every channel (i.e. each target of isotopes under investigation and reference targets) separately. This preliminary processing includes of background effects filtering, converting the time of flight into neutron energy and building the histograms of count rate and amplitude spectra for further processing.

On the base of obtained histograms cross-section were calculated.

Below the detailed description of data analysis procedure is given.

3.2.1. Noise filtering

The intense proton pulse hitting the lead target produces flash of γ-rays and other particles. Although the γ-flash is useful to provide a very precise neutron time of flight, the intensity of the produced signal saturates the detector which undershoots and, until the recovery, a ripple of the baseline is observed. The electronic distortion of the detector signal makes it impossible to extract safe conclusions for the specific energy region between above 1 MeV.

For the TDC filtering of the noise that appears after proton beam hits the target is possible due to the fact that this noise is almost identical in all the channels. So, noise signal after constant fraction discriminator appears in several channels, while probability of coincidence of two fission signals from different channels is very low. Optimal coincidence parameters were adjusted empirically: multiplicity 3 or more, coincidence window — 20 ns.

Procedure of noise filtering for FADC data is much more complicated. The detailed description of the FADC data processing is published in [50].

A correction has been applied based on the observation that all FADC outputs seem to follow the same pattern in this region, thus allowing to produce an "average" FADC output for each detector channel by adding all the signals starting from the time of the γ-flash. The rippling and undershooting effect can thus be corrected by subtracting this "average" FADC output from the actual data.

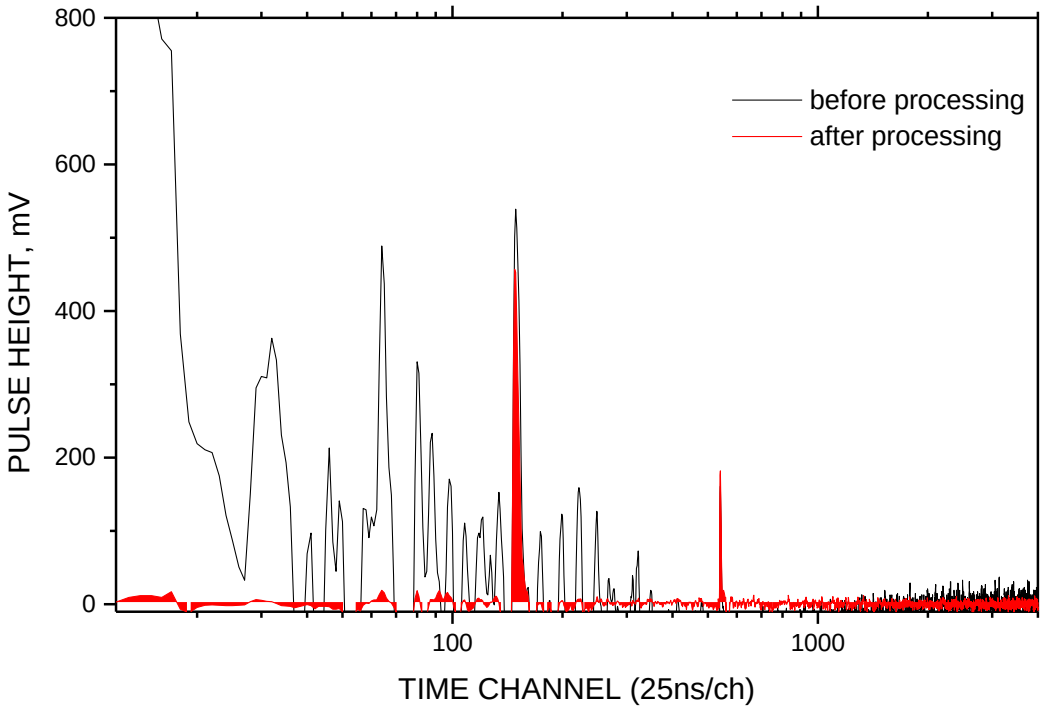

Figure 3.4. Sample of the FADC signal (black) and signal after noise filtering (red). Two fission fragments can be seen.

The sample of the signal before processing and the result of the background subtraction can be seen graphically in Figure 3.4.

3.2.2. Converting the Time-of-Flight into Energy

In case of n_TOF neutron source the well-known relation (3.1) between neutron energy, flight path and time-of-flight have to be corrected due to large volume of lead target which contribute noticeably to the moderation of neutrons.

$$E_n = 5227.29\left(\frac{L}{t}\right)^2 \quad (3.1),$$

where L is a flight path in meters,

t — flight time in microseconds.

It is well known that neutron moderation time and its path inside the medium is inversely proportional to moderator nuclear mass. Lead introduce a delay between proton burst and time when a neutron enters the neutron guide.

It is convenient to estimate this delay as a effective addition to the flight path $\lambda = v_n \Delta t$.

As a result, equation (3.1) became

$$E_n = 5227.29\left(\frac{L+\lambda}{t}\right)^2 \quad (3.2)$$

To determine λ we use resonances of ^{235}U with well-known energies. For each resonance was determined which effective length have to be added to make the energy of the resonance to coincide with existing data. The comparison of such corrected data with experimental data from EXFOR library is shown on Figure 3.5.

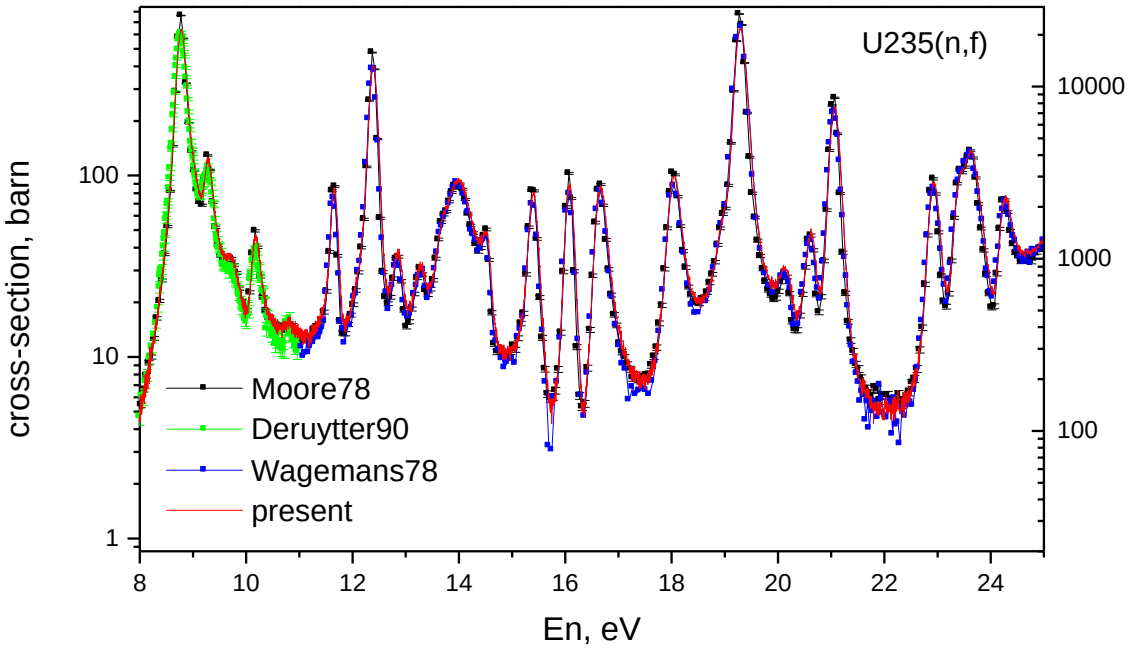

Figure 3.5. Comparison of the ^{235}U fission count rate after correction with known experimental data

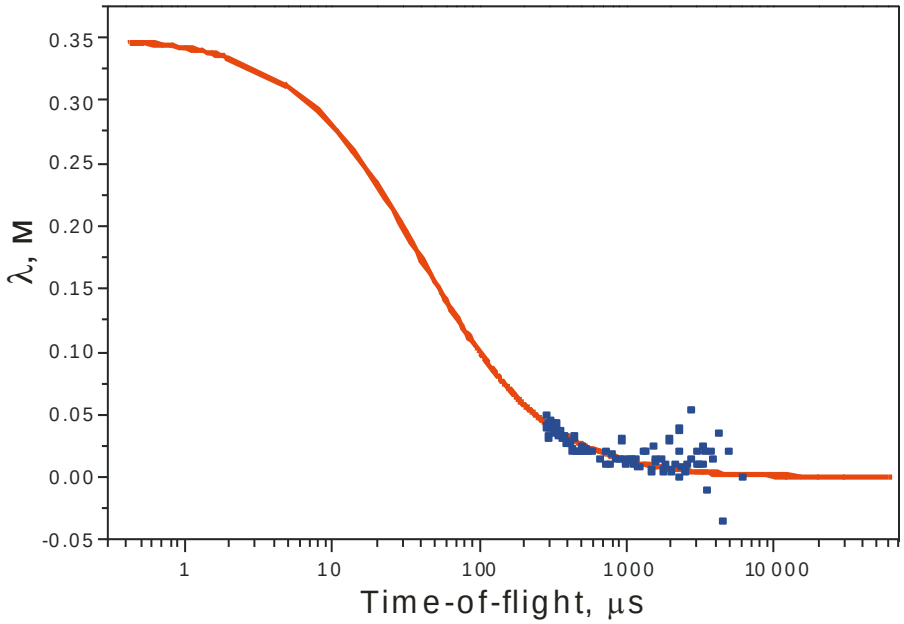

Figure 3.6. Extrapolation of the flight path correction and experimental values, obtained for ^{235}U resonances

Obtained relation together with data from capture measurements carried out on the same neutron source [50] and with results of Monte-Carlo modelling (see below) in the incident neutron energy region below 1 MeV can be described by the equation $\lambda[\text{cm}] = (0{,}094 \pm 0{,}018)\sqrt{E_n[\text{MeV}]}$. From this and (3.1) one can get final equation

$$\lambda = \frac{12{,}60 \pm 2{,}40}{t - t_0} \qquad (3.3),$$

where t_0 was determined by the gamma-flash position for every event.

This dependence is shown on Figure 3.5. On the Figure 3.6 calculated correction are shown together with results of Monte-Carlo modelling of λ as a function of neutron energy. One can see, that results of the calculation for the ^{235}U resonances are in good agreement with results of the modelling.

3.2.3. Monte-Carlo Simulation of λ Distribution and Neutron Flux

Monte-Carlo simulation of the resolution function (RF) needed to obtain measurable cross-section ^{235}U, i.e. convolution of the known cross-section (from library ENDF/B-VI point-wise) and RF. This cross-section was used to obtain neutron flux on the sample on base of count rate of the ^{235}U samples in the FIC detector. In case of n_TOF difference of time-of-flight for the given energy is mostly caused by moderation in lead and water. So, it is practically more convenient to express it as a distribution of effective flight path λ (see previous paragraph) as a function of neutron energy.

This modelling was done in two stages. First, with standard codes MCNP [52] and FLUCA [53] the interaction of the protons with lead target, neutron birth and its evolution before leaving the target was simulated. These simulation needs huge amount of calculations and were done on supercomputer of section EET CERN (64 Intel Pentium 4 2.8 MHz processors) and it took about three months of calculation time. Result of simulation was 6 parameters for each neutron, leaving the target with the angle lower, than 20° to the neutron guide tube: coordinates *x* (horizontal) and *y* (vertical), ratios of the velocity components v_X/v_Z and v_Y/v_Z, energy *E* and time τ between proton burst and neutron escape from the target (Figure 3.7). Total amount of simulated neutrons was 359,541,987.

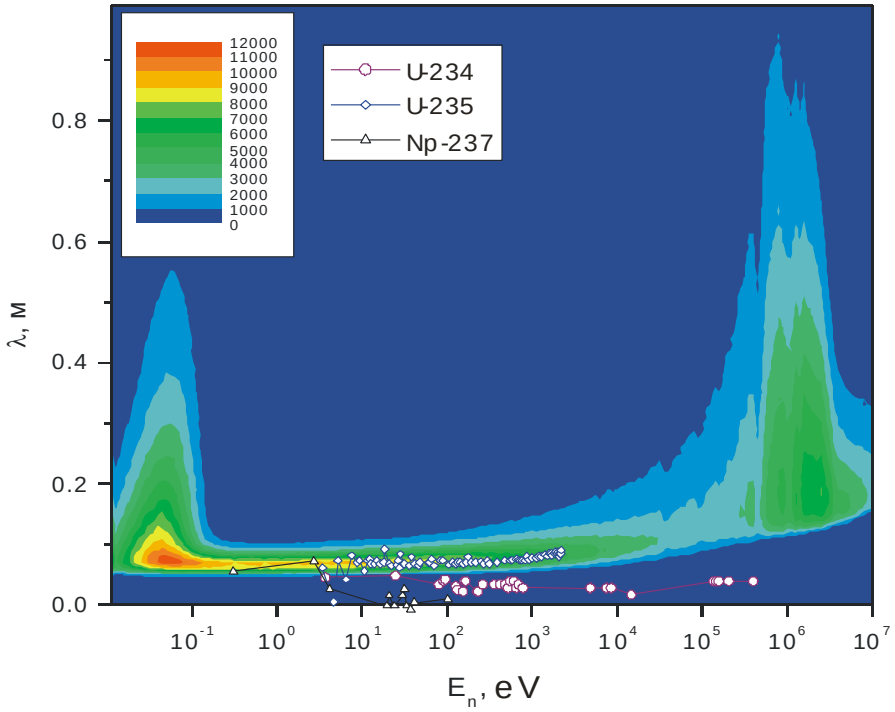

Figure 3.7. Result of the Monte-Carlo simulation and experimentally obtained λ

Direct simulation of the neutron evolution is senseless due to very small solid angle (~10^{-6} srad) in which neutrons can reach the detector. It is clear, that large enough to calculate the flux and RF number of events cannot be simulated during reasonable time.

However, taking into account that in the plane XY angular distribution of the neutrons is isotropic, one can include into simulation the neutrons, which can reach the detector after turning around the perpendicular to escape point on such an angle that velocity component $v_{\perp}$ became opposite to radius-vector **r** of escape point (see Figures 3.8 and 3.9). Since neutron guide starts directly on the surface of the target, radius-vector r can be limited to neutron guide radius which decreases the amount of calculation. Collimators and detector (with radius *d*) are also circularly symmetric. So, the task became two-dimensional.

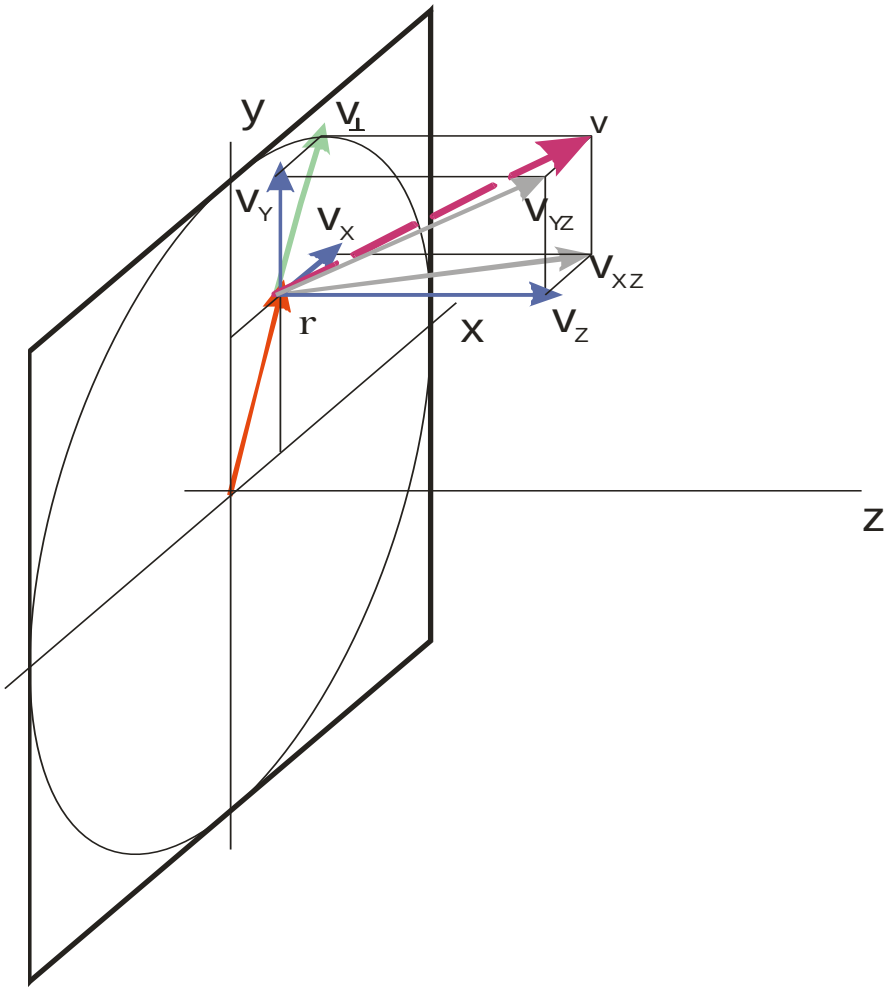

Figure 3.8. Simulation geometry

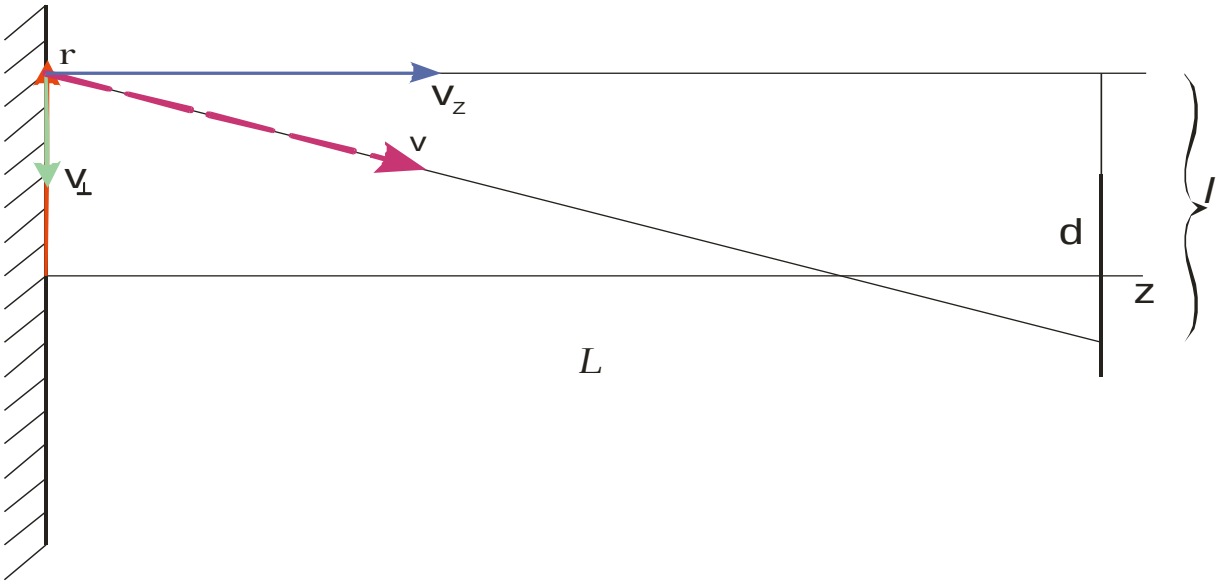

Figure 3.9. Simulation geometry after transformation

Assuming that collimators and neutron guide radius decreasing places are absolutely black one can obtain criteria for v_X/v_Z and v_Y/v_Z. for neutrons that can reach the detector.

From the Figure 3.9 it is clear that

$$\frac{v}{v_Z} = \frac{\sqrt{L^2 + l^2}}{L} \tag{3.4}$$

Substitute in (3.4) $v = \sqrt{v_X{}^2 + v_Y{}^2 + v_Z{}^2}$ and after simple math, one can obtain

$$\sqrt{\frac{v_X{}^2}{v_Z{}^2} + \frac{v_Y{}^2}{v_Z{}^2} + 1} = \frac{\sqrt{L^2 + l^2}}{L} \tag{3.5}$$

Taking into account that l can take the values in the interval $r+d \geq l \geq r–d$, where d is detector radius, and $r^2 = \sqrt{x^2 + y^2}$ one can obtain final selection criterion:

$$\frac{\sqrt{L^2 + (r-d)^2}}{L} \leq \sqrt{\left(\frac{v_X}{v_Z}\right)^2 + \left(\frac{v_Y}{v_Z}\right)^2 + 1} \leq \frac{\sqrt{L^2 + (r+d)^2}}{L} \tag{3.6}$$

Criterion (3.6) was applied to the pair of L and d for neutron guide radius change (see Figure 3.1), collimators and detector. For the histogram building contribution of each neutron was corrected on a geometrical factor connected with procedure described above (Equation 3.7).

$$w = \begin{cases} \dfrac{d^2}{(r+d)^2}, r < d \\ \dfrac{d}{2r}, r > d \end{cases} \tag{3.7}$$

Total number of simulated neutrons was 14,200,807. Measured time-of-flight t^*, measured energy $E_n{}^*$ and λ was calculated for each of them. Besides that, histograms (λ, E_n), (t^*, E_n) and (($E_n{}^*$–E_n)/E_n, E_n), neutron flux and distribution of the neutrons along the target radius were build. On the Figure 3.6 the level map of the 2-dimentional histogram (λ, E_n) together with experimental values of λ (see paragraph 3.2.2) is shown. Figure 3.10 shows the comparison of the Monte-Carlo simulation of the flux with experimental data.

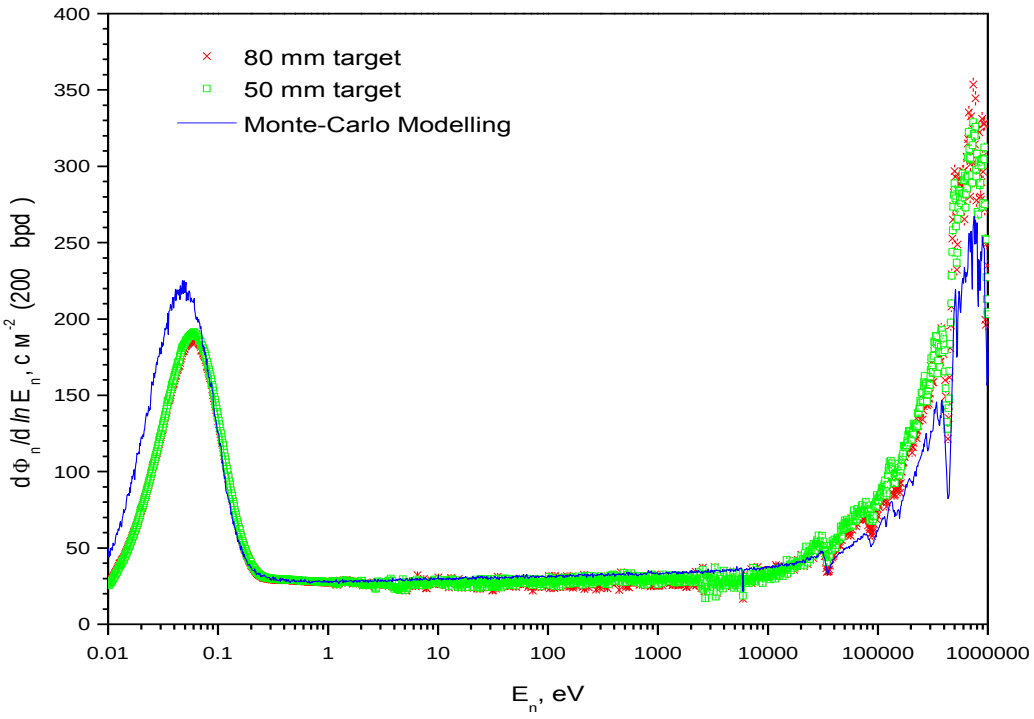

Figure 3.10. Neutron flux

3.2.4. Efficiency of Fission Fragment Registration Calculation

The signals are taken from the electrodes with deposits. Other electrodes are kept at the high voltage potential. The signal consists of three components: noise, α particle pulses and fission fragment pulses. The pulse amplitude is proportional to the energy released by the charged particle ionizing the gas. This energy, in turn, is proportional to the charged particle kinetic energy and nuclear charge.

Comprehensive study of the behaviour of the signal from heavy ionized particles in the detector was performed. It included Monte-Carlo simulation and measurements of the FADC spectra with and without neutron beam to determine all components of the signal.

Fission Fragments

The simulations started from a random generation of the emitted particles in the U_3O_8 deposit. The isotropy in the particle emission was assumed. The kinetic energy and mass of the fission fragment were randomly generated according to experimentally known distributions [36], These distributions have a dependence on the energy of the incoming neutron, however the amount of these variations is not expected to affect significantly the shape of the detector signals.

In order to study in a proper way the energy deposition of the fission fragment inside the detector, a model that calculates the complete energy loss of the particle, from its initial energy down to 0, is needed. Two approaches were considered, based on *i*) the Bethe expression, and *ii*) the use of stopping power tables.

The Bethe expression

The use of the Bethe expression for fission fragments requires some caution, because of the particular nature of the fission fragments: at sufficiently large velocities, they are completely stripped of their electrons, and the main contribution to the energy loss is due to inelastic electronic collisions, well described by the basic equation of Bethe. However, at lower velocities, the ions are partially stripped, and the energy-loss mechanism becomes more complicated due to the dependence of the effective ionic charge Z_{eff} on the velocity of the fission fragment. The Bethe expression is the following:

$$-\frac{dE}{dx}\left[MeV/(mg/cm^2)\right] = 3.072\times10^{-4}\,\frac{Z_{eff}^2}{\beta^2}\,\frac{Z_M}{A_M}\ln\left(\frac{2m_eV^2}{I}\right), \qquad (3.8)$$

where $\beta=V/c$, V is the velocity of the fission fragment, Z_M and A_M are the atomic number and mass number of the medium, m_e is the mass of the electron, I is the mean excitation energy of the atomic electrons of the medium. Z_{eff} is the effective charge and is expressed as $Z_{eff}=\gamma Z$, where γ is the effective charge parameter which has a complicated dependence on the atomic number Z and energy of the fragment. Several expressions for γ that reproduce well the data exist, see ref. [54]. We have adopted the following:

$$\gamma = 1-\left(a_0+\frac{a_1}{E}\right)\exp\left(-b_0V_R+b_1V_R^2\right),$$

where E is the fragment energy in MeV and the constants are a_0=1.005, a_1=1.296, b_0=0.988, b_1=0.218. The parameter I depends on the atomic number of the material, and according to Refs. [54-55] can be expressed by the following semi-empirical formula:

$$\frac{I}{Z} = 12+\frac{7}{Z}\,eV \qquad Z<13$$

$$\frac{I}{Z} = 9.76+58.8Z^{-1.19}eV \qquad Z\geq13.$$

For carbon and uranium more precise values have been found in Ref. [56]: I_C = 78 and I_U=890. To compute energy losses in compounds, in order to apply eq. (3.8), effective values of Z, A and I must be defined [55]:

$$Z^E = \sum_i a_i Z_i,$$
$$A^E = \sum_i a_i A_i,$$
$$\ln I^E = \sum_i \frac{a_i Z_i \ln I_i}{Z^E},$$

where a_i is the number of atoms of the ith element in the compound.

The Bethe expression has proven to reproduce correctly the experimental stopping power of fission fragments along ranges of the fission fragments up to about 2 mg/cm^2 [54], where the particle loses most of its initial energy. In fig. 2 the calculated *dE/dx* as a function of the particle range is shown. After this range, the $\beta=V/c \leq 0.025$, and many of the assumptions inherent in the Bethe-formula are no longer valid. This is a problem since it is known that ranges of fission fragments in argon and U are of approximately 4 mg/cm^2 and 10 mg/cm^2, respectively [36]. Indeed, at low velocities the logarithmic term in eq. (3.8) becomes negative, and according to this model particles of about 20 MeV do not lose any more energy. Therefore, another model needs to be used at low velocities.

Range and stopping power tables

Stopping power tables of heavy ions are available from the literature [57], or can be computed using the SRIM program. Ref. [57] contains the tabulation of range and stopping power for a large set of ions in 24 different materials.

In fig. 3 the specific energy losses for ^{98}Tc and ^{142}Nd in U and Ar calculated from the SRIM program, the Northcliffe tables and the Bethe formula are compared. These two isotopes are representative of light and heavy fission fragments, respectively. The following observation are drawn: *i*) the three curves in Ar exhibit different behaviours, the Bethe curve being clearly lower than the other two below 80 MeV. On the other hand, the Bethe formula has shown to reproduce very well the experimental data of energy loss in gases up to 2 mg/cm^2 range [54], corresponding roughly to the energy region above 40-50 MeV. *ii*) In uranium, the Northcliffe and SRIM curves have roughly the same behaviour, and differ by a constant factor, with the SRIM curve being higher by about 20%. On the contrary, the Bethe formula, especially for the heavy fission fragment, gives completely different results.

The following procedure is therefore used for the energy loss calculation:

1. In the U_3O_8 deposit, the SRIM model is adopted. A sample of 10 stopping power tables for heavy ions ranging from A=80 to A=160 in U_3O_8 and $ArCF_4$ media were calculated; for a fission fragment of a given atomic mass, the SRIM data corresponding to the closest atomic number A sampled was chosen.
2. To compute the energy loss in the gas, the Bethe formula, which has proven to reproduce well the data up to 2 mg/cm^2, is used up to this range; above 2 mg/cm^2 the SRIM model is used, scaled by 20% to match the Bethe formula, in order not to have discontinuities in the transition from one model to the other.

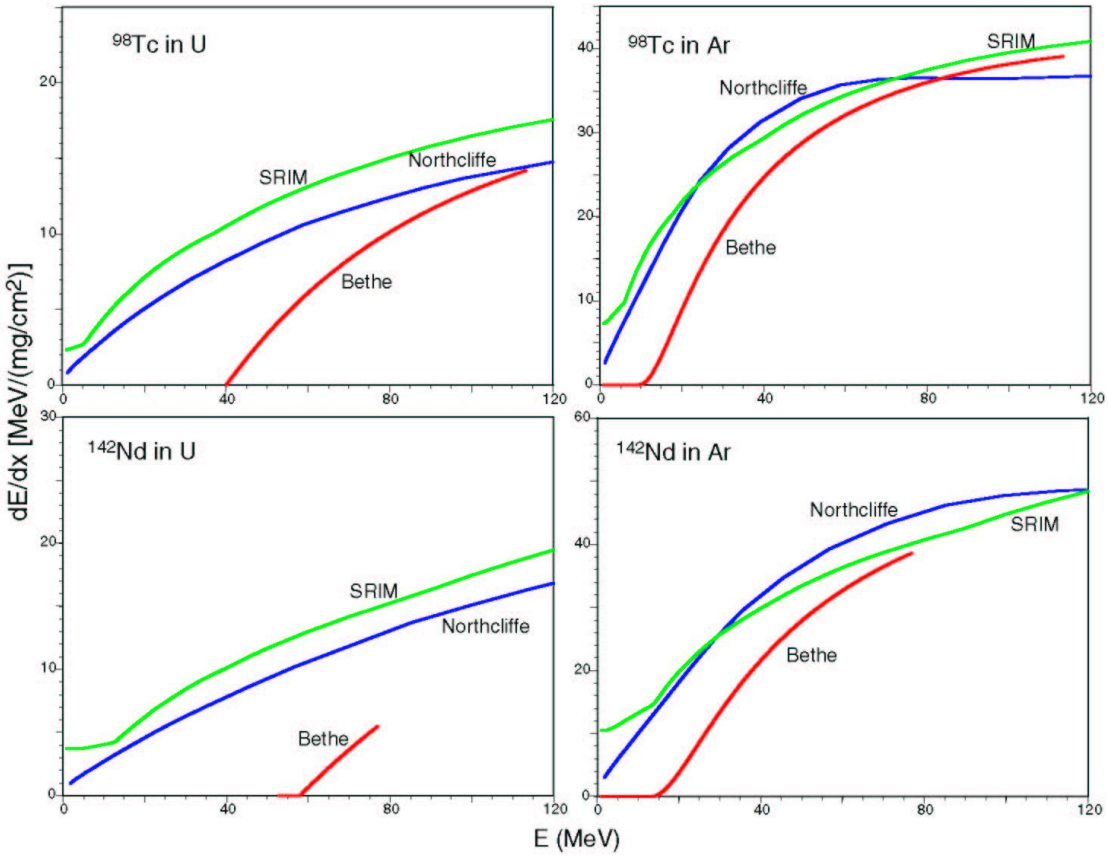

Figure 3.9. Comparison of specific energy losses as a function of the energy of ^{98}Tc and ^{142}Nd fission fragments in U and Ar media using the SRIM program, the tabulated values from [57] and the Bethe formula.

Alpha particles

As for the fission fragments, α particles were randomly generated inside the deposit. Initial energies were taken from [58]. For α particles extensive stopping power data exist from the literature [59]. The data tables calculated using SRIM were used.

In Figure 3.10 the simulated energy loss of fission fragments and α's are converted to mV and compared to the experimentally observed amplitude signal distribution. As can be seen, the overall trend of the distribution is reasonably well reproduced above 25 mV. Notable is zero energy fission fragments, i.e. fragments, which completely stopped in the target deposit due to small angle to its surface.

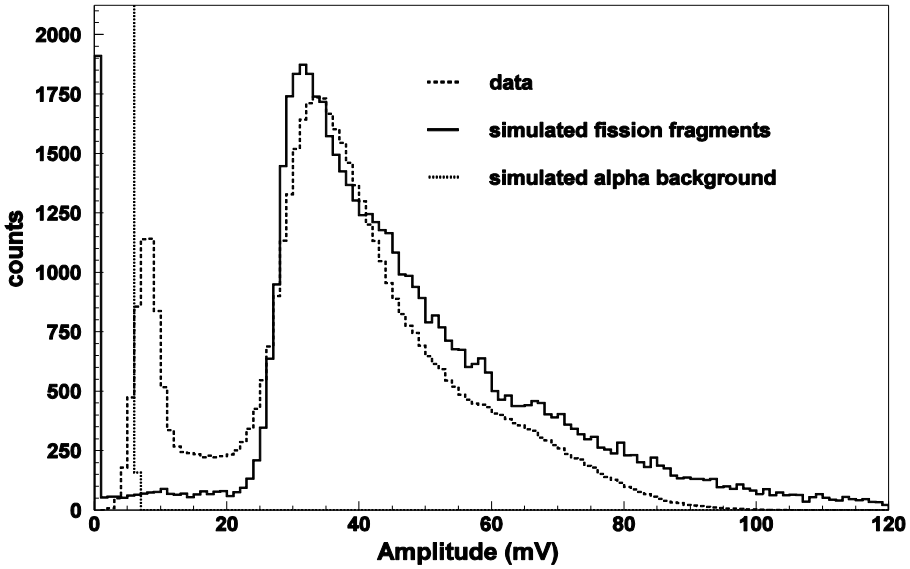

Figure 3.10. Calculated energy deposition of fission fragments and 4.5 MeV α particles from ^{235}U in the detector gas, compared with the experimental data.

Figure 3.11 shows the result of the measurements of U-234 on a neutron beam and a "background" target outside of the beam. Difference between those two spectra, normalised on sample masses, is, obviously, pure fission fragments. Different scale on the X axis on pictures 3.10 and 3.11 is due to the gain factor x10 of the preamplifiers. This procedure was done for all targets in the beam separately.

Uncertainty of the efficiency calculation directly contributes to the overall systematic error. Main component of this is the number of fission fragments which cannot leave the uranium oxide deposit (number of counts in channel No 0 on simulation, presented on Figure 3.10). Later, in turn, depends on the thickness of the deposit. Unfortunately, the technology of the layer preparation makes the targets thickness distribution non-uniform. Depending on the number of painting-baking cycles difference in thickness can be 5-10% [48]. The estimation of the average fission fragment relative losses was considered as efficiency uncertainty. If the range of the fission fragments in deposit (R) is much less than layer thickness (h), than relative loss is $\Delta\varepsilon = \frac{N_{loss}}{N} \sim \frac{h}{R}$. Average ranges of the fission fragments in U_3O_8 is about 6 mg/cm^2, thickness of ^{234}U layers is about 100 μg/cm^2, ^{235}U — 300 μg/cm^2 and ^{237}Np layers thickness is about 120 μg/cm^2 (see Table 3.2).

Efficiency of the fission fragment registration was determined from amplitude spectra, obtained from FADC data analysis (Figure 3.12). Threshold was set to 100 mV, number of fission fragments that cannot leave the target, were approximated by horizontal line, set to the average count below threshold (blue line on Figure 3.12). Efficiency is the ratio of squares under blue line and green line on Figure 3.12. Respective uncertainties are 1.7% for ^{234}U, 5% for ^{235}U and 2% for ^{237}Np.

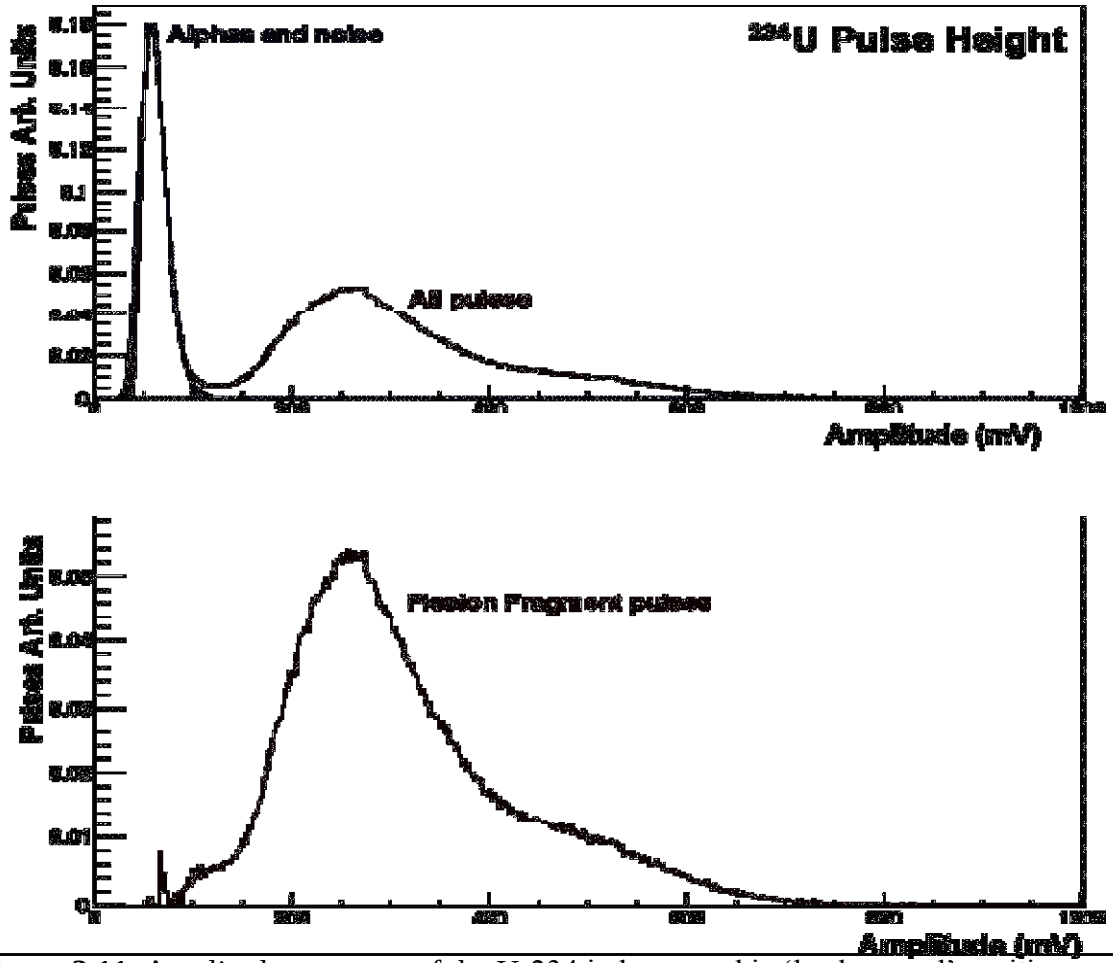

Figure 3.11. Amplitude spectrum of the U-234 in beam and in 'background' position and result of the subtraction of two spectra

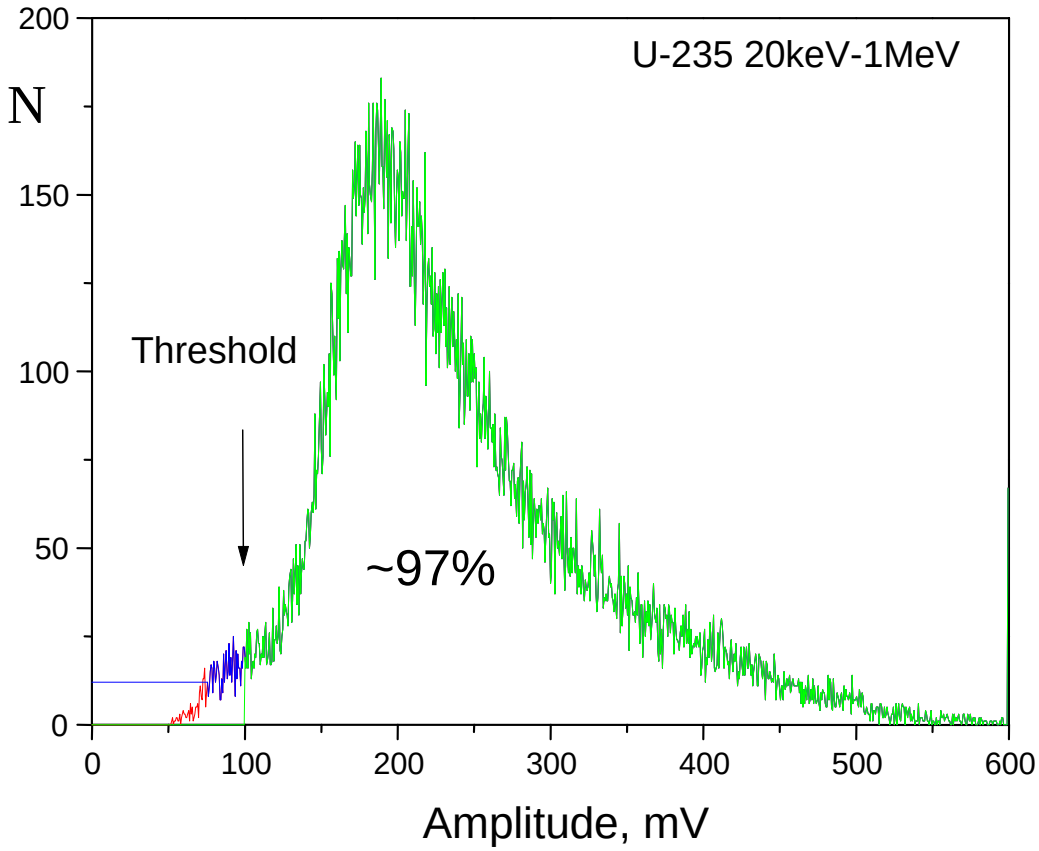

Figure 3.12. Amplitude spectrum

Results of efficiency calculation are shown in Table 3.4.

Table 3.4. Fission fragment registration efficiency.

Channel	Isotope	Mass, mg	Efficiency
1	Th-232	38.2	0.96
2	U-235	35.6	0.95
3	U-236	11.15	0.97
4	Np-237	12.82	0.97
5	U-236	10.2	0.97
6	U-238	23.3	0.96
8	U-238	25.4	0.96
9	Th-232	37.6	0.95
11	U-234	5.46	0.98
12	U-234	5.28	0.98
13	U-234	5.4	0.98
14	U-235	5	0.96
15	U-238	20	0.96
16	U-235	12.79	0.95

3.2.5. Count Rate Histogram Analysis: Corrections and Cross-sections Determination

After obtaining count rate histograms several corrections have to be introduced: background, other isotopes admixtures, neutron absorption in the electrodes, beam divergence. For the cross-section calculation neutron flux and fission fragment registration efficiency are needed.

Measurements done in 2002 (see Figure 3.32 in Section 3.4) shows that background from scattered neutrons, correlated with the beam is neglecting. So, only background from alpha-particles pile-ups was taken into account. It is constant in time and in lethargy scale can be expressed as $BG=cE^{-b^2}$. Square in parameter b is introduced for exponent index for E being always negative. Together with background contribution of another isotopes admixture was determined. In case of ^{234}U and ^{236}U most important one is ^{235}U. Even very small admixture (about 10^{-4} nuclei) gives a contribution to count rate comparable with one of isotope under investigation (Figure 3.13, red line).

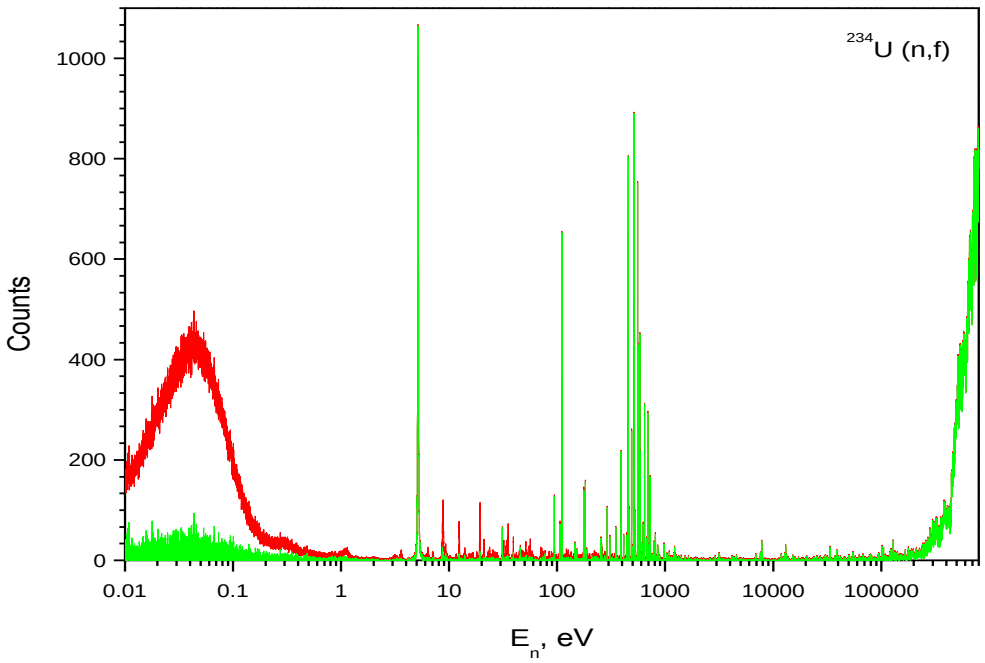

Figure 3.13. Background and ^{235}U admixture correction

Background level and ^{235}U admixture was determined by fitting by program MINUIT in the intervals where no resonances of the isotopes under investigation were, according to [18] and [35]. Fitting was done with a relation

$$N_i^{BG} = \frac{m}{m^{ref}} A \cdot N_i^{ref} + cE_i^{-b^2} \quad (3.9)$$

where: N_i^{BG} — number of BG counts in bin no i

N_i^{ref} — number of counts in the same bin of ^{235}U spectrum

m^{ref} — mass of the ^{235}U sample

m — mass of the investigated sample

This procedure was done separately for each target. Result is shown on Figure 3.10, green line.

The uncertainty of the background determination was calculated as follows. Despite the program MINUIT calculate errors (one standard deviation) for each of the parameters *A*, *b*, *c*, it is practically more convenient, due to complication of the function (3.9) to calculate its value with parameters on one standard deviation higher (or lower) obtained values. Half of the difference between those values can be used as an estimation of the BG level uncertainty. Since parameter A is very small (about 10^{-4}), its uncertainty is neglecting. So,

$$\Delta N_i^{BG} = \frac{1}{2}\frac{m}{m^{ref}}\left((A+\Delta A)\cdot N_i^{ref} + (c+\Delta c)E_i^{-(b+\Delta b)^2} - (A-\Delta A)\cdot N_i^{ref} + (c-\Delta c)E_i^{-(b-\Delta b)^2}\right) \quad (3.10)$$

Neutron flux Φ_i was determined from the ^{235}U reference target count rate:

$$\Phi_i = \frac{N_i^{ref}}{\varepsilon \cdot \sigma_{(n,f)}^{ref}(E_i)} \quad (3.11)$$

where ε — efficiency of the ^{235}U fission fragment registration, $\sigma_{(n,f)}^{ref}(E_i)$ — convolution of the recommended cross-section and RF obtained from Monte-Carlo simulation.

Uncertainty of the recommended cross-section was taken from estimation given in ENDF-B/VI library and shown in Table 3.3. Since convolution with RF changes the cross-section behaviour less than on 5%, its uncertainty is neglecting.

Table 3.3. Estimated uncertainties of the ^{235}U fission cross-section.

Energy (keV)	Uncertainty estimation (%)
2.53E-05	0.2
150-600	1.5
600-1000	1.6
1000-3000	1.8
3000-6000	2.3
6000-10000	2.2
10000-12000	1.8
12000-14000	1.2
14000-14500	0.8
14500-15000	1.5
15000-16000	2.0
16000-17000	2.5
17000-19000	3.0
19000-20000	4.0

Finally, neutron flux uncertainty is:

$$\Delta\Phi_i = \Phi_i \sqrt{\frac{1}{N_i^{ref}} + \left(\Delta\sigma_{(n,f)}^{ref}(E_i)\right)^2 + \Delta\varepsilon^2} \qquad (3.12)$$

Efficiency of the fission fragment registration and its uncertainty is shown in Table 3.4.

Distance between first and last targets in chamber was 180 mm, so the neutron flux on the different targets differs a little bit due to absorption of neutrons in Aluminium electrodes and target support. This absorption is not neglecting only in the areas of strong Al resonances at 35 keV, 90 keV and 137 keV (see Figure 3.14).

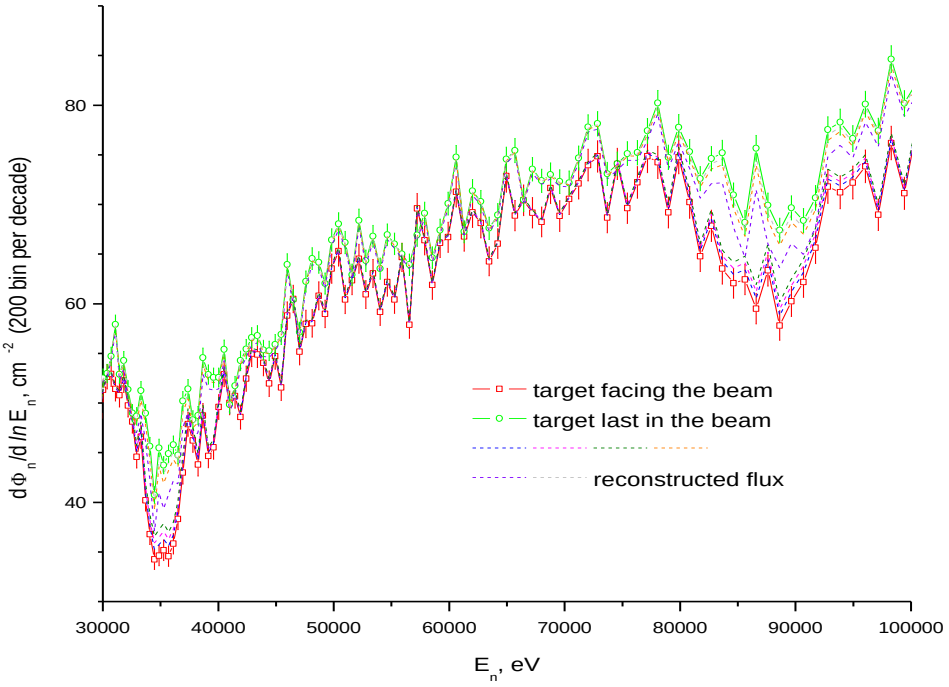

Figure 3.14. Neutron flux on the different targets

The first and the last targets was ^{235}U targets (Figure 3.2).

Flux on intermediate targets was calculated as $\Phi^* = \frac{\Phi}{\exp(-n\sigma_{tot}^{Al})}$, where n — number of Aluminium nuclei in between the layers, Φ — flux on the first target (Figure 3.14). Uncertainty of the total cross-section of Aluminium is few per cent and the correction introduced is also on the level of per cents, so, uncertainty of the correction is negligible.

Thus, final cross-section is:

$$\sigma_f = \frac{\varepsilon \cdot N \cdot M}{\Phi^* \cdot m \cdot N_A}, \tag{3.13}$$

where: ε — fission fragment registration efficiency,

N — number of counts,

Φ^* — flux through the target during the measurements,

m — target mass,

M — molar mass of the target nuclei,

N_A=6,02·10^{23} mol^{-1} — Avogadro number.

As one can see from the description of the FIC and from Equations 3.11 and 3.12, the measurements of the standard (to determine the neutron flux) and isotopes under investigation were done in exactly the same conditions, thus cancelling out most of the systematical errors.

The remaining sources of the systematical errors are determination of sample mass and fission fragment registration efficiency, which are described above. Overall systematical error for all of the isotopes is about 7%.

3.3. Results and discussion

3.3.1. ^{234}U fission cross-section

Figure 3.15 shows ^{234}U fission cross-section in all energy range achieved during the measurements. It is clearly seen that in the interval where data from FADC and TDC are overlapping, the results is quite consistent.

Figures 3.15 to 3.23 shows comparison of the obtained energy dependence of the ^{234}U cross-section (dots) and recommended data from ENDF-B/VII library (blue line). In the energy range below 1.5 keV or data is coincide with evaluated data. Data shown on Figure 3.24 confirms the data of [20] for the 780 eV resonance. For the energies where resolution of n_TOF source is higher than one for all previous measurements, our cross-section demonstrate the structure which is connected with second and, probably, third well in the fission barrier. On the barrier our cross-section demonstrates pronounced structure, which is connected with vibration resonances and third well.

The most pronounced structures attributed to vibration resonance, are ones around 310 keV (Figures 3.21 and 3.24) and 540 keV (Figure 3.22 and 3.25).

In the vibration resonance structure around 310 keV seven resonance-like structures are clearly seen. Average distance between them is about 10 keV, while, according to [13], average distance between class-II levels should be about 1 keV. In the meantime, this structure is similar to one in [18], while our data shows better resolution (Figure 3.24). Same situation can be observed around 540 eV. There are 12 resonance-like structures with average distance

between them about 5 keV (Figure 3.25). Again, the structure is similar with [18] but with better resolution.

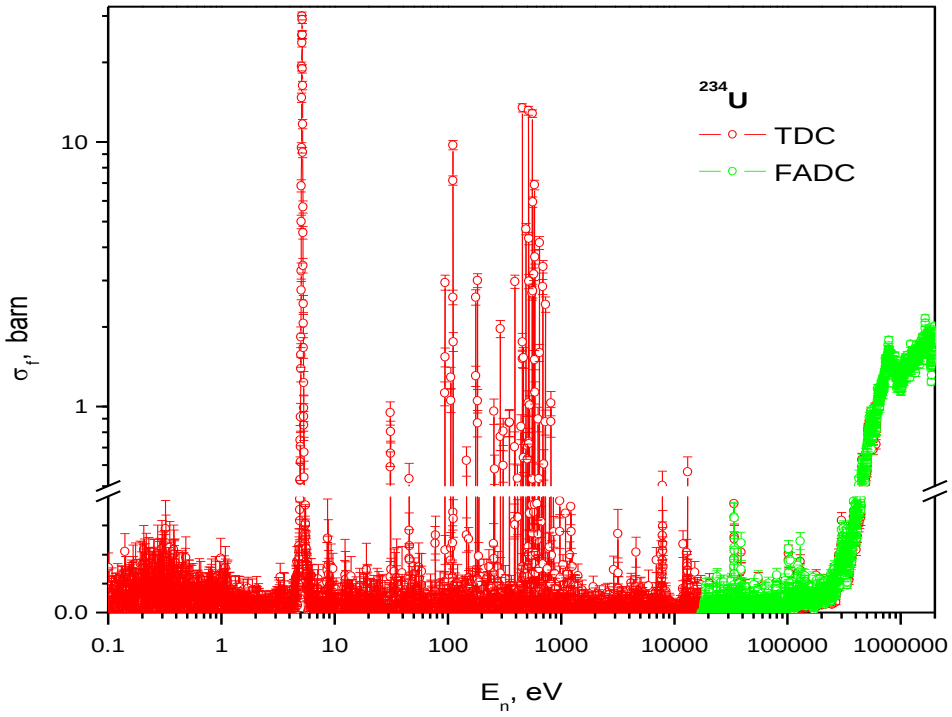

Figure 3.15. ^{234}U Fission cross-section

To explain the effect, same analysis as in [18] was used. The procedure, described below, give the possibility to model observed period of the resonance structures taking into account structure of the cross-section and experimental resolution. The cross-section was calculated from the fission width of class-I and class-II levels taking into account intermediate coupling between them [13]:

$$\Gamma_{vib(f)} = \frac{D_{vib}}{2\pi\left[1+\exp\left(2\pi(V_B - E_{vib})/\hbar\omega_B\right)\right]} \tag{3.14}$$

$$\Gamma_{II(f)} = \frac{D_{II}\cdot W\cdot\Gamma_{vib(f)}}{2\pi\left[(E_{II}-E_{vib})^2 + \frac{1}{4}(W+\Gamma_{vib(f)})^2\right]} \tag{3.15}$$

$$\Gamma_{II(c)} = \frac{D_{II}}{2\pi\left[1+\exp\left(2\pi(V_A - E_{vib})/\hbar\omega_A\right)\right]} \tag{3.16}$$

$$\Gamma_{I(f)} = \frac{D_I\cdot\Gamma_{II(c)}\cdot\Gamma_{II(f)}}{2\pi\left[(E_{II}-E_I)^2 + \frac{1}{4}(\Gamma_{II(c)}+\Gamma_{II(f)})^2\right]} \tag{3.17}$$

$$\left\langle \sigma_f \right\rangle = \sum_J \frac{2\pi^2 \lambda^2 g \left\langle \Gamma_n \right\rangle \left\langle \Gamma_{I(f)} \right\rangle F}{D_I \left\langle \Gamma_n + \Gamma_{I(f)} + \Gamma_\gamma + \sum \Gamma_{n'} \right\rangle} \tag{3.18}$$

Where V_A и V_B – heights of intermediate and outer potential barriers above neutron binding energy (B_n = 5,31 MeV for ^{234}U); E_{vib}, $\Gamma_{vib(f)}$ and D_{vib} – resonance energy, fission width and distance between levels for vibration resonance; E_{II}, $\Gamma_{II(f)}$ and D_{II} – resonance energy, fission width and distance between class-II levels; W – damping width of vibration level with class-II levels ; E_I, $\Gamma_{I(f)}$ and D_I – resonance energy, fission width and distance between class-II level; $\Gamma_{II(c)}$ – coupling width between class-I and class-II levels; $2\pi\lambda$ – neutron wavelength; g – spin factor; Γ_n and Γ_γ – neutron and fission widths of class-I levels; $\Gamma_{n'}$ – inelastic scattering neutron withs for levels above 310 keV; F – fluctuation factor ($<\Gamma_n \Gamma_f / \Gamma><\Gamma>/<\Gamma_n><\Gamma_f>$)[13, 18].

All these parameters were taken from [13], except for potential barrier heights (from [18]) and damping width, which was obtained from our experimental data and was ~48 keV and ~54 keV for 310 keV and 540 keV levels, respectively.

In the energy interval containing vibration resonance, class-II levels were equidistantly set and their fission widths were randomly chosen according to Porter-Thomas distribution. Fission cross-section, obtained according to equations 3.14–3.18, is shown on figure 3.27. Convolution of this cross-section with experimental resolution produces a structure shown on Figure 3.28. The period of the obtained structure is close to experimental one.

The detailed calculations for 310 keV resonance performed using MathCAD are shown in Appendix III.

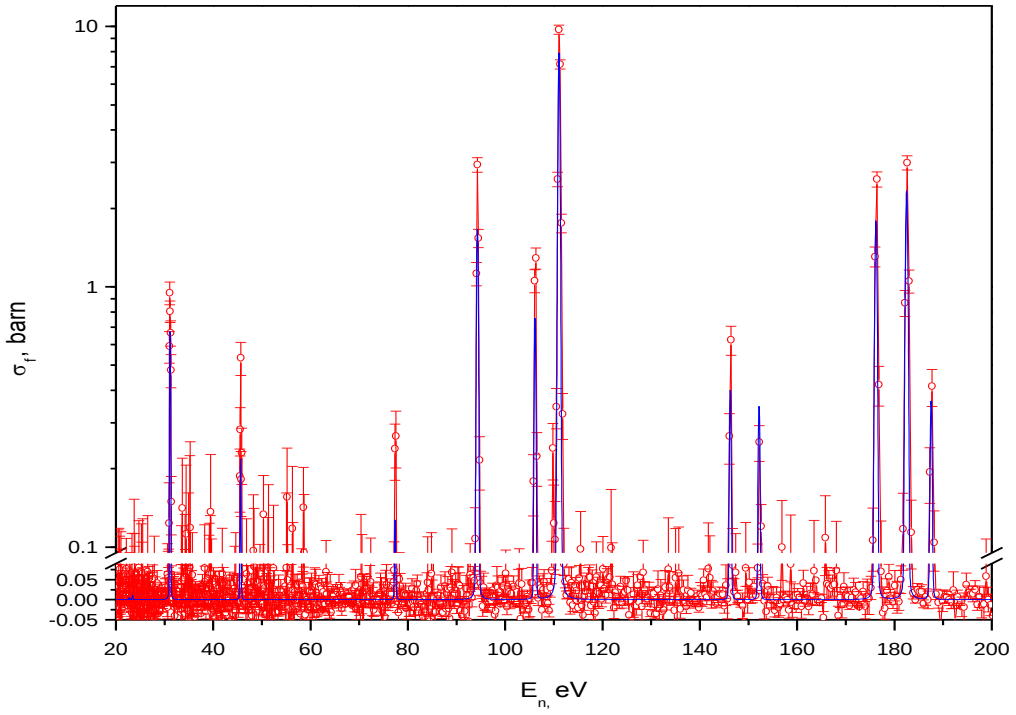

Figure 3.16. Comparison of obtained ^{234}U fission cross-section with data from ENDF-B/VII

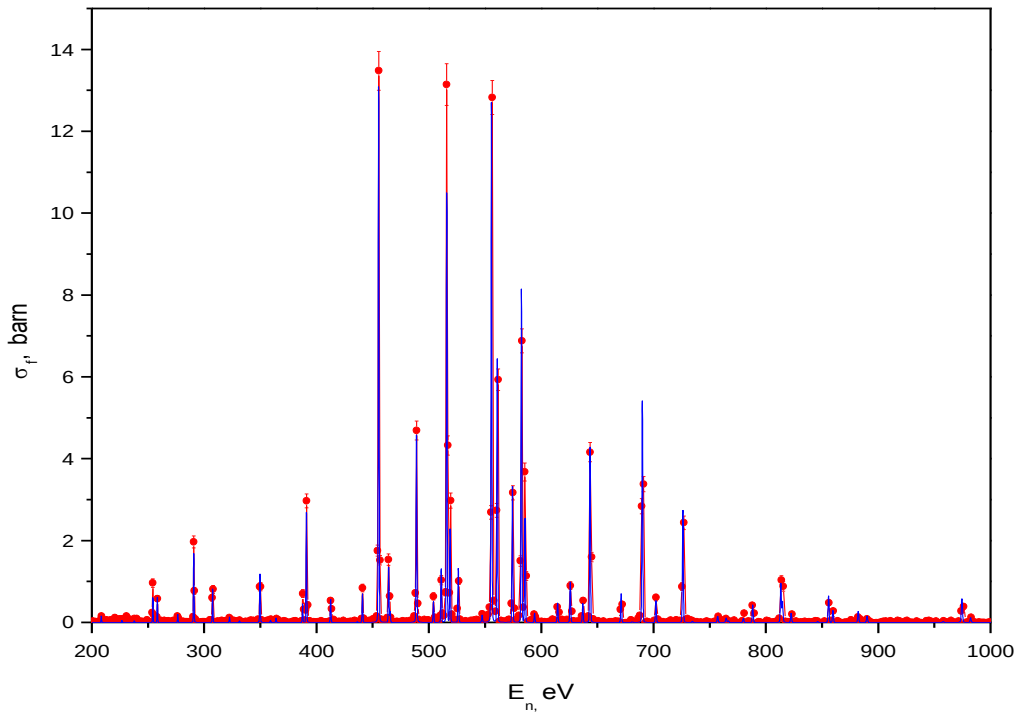

Figure 3.17. Comparison of obtained ^{234}U fission cross-section with data from ENDF-B/VI

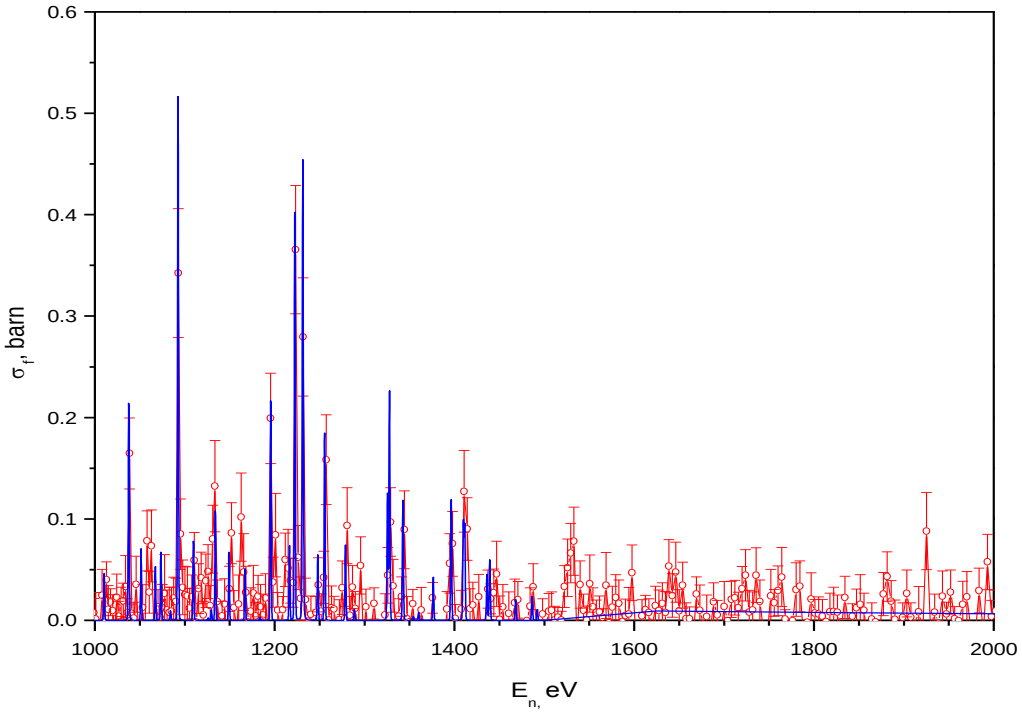

Figure 3.18. Comparison of obtained ^{234}U fission cross-section with data from ENDF-B/VII

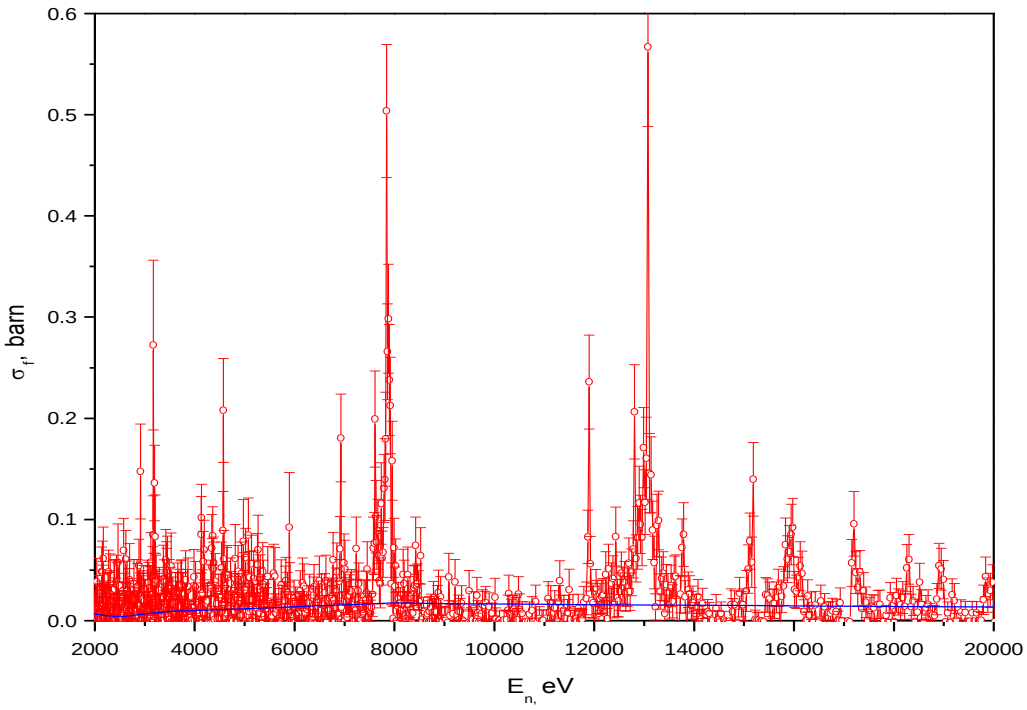

Figure 3.19. Comparison of obtained ^{234}U fission cross-section with data from ENDF-B/VII

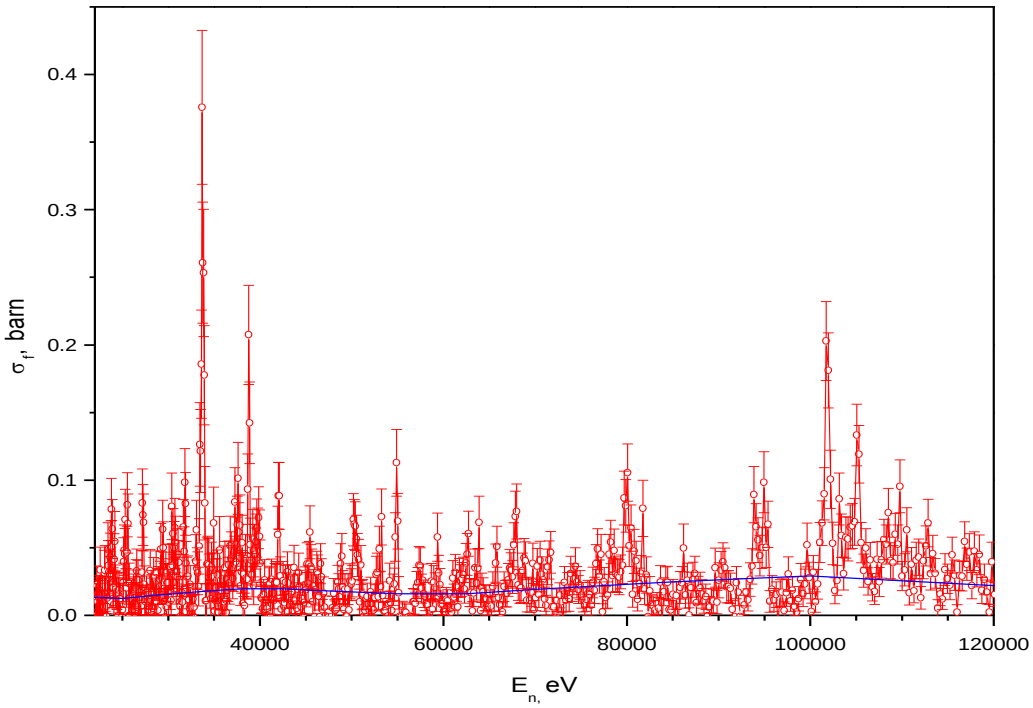

Figure 3.20. Comparison of obtained ^{234}U fission cross-section with data from ENDF-B/VII

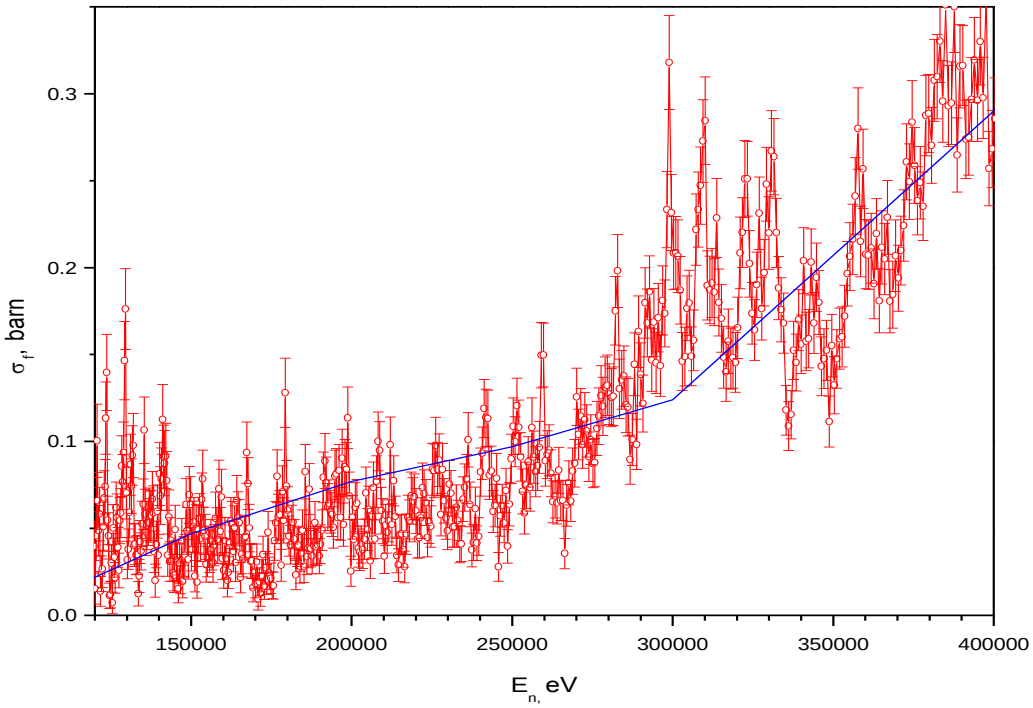

Figure 3.21. Comparison of obtained ^{234}U fission cross-section with data from ENDF-B/VII

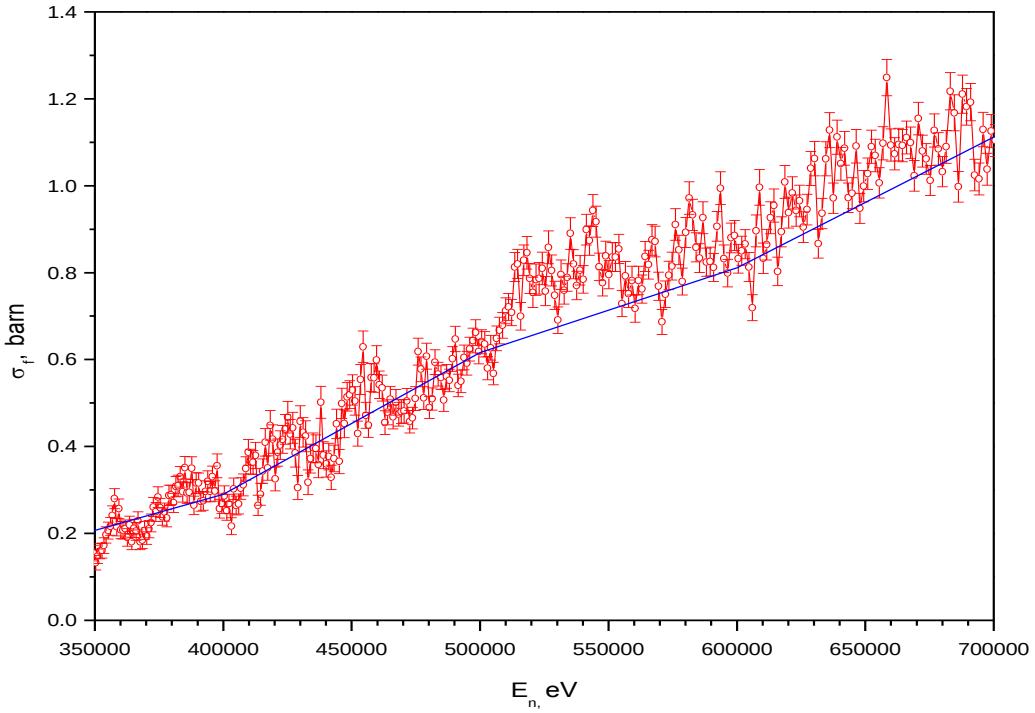

Figure 3.22. Comparison of obtained ^{234}U fission cross-section with data from ENDF-B/VII

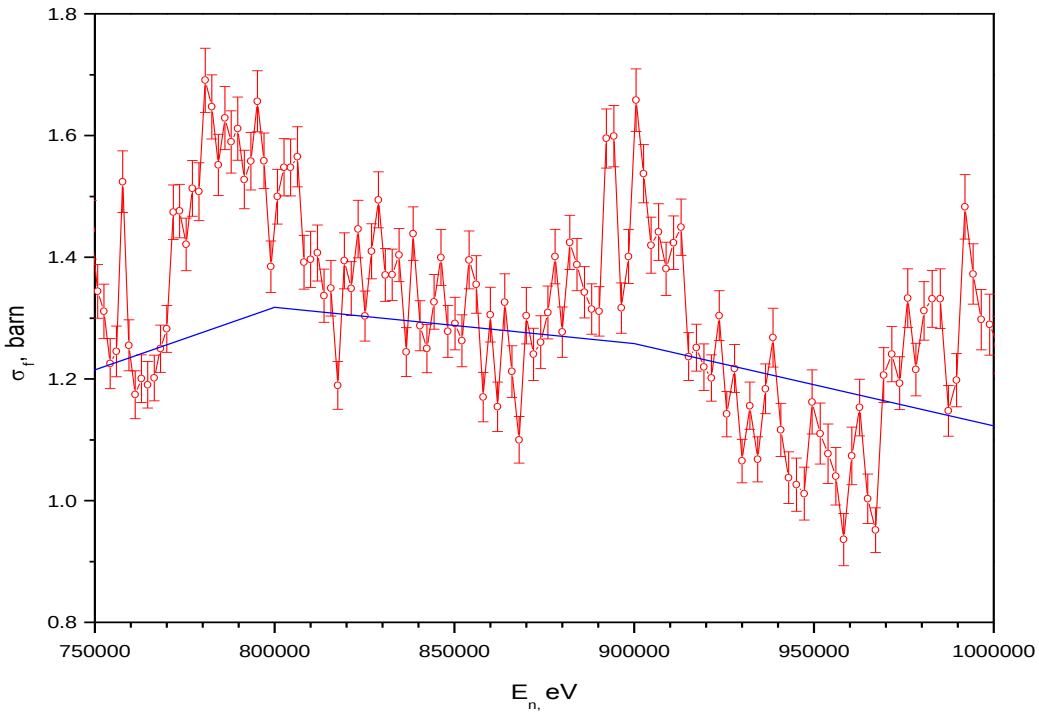

Figure 3.23. Comparison of obtained ^{234}U fission cross-section with data from ENDF-B/VII

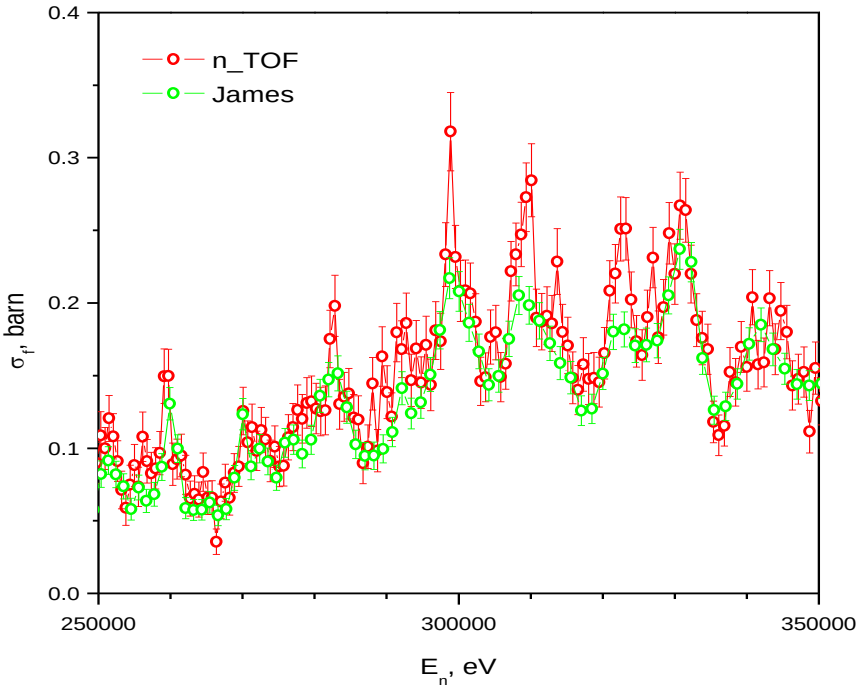

Figure 3.24. Vibration resonance with E_{vib}=310 keV. Data from current work (red) and from [18] (green)

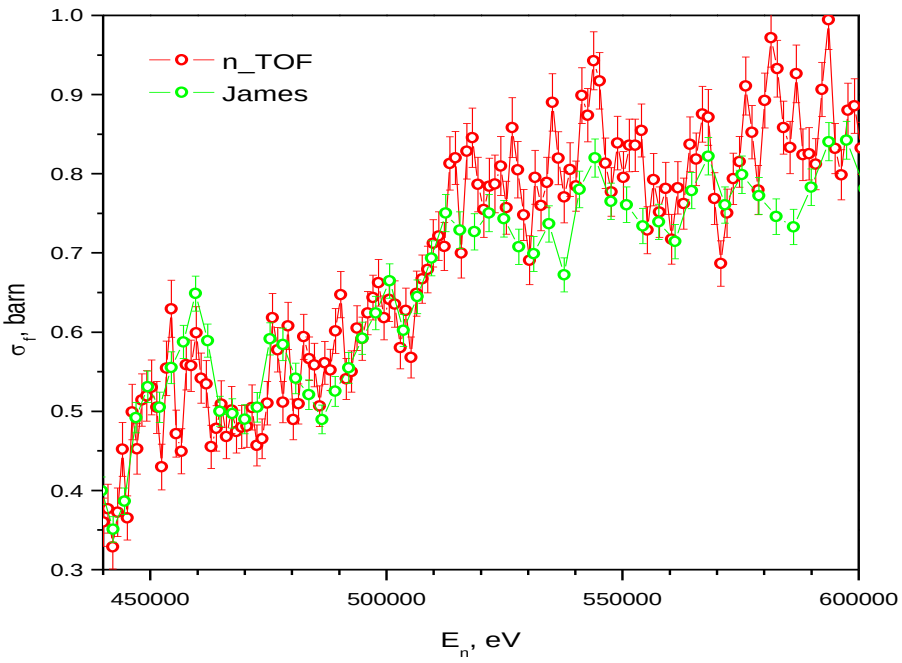

Figure 3.25. Vibration resonance with E_{vib}=540 keV. Data from current work (red) and from [18] (green)

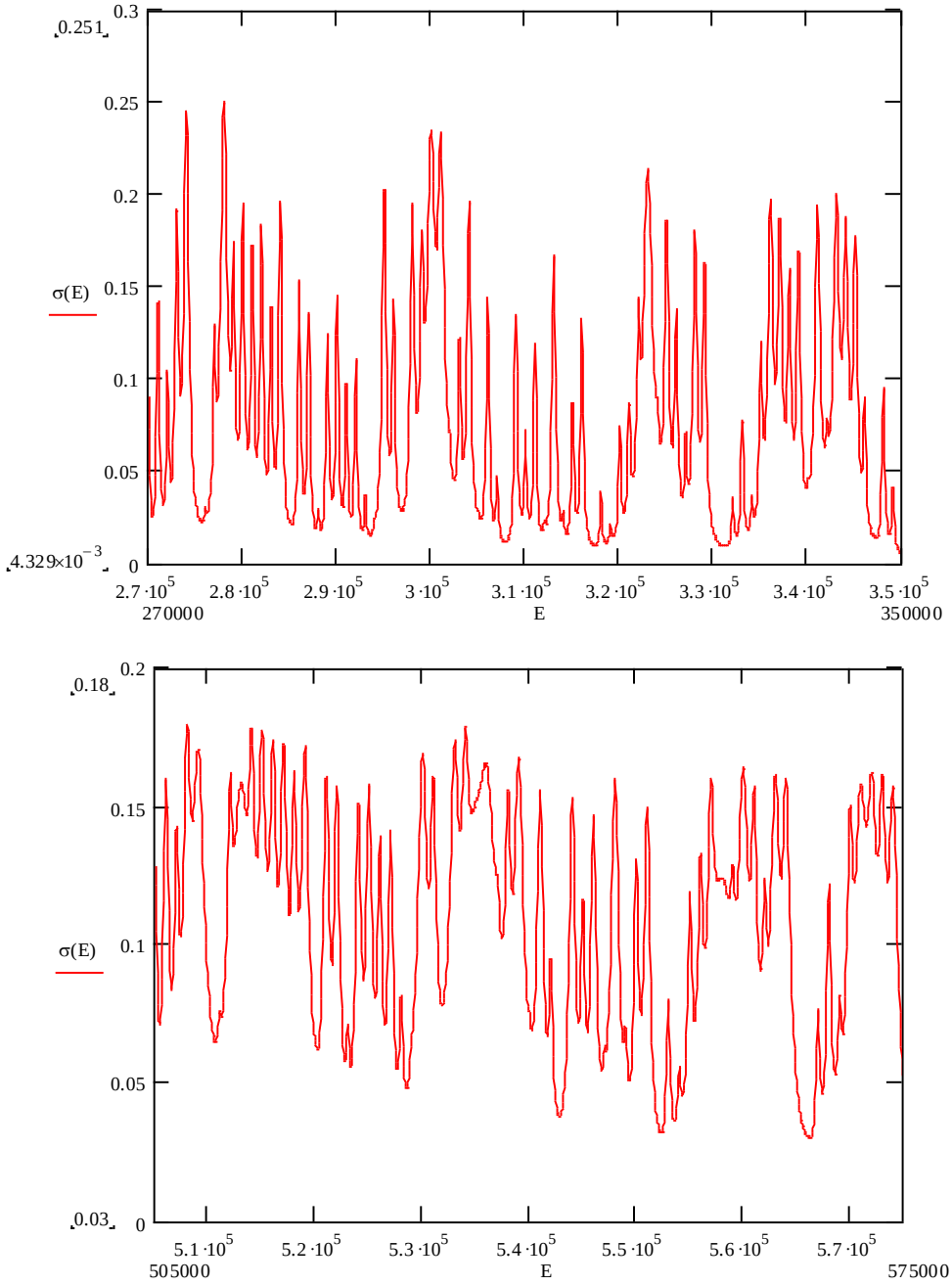

Figure 3.26. Simulated cross-section in vicinity of vibration resonances with E_{vib}=310 keV (top) and E_{vib}=540 eV (bottom)

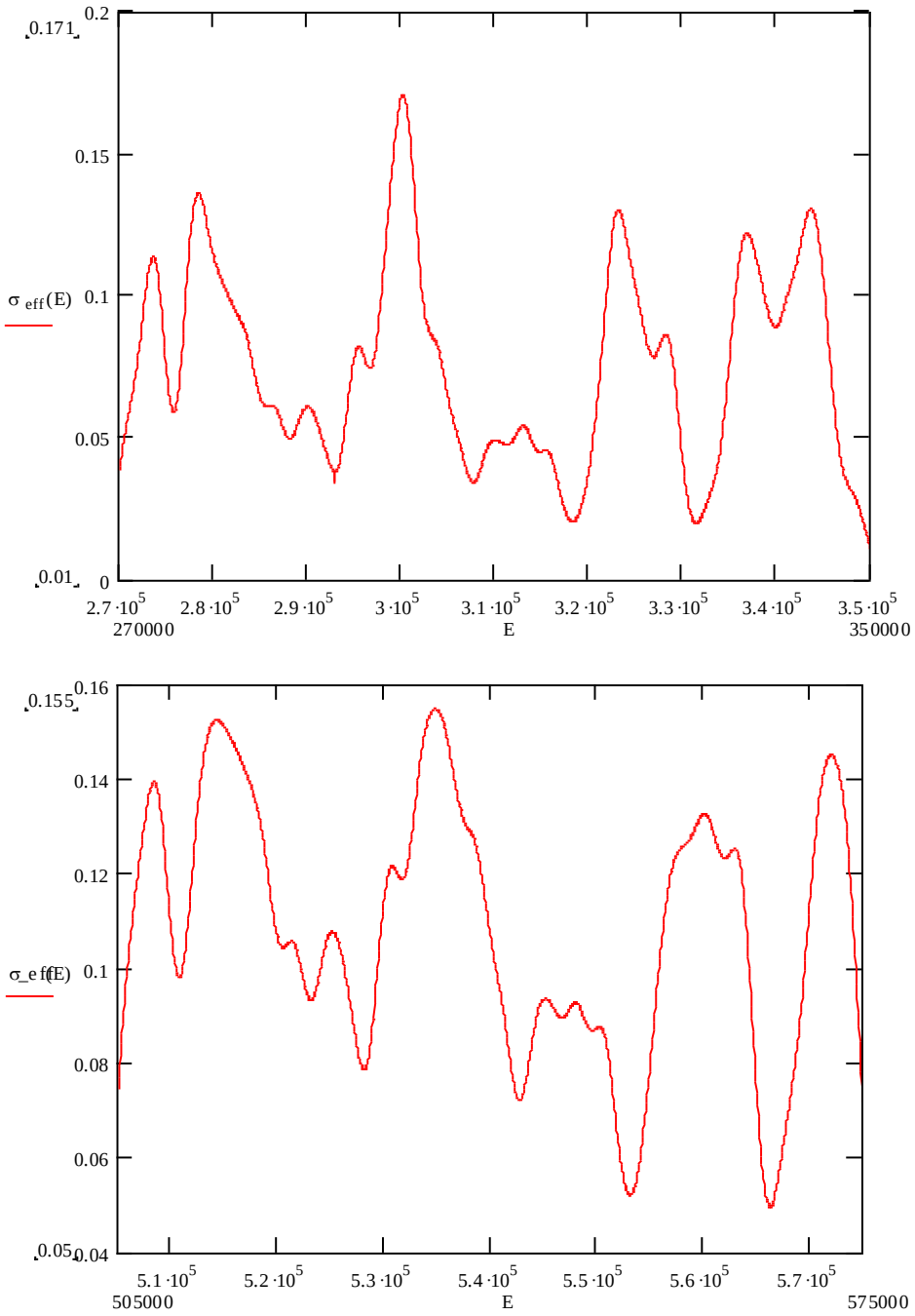

Figure 3.27. Simulated cross-section corrected on experimental resolution in vicinity of vibration resonances with E_{vib}=310 keV (top) and E_{vib}=540 eV (bottom)

3.3.2. ^{237}Np fission cross-section

The procedure to obtain fission cross-section of ^{237}Np is the same as described in Section 3.2. The results of the measurements were published in [60] and [61].

Figure 3.28 shows the obtained fission cross-section of ^{237}Np and Figure 3.29 — comparison of the cross-section with recommended values and previous experimental data. In the vicinity of the first cluster (39 eV) our cross-section is about 3 times higher, than evaluated one. That confirms data of [7] and results, obtained in Dubna [62]. Picture 3.30 shows the

comparison of the obtained data with earlier experiments and evaluation for neptunium in the fast neutrons region. One can see systematical deviation of present data from ENDF/B-VI for energies higher than 450 keV. Obviously, all TOF experiments show higher cross-section than it is expected from evaluation. Discrepancy is about 6-7%.

Comparison with newer library, ENDF/B-VII, is discussed in Chapter 4.

In the energy region from 200 eV to 1 keV, where resolution of the n_TOF measurements is significantly higher, than in all previous measurements, one can see fine structure of the resonances, attributed to second well levels. The distance between resonance clusters of 4-7 resonances is about 80 eV, which corresponds to the distance between Class-II levels for ^{237}Np (Figure 3.31).

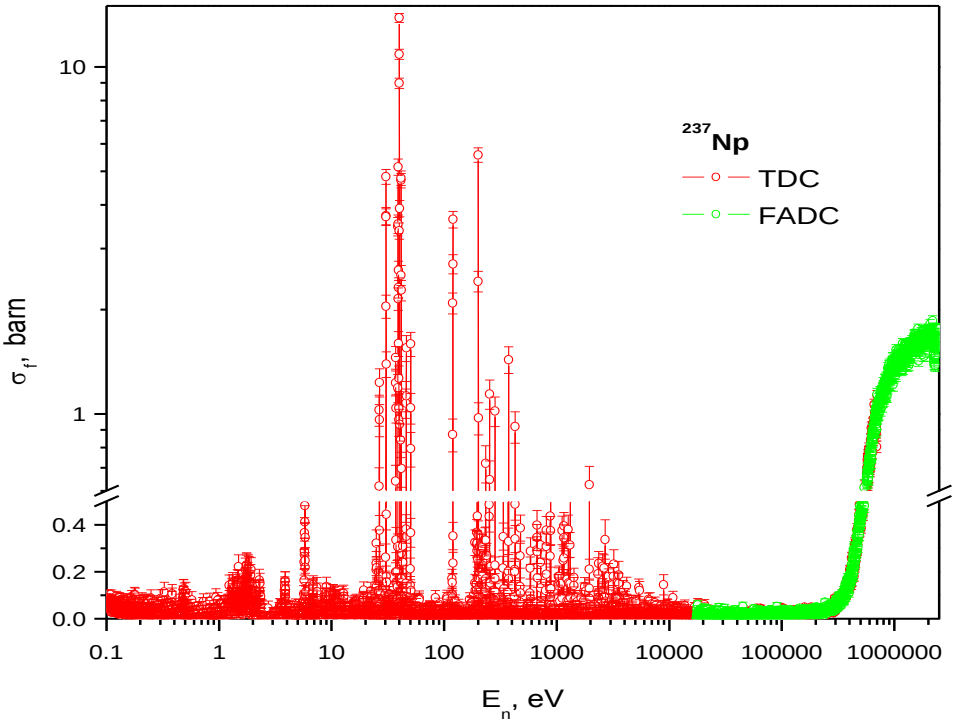

Figure 3.28. ^{237}Np fission cross-section

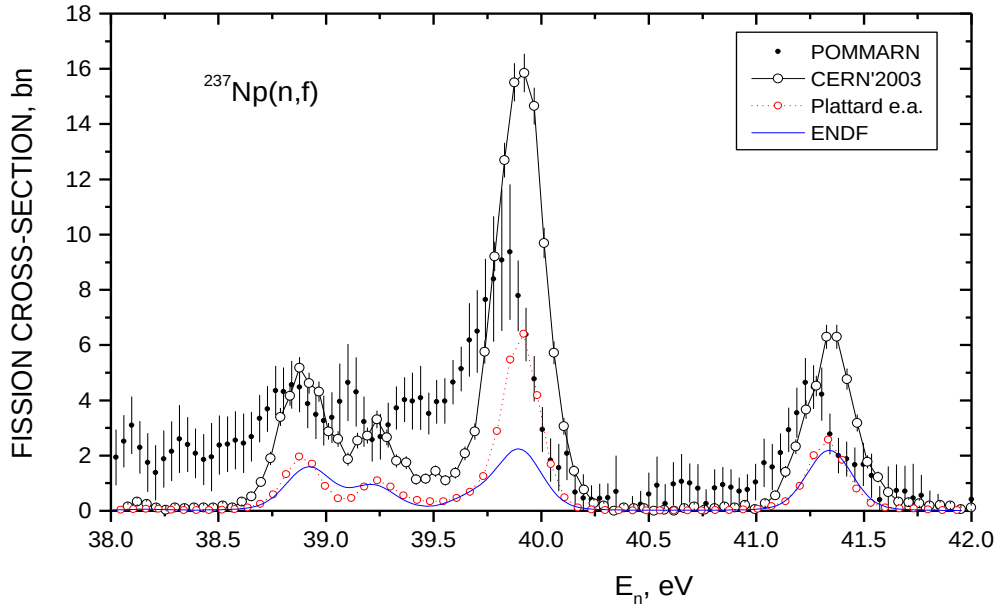

Figure 3.29. Comparison of obtained ^{237}Np fission cross-section (black circles and solid line) with experimental data [63] (black triangles) and [64] (red circles and dotted line) and data from ENDF-B/VI in the region of first resonance cluster

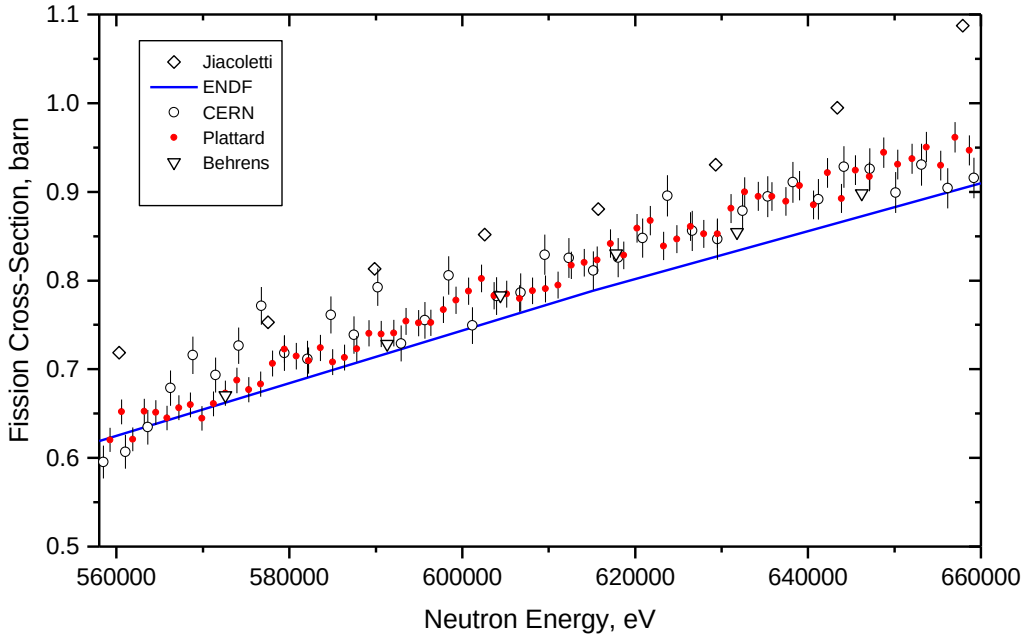

Figure 3.30. Comparison of obtained ^{237}Np fission cross-section with experimental data and data from ENDF-B/VI in the fast energy region

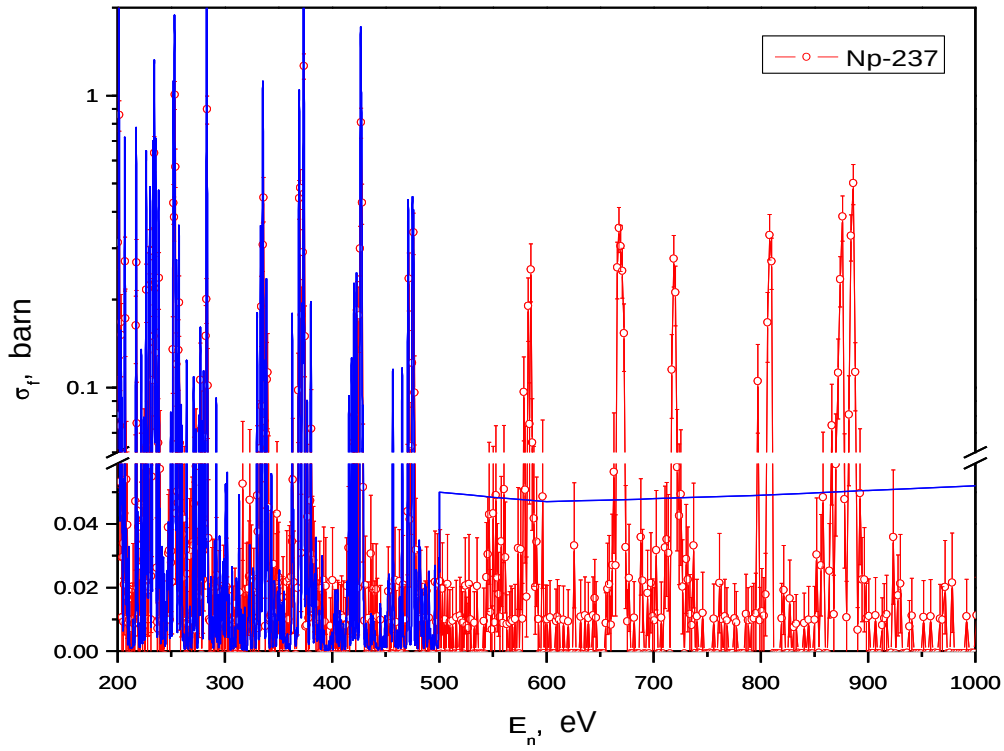

Figure 3.31. Comparison of obtained ^{237}Np fission cross-section with data from ENDF-B/VII

3.4. Measurements of the Thermal Cross-section of ^{234}U on n_TOF Neutron Source

Measurements were done with same FIC detector. There is also another stack of electrodes (3 targets of ^{234}U, ^{235}U and ^{238}U and 4 electrodes) mounted perpendicularly to the previous one, that could be equipped with reference isotopes to evaluate the background produced by scattered neutrons. The ^{234}U, samples installed in the beam has the mass 37±1 mg, in the background position 5.41±0.16 mg. These samples have an admixture of the ^{235}U on the level $C^{U\text{-}235}$=(0.3159±0.0052)% of the mass. The ^{235}U sample with a same diameter was also installed into the beam to be used as the reference. The mass of this sample is (5.06±0.05) mg with ^{235}U isotope content— (99.9±0.05) %

To check the background conditions additional set of measurements with black filters (Ag, Al, Mo, W) in the beam. One could see from the spectra obtained (Figure 3.32) that the background, caused by scattered neutrons in the area is negligible.

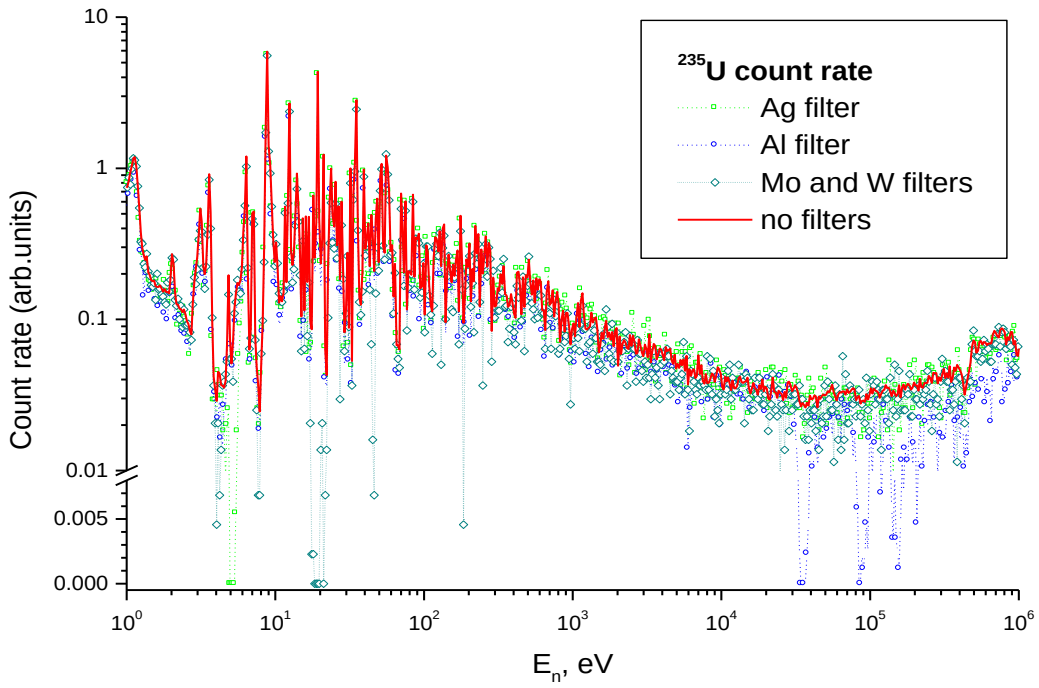

Figure 3.32. Background measurements with black filters

After normalizing of all the spectra on the samples masses the count rate of the fission events of ^{234}U sample could be calculated as seen on the Figure 3.33.

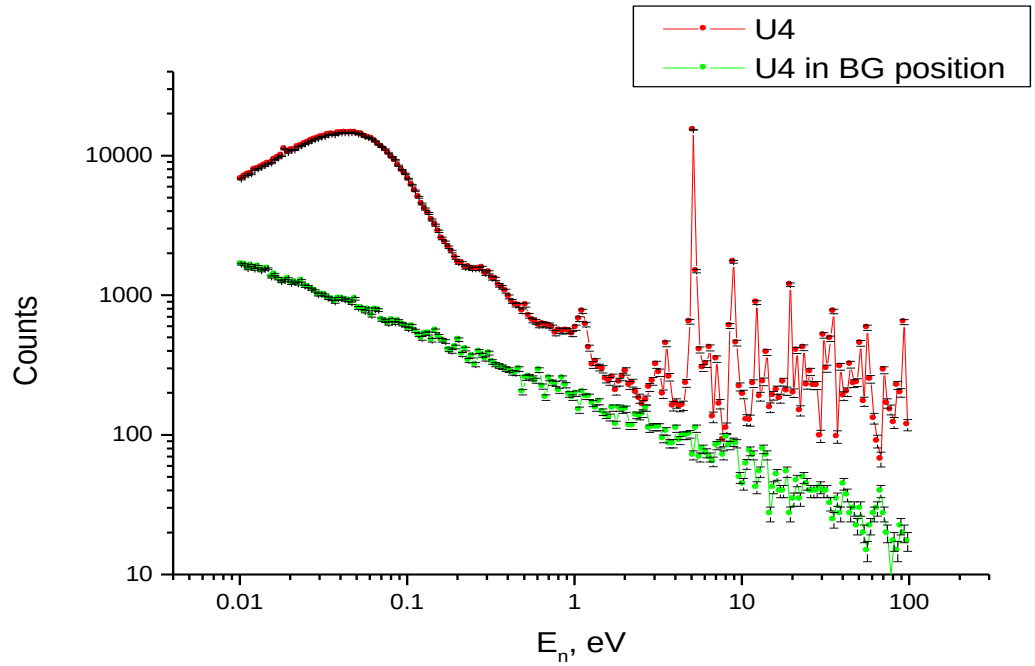

Figure 3.33. TOF spectrum of ^{234}U fissions and BG spectrum

Procedure of cross-section calculation was the same as in paragraph 2.2.2.

One can calculate ^{235}U admixture using TOF spectra. Obtained value, (0.36±0.03)%, are in good agreement with mass-spectrometry data.

The finally obtained cross-section together with results from [30–31] is presented on the Figure 4.6 in the Chapter 4.

The interpolated value σ_f^{th}=197±18 mbarn are in good agreement with previous data obtained by TOF technique. All these data gives average value σ_f^{th}=196±10 mbarn.

The results of this measurement together with ones described in Paragraphs 2.2.2.and 2.2.3 are discussed in the Final Chapter.

Chapter 4. Results and Conclusions

The Dissertation present the results of measurements of the fission cross-section of ^{234}U in the energy range from thermal to 1 MeV, ^{237}Np and ^{243}Am in the resonance region. The data of ^{234}U are recommended by IAEA [5] as a first priority needs for transmutation problem.

The current work summarizes more, than 10 years of the experiments, performed on the pulsed neutron sources IBR-2 and IBR-30 of Frank Laboratory of Neutron Physics of the Joint Institute for Nuclear Research (FLNP JINR) in Dubna, Russia; "Fakel" of RSC "Kurchatov's Institute" and n_TOF of CERN. The TOF technique was used for neutron energy spectrometry and various kinds of detectors (mostly ionization chambers) to mark the fission events.

The independent measurements of the same isotopes done on different neutron sources and sometimes with different techniques gives strong, self-consistent set of data.

Below the results obtained for each measured isotope is discussed.

4.1. Fission Cross-section of ^{237}Np

Several measurements of the fission cross section of ^{237}Np have been made previously, below and above threshold. However, the quality of the data is not always acceptable, in accuracy as well as concerning the energy range covered. In particular, in the sub-threshold resonance energy region, ^{237}Np has a small fission cross section which is important for transmutation studies in Pb or Pb-Bi cooled systems, where the epithermal neutron flux is not negligible in the periphery of the fuel core, and where some proposal to perform heterogeneous transmutation of minor actinides has been made. Recent measurements by Yamanaka *et al*. [7] carried out at the Kyoto University Lead Slowing-down Spectrometer (KULS) and used in JENDL-3.2 are a factor of three higher than those measured by Plattard *et al*. [8] on which the ENDF/B-VI evaluated file is based. There was also the measurements done in Dubna [53] using the same technique, as described in paragraph 2.1.1 (Chapter 2). The cross-section obtained in these measurements was about three times higher, than ENDF/B-VI.

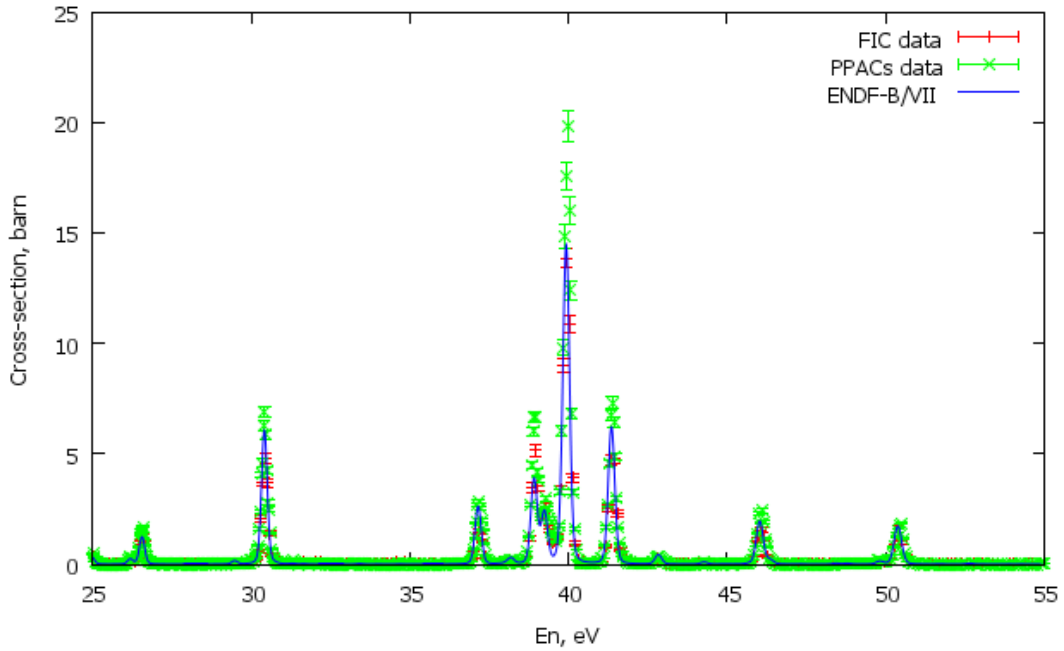

Figure 4.1. Comparison of the obtained fission cross-section of ^{237}Np with data from PPACs detector measured on the same neutron source [65] and with ENDF-B/VII library

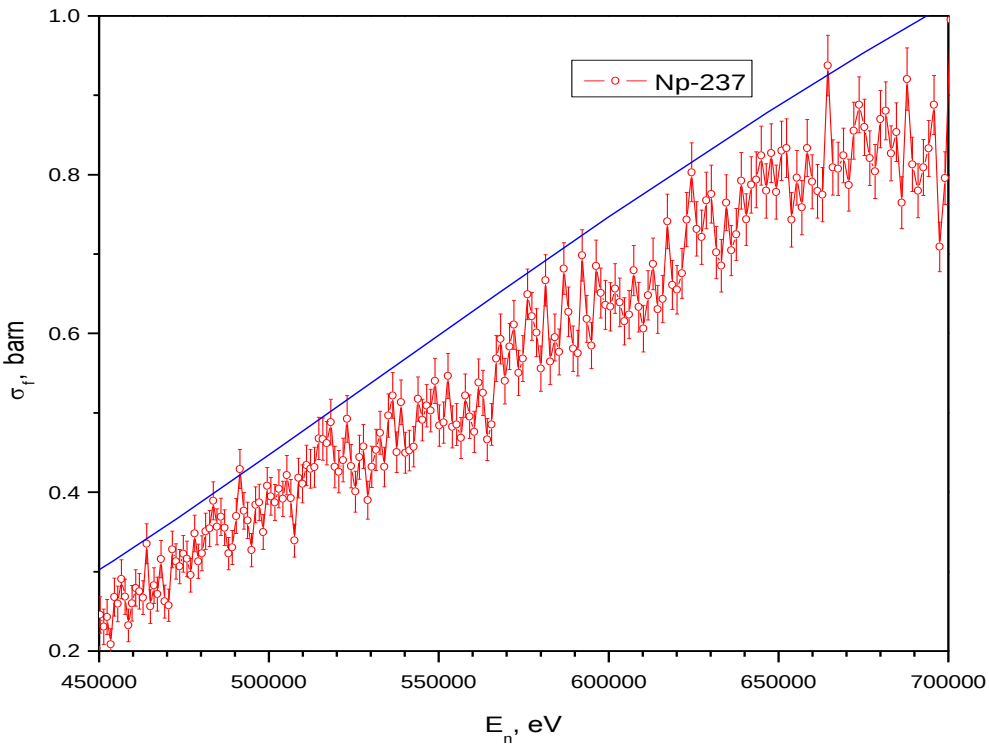

Figure 4.2. Comparison of the obtained fission cross-section of ^{237}Np with ENDF-B/VII data in fast neutron region.

Figures 4.1 to 4.3 shows the comparison of the ^{237}Np fission cross-section obtained on n_TOF neutron source with recommended values.

Our data on fission cross-section of ^{237}Np allows one to resolve contradiction between two main libraries of nuclear data, JENDL-3.2 and ENDF-B/VI, which are based on results of [7] and [8], respectively and differs in a factor of three. Our data coincide with [7]. Later version of ENDF, ENDF-B/VII, published after our measurements, does not have this contradiction (Figure 4.1). Recently published n_TOF collaboration data on results of the measurements with Parralel Plates Proportional Chambers (PPACs) detector [65] are 20–25% higher, than our data and the latest evaluated one in the region of the first resonance cluster.

In the region of the fission barrier our data shows fair agreement with evaluated data and with [65]. In the region 510–900 keV our data are systematically lower (on about 10%), than data from [65] and ENDF-B/VII (Figures 4.2 and 4.3). High resolution (1000 bins per decade) data (Figure 3.31) shows pronounced structure which was not observed before.

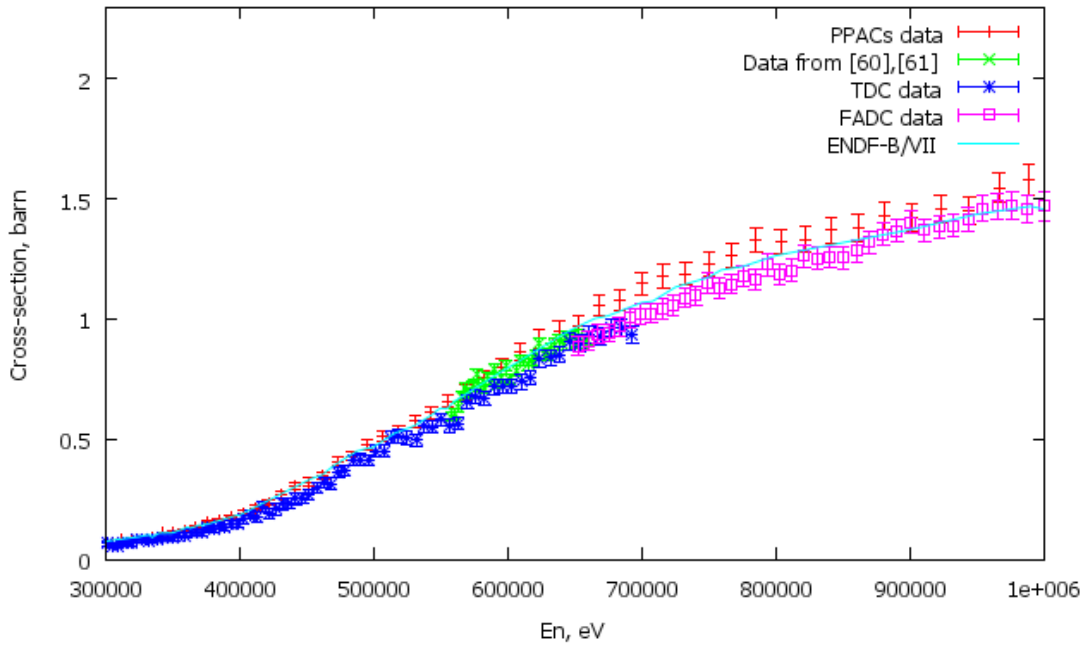

Figure 4.3. Comparison of the obtained fission cross-section of ^{237}Np with data from PPACs detector measured on the same neutron source [65] and ENDF-B/VII library in fast neutron region. For our data (red and green) only the statistical errors are given

The careful analysis of the fission cross-section data together with data on neutron capture cross-section, obtained on the same neutron source [66], will give a new set of the resonance parameters data.

4.2. Fission cross-section of the ^{234}U

4.2.1. Resonance region data

Cross-section measurements of the ^{234}U neutron induced fission in the area below 1 keV, performed in Dubna and described in Chapter 2, shows very good agreement with the existing data [18]. The resolution of the IBR-30 neutron source is not high enough to resolve even the first resonance cluster at 600 eV, however the resonance analysis were done and obtained fission widths were in good agreement with [18], too. These measurements give a necessary experience, which was crucial for measurements on n_TOF neutron source.

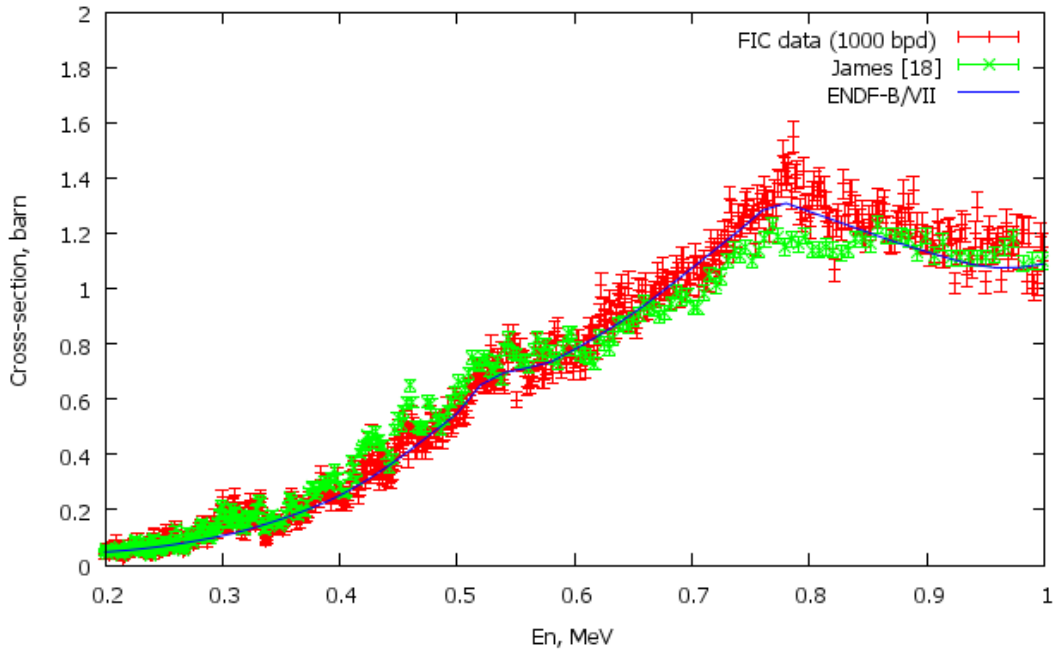

Figure 4.4. Comparison of the obtained data (red) with existing experimental works [18] (green) and with evaluated data.

High-resolution data for ^{234}U obtained on n_TOF neutron source (see Chapter 3) confirms the results of [18] for the fine structure connected with vibrational resonances and a third well. Around 780 keV our data shows the resonance, that can be seen in [20] and absent in [18]. Cross-section in the area from 600 keV to 1 MeV, obtained in our measurements, appeared to be about 12-15% higher, than evaluations. This energy region is near the maximum of the neutron flux of the fast reactors supposed to be used in Thorium cycle as well as of ADS. Since results of [65] have lower systematical errors then our ones, while our results shows better resolution with same statistical uncertainty, after discussion on the n_TOF Collaboration meeting we normalize our result on the [65] integral value in the region from 450 keV to 1 Mev, as shown on Figure 4.5.

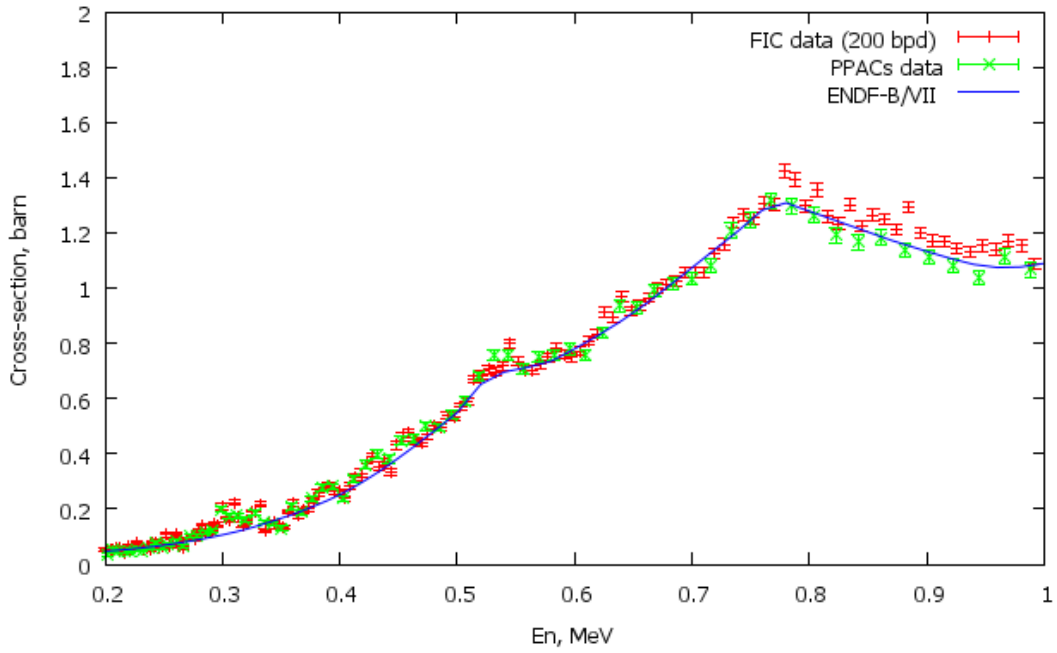

Figure 4.5. Comparison of the obtained fission cross-section of ^{234}U with data from PPACs detector measured on the same neutron source [65] and ENDF-B/VII library in fast neutron region.

Resolution of our measurements in the region of vibrational resonances (hundreds of keV) is much higher, than in [20] and about 30% better, than [18]. For the energies where resolution of n_TOF source is higher than one for all previous measurements, our cross-section demonstrate the structure which is connected with second and, probably, third well in the fission barrier. On the barrier our cross-section demonstrates pronounced structure, which is connected with vibration resonances and third well. The most pronounced structures attributed to vibration resonance, are ones around 310 keV (Figures 3.19 and 3.23) and 540 keV (Figure 3.20 and 3.24).

In the vibration resonance structure around 310 keV seven resonance-like structures are clearly seen. Average distance between them is about 10 keV. This structure is similar to one in [18], while our data shows better resolution (Figure 3.23). Same situation can be observed around 540 eV. There are 12 resonance-like structures with average distance between them about 5 keV (Figure 3.24). Again, the structure is similar with [18] but with better resolution.

Expected average distance between class-II levels should be about 1 keV, according to [13], which is lower than period of the observed structure. To explain the observed data, the analysis, similar to [18] was done (see Paragraph 3.3. and Figures 3.23–3.26). The analysis takes into account parameters of the barrier as well as the experimental resolution.

Analysis of the 310 keV vibrational resonance (Paragraph 3.3 and Figures 3.23–3.26) gives a similar with [18] results and analysis of the 540 eV resonance was done in the first time. Despite the resolution which is lower than distance between Class-II levels, the observed structure of the cross-section is in good agreement with results of the modeling.

The measurements of the cross-section could be only the first step in careful study of the vibrational resonances. To investigate the coupling between second well compound states and vibrational resonances the measurement of the angular and mass distribution of fission fragments for sub-barrier vibrational resonances need to be performed.

For simultaneous measurements of the mass and angular distribution Author proposed [67] to use the detector that is shown schematically on the Figure 4.6.

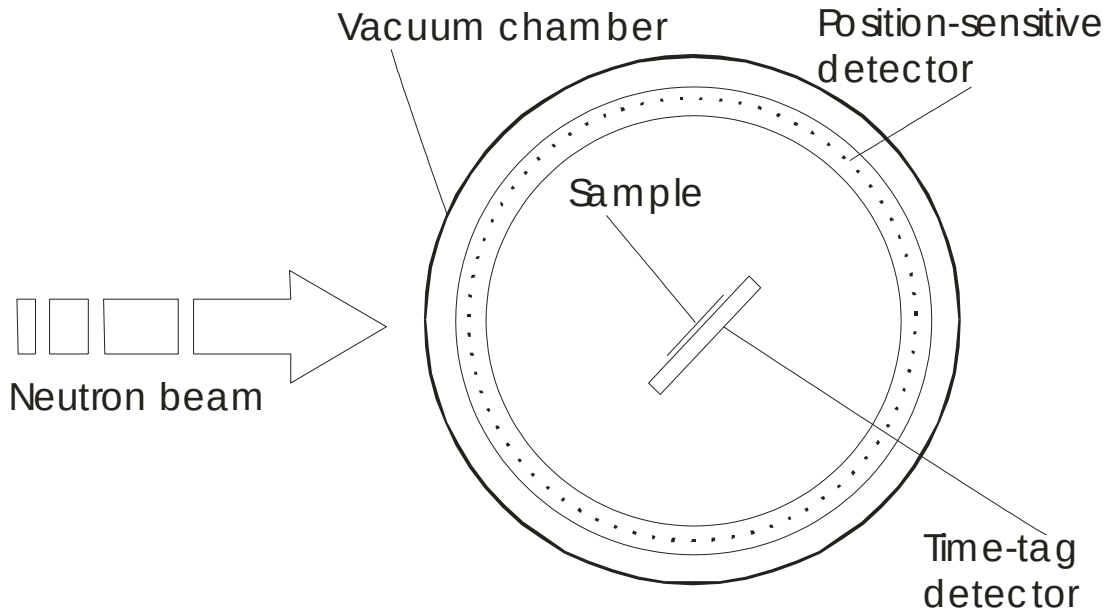

Figure 4.6. Sketch of the detector for mass and angular distribution measurements

Thin (allowing both fragments to go out) target is located in the center of the detector on the 45 degrees angle relative to the beam direction. Angular distribution of the fission fragments is measured by cylindrical fast position-sensitive detector (such as MicroMegas, or semiconductor detector, or photovoltaic cells or avalanche chamber). The same detector determines the kinetic energy of the both fission fragments (and so, the fragments mass ratio) by the time-of-flight of the both fission fragments. “Start” for time measurement (and time mark for neutron time-of-flight spectrometry) is obtained from time-tag detector that should be transparent for the fission fragments.

Figure 4.7 shows expected count rate per proton pulse ($7 \cdot 10^{12}$ protons) for the 5 mg ^{234}U sample on the planning 20 m flight path. The binning is chosen to be 200 bins per decade ($\Delta E/E \approx 1\%$) that roughly correspond to intrinsic resolution of the n_TOF facility at this flight distance. Let’s assume that statistical accuracy of double-differential (mass and angle) distribution for each energy bin should be around 3% (≈1000 counts) and we want to measure 25 points in angular distribution and 20 points in mass one (just to distinguish between

Standard 1 and Standard 2 fission modes), so we need about 500000 counts per bin on the middle of the barrier. Thus, we need about one million proton bunch or $7 \cdot 10^{18}$ protons.

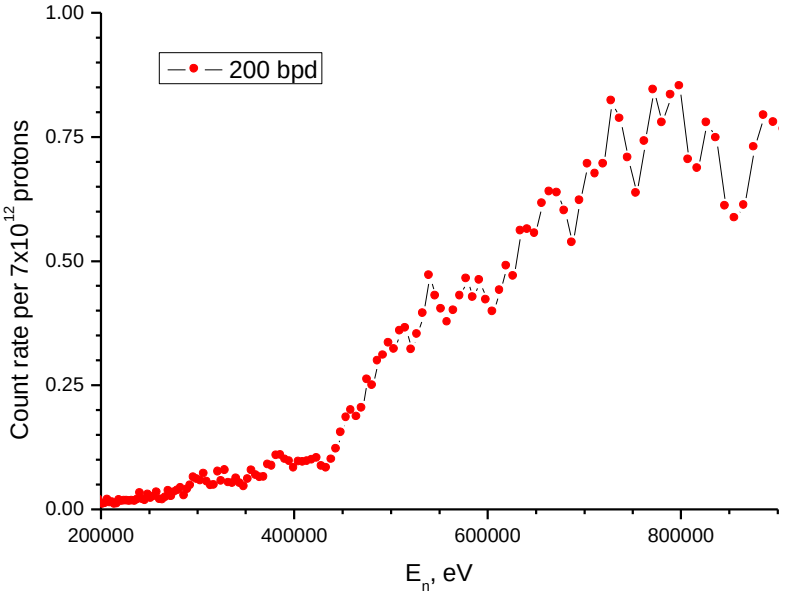

Figure 4.7. Expected integral count rate for ^{234}U (5 mg) on the 20 m flight path

Such kind of investigations of neutron induced fission with high energy resolution allow one to get essentially new information on basic mechanism of nuclear fission.

The resonance analysis of the Dubna's data [30] was done in the assumption that gamma-width of all the resonances is equal to $<\Gamma_\gamma> = 25$ meV. Careful analysis of the fission cross-section data together with data on neutron capture cross-section, obtained on the same neutron source [54], will give a much more accurate new set of the resonance parameters data.

4.2.2. Thermal Fission Cross-section

There exist several papers: by C. Wagemans and co-authors [27-29] and papers, describing the results of the Dubna's group measurements [30, 31]. The papers [27] and [30] were presented on IInd International Workshop on Nuclear Fission Physics and Fission Products Spectroscopy, 22-26 April, 1998, Seyssins, France. Measurements described in the paper [27] were carried out on the ILL high-flux reactor on the neutron beam having Maxwellian spectrum with average energy 11 meV and gives the value of σ_{th}=300±20 mb, then was also published as [28]. Few years later the same authors had published another value, σ_{th}=67±14 mb [29]. Value given in [30] and described in the Paragraph 2.2.1, 140±45 mb, was obtained by averaging of time-of-flight (TOF) spectrum measured on the IBR-30 pulsed booster over energy interval 14–37 meV. Results of the more careful analysis of that data showing the energy dependence of the fission cross-section near the thermal point are presented in [31]. Results of the another measurements of the energy dependence of the fission cross-section,

performed on IBR-2 pulse reactor in Dubna and described in Paragraph 2.2.2, was presented on ISINN-7, May 25-28, 1999, Dubna, Russia. The shown value of the fission cross-section in the thermal point was σ_{th}=210±30 mb.

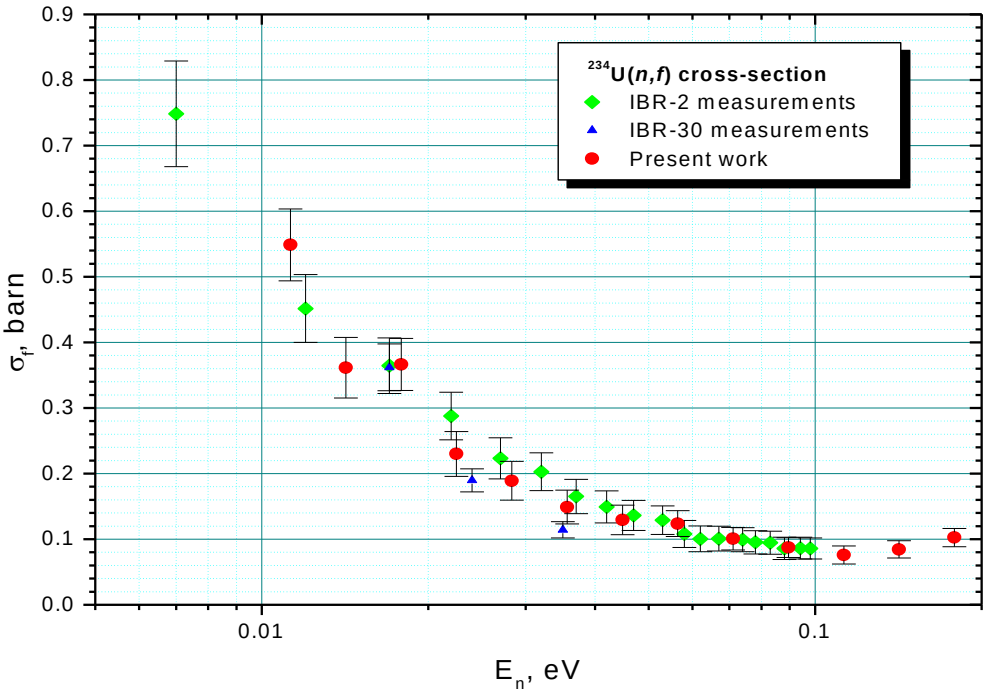

Figure 4.8. ^{234}U Fission cross-section in the vicinity of thermal point

The results of the independent measurements of ^{234}U fission cross-section near the thermal point, carried out with time-of-flight (TOF) technique on the pulsed neutron sources, described in the current dissertation and in [30, 31], are in good agreement with each other. Results of these measurements presented together on Figure 4.8. Average cross-section for the thermal point, is σ_f^{th} =196±10 mbarn.

4.3. Fission Cross-section of the ^{243}Am

Obtained fission widths [30] shown in the Table 2.4 together with data from [10] and [36] are in the reasonable agreement with data [10] for the energy region up to 10 eV with the exception of a two resonances: 7.8 and 9.9 eV. In the paper [10] for energy region above 20 eV the Γ_f values are given only for few resonances. The area $\sigma_0\Gamma_f$ of them are much higher then our one, probably, due to neibouring unresolved resonances. For some groups of resonances that could not be resolved, only total area given in this table.

The fission widths accuracy below 20 eV, obtained in our measurements, is better, than in [10]. Above 20 eV, where our resolution is slightly better, than in [10], our data is more detailed.

References

1. The recent European Commission's GREEN PAPER: "Towards a European strategy for the security of energy supply", December 2000, Brussels.
2. C. Rubbia et al., "An Energy Amplifier for Cleaner and Inexhaustible Nuclear Energy Production Driven by a particle Accelerator", CERN/AT/93-47(ET) 1993.
3. C. Rubbia, et al., "Conceptual Design of a fast Neutron Operated High Power Energy Amplifier", CERN/AT/95-44 (ET); see also C. Rubbia, "A High Gain Energy Amplifier Operated with fast Neutrons", AIP Conference Proceedings 346, International Conference on Accelerator-Driven Transmutation Technologies and Applications, Las Vegas, 1994.
4. C. Rubbia et al., "A Realistic Plutonium Elimination Scheme with Fast Energy Amplifiers and Thorium-Plutonium Fuel", CERN/AT/95-53 (ET); C. Rubbia et al., "Fast Neutron Incineration in the Energy Amplifier as Alternative to Geological Storage: the Case of Spain", CERN/LHC/97-01 (EET).
5. Summary Report of the Consultants' Meeting on "Assessment of Nuclear Data Needs for Thorium and other Advanced Cycles", INDC(NDS)–408, IAEA, Vienna, August 1999.
6. Y. Kadi et al., "Sensitivity Analysis of Neutron Cross Sections Relevant for Accelerator Driven Systems", International Conference on Nuclear Data for Science and Technology, October 7–12 2001, Tsukuba, Japan.
7. A. Yamanaka et al., J. Nucl. Sci. Techn., **36** (1993), p. 863.
8. P.A. Seeger et al., LA-4420 (LANL, 1970).
9. K. Wisshak et al., Nucl. Sci. Eng., 85 (1983) 251.
10. H.H. Knitter et al., Nucl. Sci. Eng., 99 (1988) 1.
11. Kobayashi et al., in Proc. Int. Conf. Nucl. Data for Science and Technology, Trieste, Italy, 1997, SIF, Vol.59, Part 1, p. 638 (1997).
12. V.M. Strutinsky, Nucl. Phys. A95 (1967) 420.
13. Bjornholm S. and Lynn J.E, Rev.Mod.Phys. 52 (1980) 725
14. P. Moeller and J.R. Nix, Proc. Int. Conf. on physics and chemistry of fission, Rochester, 1973 (IAEA, Vienna, 1974) p. 103.
15. A. Bohr, Proc. Int. Conf. on peaceful uses of atomic energy, Geneva, 1955 (United Nations, New York, 1956) vol. 2 p. 220.
16. Blons et al, Nucl. Phys. A414 (1984) 1.
17. Polikanov S.M. et al, JETF 42 (1962) 1016
18. James G.D, Phys. Rev. C15 (1977) 2083
19. Lamphere R.W, Nucl. Phys. 38 (1962) 561
20. Meadows J.W, Nucl. Sci. Eng., **65** (1978) 171
21. G.V.Danilyan. Usp.Fiz.Nauk,131, 1980, 329. Transl.Sov.Phys.Usp.23, 1980, 323.
22. A.M.Gagarski, G.A.Petrov, A.Koetzle et al., Proc. of the ISINN-6, JINR, Dubna, 1998.
23. O.P.Sushkov and V.V.Flambaum, Sov.Phys.Usp., 25, 1982, 1.
24. V.E.Bunakov and V.P.Gudkov, Nucl.Phys., A401, 1983, 93.
25. N.V.Borovikova, V.M.Lobashov et al., Pis'ma JETF, 31, 1980, 704.
26. J.D.Bowmann. in "Parity and TRI in Compound States and Related Topics". Ed. N Auerbach, World Scientific, 1996, p.65
27. Wagemans, C., Wagemans, J., Getlenbort, P., Zimmer, O., Gönnenwein, F. Determination of the $^{234}U(n_{th}, f)$ Cross-section and Some Underlying Physics. Nuclear Fission and Fission-product Spectroscopy. Second International Workshop, Seyssins, France, April 1998. AIP Conference Proceedings 447, Woodbury, New York, p. 262, 1998

28. Wagemans, C., et al., Nucl. Sci. Eng., v.132 (1999) p.308
29. Wagemans, C., et al., Nucl. Sci. Eng., v.141 (2002) p.171
30. Borzakov S.B., Florek M., Konovalov V. Yu., Ruskov I., Zamyatin Yu.S. Zeinalov Sh.S. Measurements of the Subthreshold Neutron Induced Fission Cross-sections of ^{234}U, ^{237}Np and ^{243}Am. Nuclear Fission and Fission-product Spectroscopy. Second International Workshop, Seyssins, France, April 1998. AIP Conference Proceedings 447, Woodbury, New York, pp.269-276, 1998
31. Florek, M., Konovalov, V. Yu., Pikelner, L.B., Zamyatnin, Yu.S., Zeinalov, Sh.S. The ^{234}U Neutron Induced Fission Cross-section Near the Thermal Point. In: Proceedings of the XIV International Conference of Nuclear Fission Physics, 24–26 October 1998, Obninsk, Russia
32. Neutron Experimental Facilities for Nuclear Physics Investigations.— V.V. Sikolenko (Ed.), Dubna, 1997
33. Muradian G.V., Petrenko V.V., Shatrov O.Ya., et al.— In Proc. of ISINN-4, Dubna, April 27-30, 1996.— E3-96-336, Dubna 1996, p 276–284
34. Zeinalov, Sh.S., Smirnov, V.I., Stempinsky, M., Florek, M., Shalansky, P., Very Fast Fission Fragment Detector, Dubna: P13-97-222.
35. Mughabhab, S.F., Neutron Cross-Section, New York: Academic Press, vol. 1 Part B.
36. Schopper, H. (ed.) Landolt-Börnstein vol I/16B, Springer-Verlag, 1998
37. Florek M., Konovalov V. Yu., Zamyatin Yu.S., Zeinalov Sh.S. Neutron induced fission cross-section of ^{243}Am in the energy region from 0.8 to 50 eV. The XIV-th International Workshop on Nuclear Fission Physics, Obninsk, Russia, 12-15. October, 1998.
38. Muradyan G.V. et al., Nucl. Sci. Eng., 90 (1985) 60.
39. G.V.Muradyan, M.A.Voskanyan, L.P.Yastrebova, V.L.Volkov, O.Ya.Shatrov, V.I.Furman, V.Yu.Konovalov. Measurements of Neutron Capture Cross Sections of ^{234}U and ^{236}U and Fission Cross Section of ^{236}U JINR-E3-98-212, p. 287,1999
40. Yu.S.Zamyatnin, Sh.S.Zeinalov, V.Yu.Konovalov, V.I.Smirnov, E.A.Sokol, M.Stempinski, P.Szalanski, "Experimental Set-up for Prompt Neutron Distribution Measurements on Resonance Neutron Induced Fission", Proceedings of the VII International Seminar on Interaction of Neutrons with Nuclei (ISINN-7) "Neutron Spectroscopy, Nuclear Structure and Related Topics", Dubna (Russia), May 25-28, **1999**, pp. 263-268
41. G.F. Knoll: Radiation Detection and Measurement. - John Wiley and Sons, New York, 1979
42. Abagyan L.P, Bazazyanc N.S., Nikolaev M.N., Cybula A.M., The group constants for calculation of reactors and shielding. M., 1981
43. Rose P.F., ENDF-201. ENDF/B-VI Summary documentation. (4th edition) BNL-NCS-17541, New-York (1991).
44. Kikuchi Y. JENDL-3 Revision-2 JENDL-3.2. Int. Conf. on Nuclear Data for Science and Technology, Gatlinburg, Tennessee, (1994) p. 685
45. n_TOF Collaboration. CERN n_TOF facility. Performance report. CERN/INTC-O-011; INTC-2002-037; CERN-SL-2002-053 ECT (2002).
46. P. Cennini et al., Fission Fragment Detector to be installed at the Measuring Station in the TOF Facility, SL-Note-99-026 EET (16-02-99).
47. A. Doroshenko, P. Cennini A. Goverdovsky, W. Furman, V. Ketlerov, V. Konovalov, V. Mitrofanov, V. Pavlovich, B. Samylin. *Alpha-radioactive Samples Fabrication and Testing for Fundamental and Applied Purposes* (to be published).
48. P. Cennini et al., Handling of the Radioactive Samples for the Fast Induction Chamber (FIC) for the measurement of Fission Reactions at the n-TOF Facility at CERN, Technical Note CERN-TIS-2002-039-RP-TN, (August 2002)

49. U. Abbondanno et al. (The n_TOF collaboration) The data acquisition system of the neutron time of flight facility n_TOF at CERN. NIM A, v. 538 issues 2-3 (2005) p. 692
50. G. Lorusso et al. (The n_TOF collaboration) Time-energy relation of the n_TOF neutron beam: energy standards revisited. NIM A, v. 532, issue 3 (2004) p. 622
51. D. Karadimos, R. Vlastou, K. Ioannides, P. Assimakopoulos, N. Tsagas, P. Pavlopoulos, D. Karamanis, C. Papachristodoulou, K. Stamoulis, V. Vlachoudis, P. Cennini, V. Ketlerov, V. Konovalov, for the n_TOF collaboration. *Analysis of the FIC detector data at the n_TOF facility.* NIM B 268 (2010) pp. 2556-2562
52. H.G. Hughes et al., MCNPX for Neutron-Proton Transport, Mathematical and Computation Topical Meeting, American Nuclear Society, Madrid, Spain (27–30 September 1999).
53. A. Ferrari and P.R. Sala, Intermediate and High Energy Physics Models in FLUKA: Improvements, Benchmarks and Applications, Proc. of Int. Conf. on Nuclear Data for Science and Technology, NDST-97, ICTP, Miramare, Trieste, Italy, (19-24 May 1997).
54. D. C. Biswas, M. N. Rao and R. K. Choudhury, *Specific energy-loss behaviour of fission fragments along their range in P-10 gas*, Nucl. Instrum. Meth. **B 53**, 251 (1991), and references therein.
55. W. R. Leo, *Techniques for Nuclear and Particle Physics Experiments*, Springer-Verlag editor, 1994.
56. R. M. Sternheimer, S. M. Seltzer and M. J. Berger, Phys. Rev. **B 26**, 6067 (1982).
57. L. C. Northcliffe and R. F. Schilling, *Range and stopping power tables for heavy ions*, Nucl. Data Tables A7, 233 (1970).
58. R. B. Firestone, *Table of Isotopes, eighth edition, Volume II:A=151-272*, V. S. Shirley editor, John Wiley & Sons, Inc., New York, 1996.
59. J. F. Ziegler, Helium Stopping Powers and Ranges in All Elemental Matter, Pergamon Press, New York, 1977.
60. W. Furman, P.Cennini, V.Ketlerov, A.Goverdovski, V.Konovalov and n_TOF collaboration. *High-Resolution Study of ^{237}Np Fission Cross Section from 5 eV to 1 MeV.* JINR-E3-2004-16N: 18 Int. Sem. on Interactions of Neutrons with Nuclei, No.12, p.456 (2004)
61. W. Furman, P.Cennini, V.Ketlerov, A.Goverdovski, V.Konovalov and n_TOF collaboration. *High-Resolution Study of ^{237}Np Fission Cross Section from 5 eV to 1 MeV.* In AIP Proceedings CP769: International Conference on Nuclear Data for Science and Technology. Edited by R.C Haight, M.B. Chadwick, T. Kawano and P. Talou, p. 1039 (2005)
62. S.B. Borzakov, E. Dermendjiev, Yu.S. Zamyatnin, V.M.Nazarov, S.S. Pavlov, A.D. Rogov, I. Ruskov, Atomnaya Energiya, v. 79, p. 231, 1995 (in Russian).
63. W.K. Brown et al. – Nucl. Phys. A156, 609 (1970).
64. S. Plattard – Ph.D. thesis, Saclay, 1973.
65. C. Paradela and n_TOF collaboration. *Neutron-induced fission cross section of ^{234}U and ^{237}Np measured at the CERN Neutron Time-of-Flight (n_TOF) facility.* Phys. Rev. C 82, 034601 (2010)
66. n_TOF collaboration. Neutron Capture Cross Section Measurements at n_TOF of ^{237}Np, ^{240}Pu and ^{243}Am for the Transmutation of Nuclear Waste. CAPTURE GAMMA-RAY SPECTROSCOPY AND RELATED TOPICS: 12th International Symposium. AIP Conference Proceedings, Volume 819, pp. 318-322 (2006).
67. V. Konovalov and n_TOF collaboration. *Neutron Induced Fission Cross-Section Measurements with FICs Detectors*. International Symposium on Neutrons in Basic Science and Nuclear Technologies n_BANT CERN, Geneva - March 22-23, 2005 http://pceet075.cern.ch/n_BANT/files/Talks/Afternoon-22/Konovalov.ppt

Appendix I. Resonance Parameters Calculation

	From	To	Width	Middle	S	d_S	Average	d_Averag	rel_error
resonance	2700	2850	150	2775	2676	51.7301			0.019331
BG left (1)	2550	2700	150	2625	484	22	3.226667	0.146667	0.045455
BG right (1)	2850	3000	150	2925	422	20.5426	2.813333	0.136951	0.048679
	a=		3.123333	2.916667	453	30.17053			0.066602
	b=								
BG left (2)	2400	2700	300	2550	994	31.5278	3.313333	0.105093	0.031718
BG right (2)	2850	3150	300	3000	809	28.4429	2.696667	0.09481	0.035158
	a=		3.107778	2.902222	450.75	21.34352			0.047351
	b=								

Φ=	2.69E+07
ΔΦ=	3.03E+05
ΔΦ/Φ=	0.011264
S=	2167.5
d_S=	53.2
d_S/S=	0.025
m=	6.33E-02
d_m=	0.001899
d_m/m=	0.03
σ_0*Γ_f=	**1.38E-24**
abs. error=	**5.57E-26**
rel. error=	**0.040363**

E_n	TOF-BG	TOF	BG	d_TOF	d_BG (apr	d_(TOF-B(	rel_err(TC	sigma_0*Gamma_f	
5.16	269684.5	313861	45451.92	560.233	2272.596	2340.631	0.008679	1.38E-24	5.57E-26
31.13	6460.773	12782	6269.912	113.0575	313.4956	333.2589	0.051582	1.67E-25	1.09E-26
45.61	1831.398	8861	6762.12	94.13288	338.106	350.9653	0.191638	6.66E-26	1.3E-26
94.29	9428.558	20184	10729.51	142.0704	536.4757	554.9686	0.05886	6.59E-25	4.7E-26
106.13	2907.15	17560	7575.746	132.5142	378.7873	401.2977	0.138038	2.26E-25	3.25E-26
111.06	40500.99	58673	15413.29	242.2251	770.6644	807.8345	0.019946	3.28E-24	1.48E-25
146.25	2797.835	10469	7662.629	102.3181	383.1315	396.5586	0.141738	2.9E-25	4.28E-26
152.16	1783.427	8389	6605.953	91.59148	330.2977	342.7616	0.192193	1.92E-25	3.77E-26
176.18	7666.642	23304	11897.21	152.6565	594.8604	614.1359	0.080105	9.41E-25	8.44E-26
182.49	10818.63	12335	5089.714	111.063	254.4857	277.6652	0.025665	1.37E-24	6.55E-26
254.3	5141.621	16754	11369.9	129.4372	568.495	583.0442	0.113397	8.78E-25	1.06E-25
290.7	7098.411	21101	14072.31	145.2618	703.6154	718.4536	0.101213	1.37E-24	1.49E-25

E_n	sigma_0*Gamma_f	G_n	d_G_n	rel_err	G_gamma	G_total	G_f (meV)	d_G_f	d_G_f
5.16	1.38E-24	0.040363	3.92	0.02	0.005102	25	28.92	0.0201	0.0008	0.040684
31.13	1.67E-25	0.065497	7.2	0.79	0.109722	25	32.2	0.0089	0.0011	0.127784
45.61	6.66E-26	0.195842	0.43	0.031	0.072093	25	25.43	0.0689	0.0144	0.20869
94.29	6.59E-25	0.07137	41.7	2.3	0.055156	25	66.7	0.0381	0.0034	0.090199
106.13	2.26E-25	0.143818	4.05	0.28	0.069136	25	29.05	0.0660	0.0105	0.159573
111.06	3.28E-24	0.045023	18.5	1.4	0.075676	25	43.5	0.3285	0.0289	0.088056
146.25	2.9E-25	0.147373	13.39	0.74	0.055265	25	38.39	0.0467	0.0073	0.157394
152.16	1.92E-25	0.196385	17.88	0.75	0.041946	25	42.88	0.0268	0.0054	0.200815
176.18	9.41E-25	0.089699	39.3	1.4	0.035623	25	64.3	0.1040	0.0100	0.096514
182.49	1.37E-24	0.047832	47.1	1.6	0.03397	25	72.1	0.1468	0.0086	0.058668
254.3	8.78E-25	0.120366	1.48	0.12	0.081081	25	26.48	1.5313	0.2222	0.145128
290.7	1.37E-24	0.108965	37.2	1.5	0.040323	25	62.2	0.2547	0.0296	0.116186

Appendix II. Group Fission Cross-section Calculation

$$I(a,b) = \frac{\int_a^b \frac{\sigma_f(E_n)}{E_n} dE_n}{\int_a^b \frac{1}{E_n} dE_n}$$

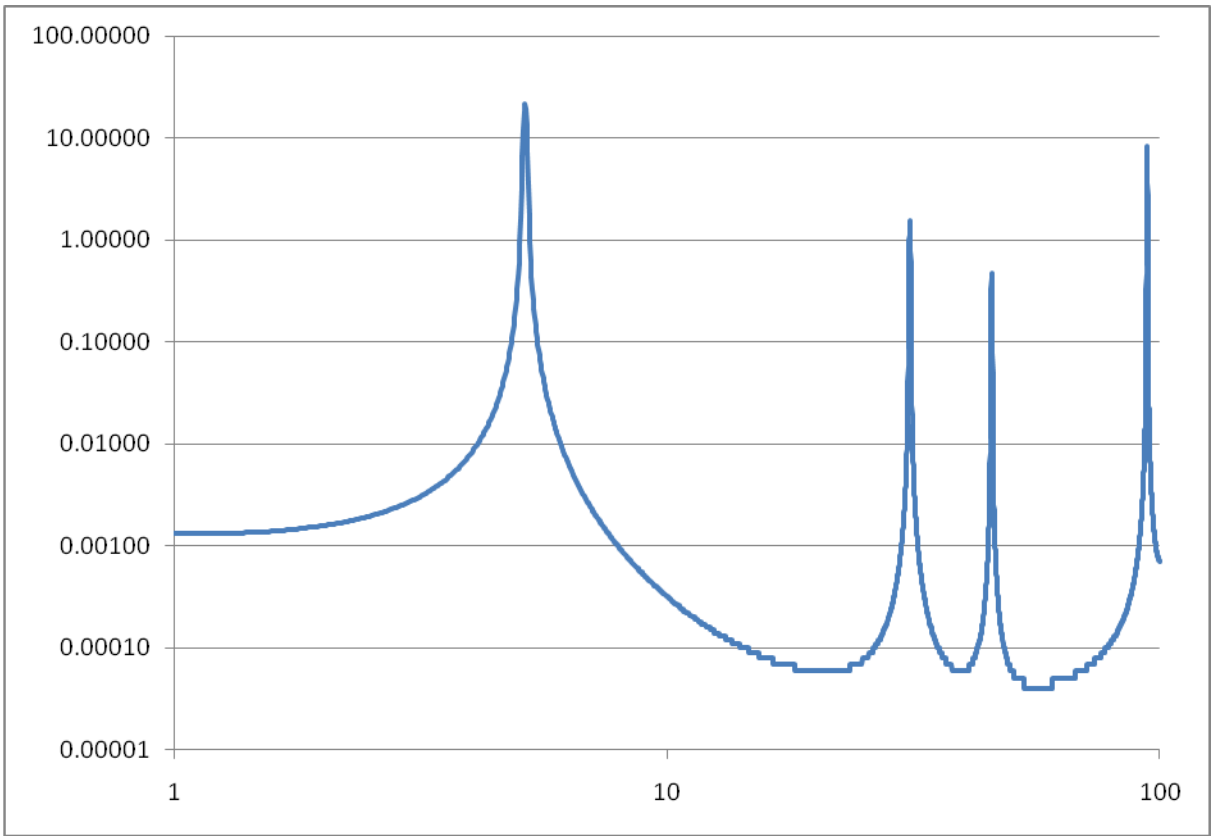

U-234 Group cross-sections:

Group No	E1	E2	σ
23	1	2.15	0.0014
22	2.15	4.65	0.005854
21	4.65	10	0.590068
20	10	21.5	0.000122
19	21.5	46.5	0.017817
18	46.5	100	0.038106

Appendix III. Analysis of the Observed Cross-section in the Vibrational Resonance Region

$E\_vib := 310000$ $DI := 10.64$ $DII := 2100$ $V\_a := 101000$ $h\omega\_a := 1000000$

$V\_b := 590000$ $h\omega\_b := 520000$

$D\_vib := 500000$

$W := 50000$

$$\Gamma\_vib := \frac{D\_vib}{2 \cdot \pi \cdot \left[1 + e^{-2 \cdot \pi \cdot \frac{(V\_b - E\_vib)}{h\omega\_b}}\right]}$$

$$EII\_0 := \left| \begin{array}{l} \text{for } i \in 0..79 \\ \quad e0_i \leftarrow 270000 + i \cdot 1000 \\ \text{return } e0 \end{array} \right.$$

$$\Gamma II\_f\_ave := DII \cdot W \cdot \frac{\left[\sum_{i=0}^{79} \frac{\Gamma\_vib}{2 \cdot \pi \cdot \left[(EII\_0_i - E\_vib)^2 + \frac{(W + \Gamma\_vib)^2}{4}\right]}\right]}{80}$$

$\Gamma II\_f\_ave = 41.027$

$Y := rnorm(80, 0, \sqrt{\Gamma II\_f\_ave})$

$\Gamma n := 0.5$

$$\Gamma II\_f := \left| \begin{array}{l} \text{for } i \in 0..79 \\ \quad e0_i \leftarrow (Y_i)^2 \\ \text{return } e0 \end{array} \right.$$

$\Lambda := 4.1 \cdot 10^6$

$EII\_0 =$

	0
0	$2.7 \cdot 10^5$
1	$2.71 \cdot 10^5$
2	$2.72 \cdot 10^5$
3	$2.73 \cdot 10^5$
4	$2.74 \cdot 10^5$
5	$2.75 \cdot 10^5$
6	$2.76 \cdot 10^5$
7	$2.77 \cdot 10^5$
8	$2.78 \cdot 10^5$
9	$2.79 \cdot 10^5$
10	$2.8 \cdot 10^5$
11	$2.81 \cdot 10^5$
12	$2.82 \cdot 10^5$
13	$2.83 \cdot 10^5$
14	$2.84 \cdot 10^5$
15	$2.85 \cdot 10^5$
16	$2.86 \cdot 10^5$
17	$2.87 \cdot 10^5$
18	$2.88 \cdot 10^5$
19	$2.89 \cdot 10^5$
20	$2.9 \cdot 10^5$

$\Gamma II\_f =$

	0
0	7.906
1	18.938
2	9.19
3	37.141
4	116.58
5	0.078
6	0.597
7	12.702
8	197.091
9	26.834
10	39.817
11	30.501
12	34.391
13	18.582
14	44.744
15	0.196
16	23.423
17	19.913
18	1.357
19	17.037
20	21.451

$$\Gamma II\_c := \frac{DII}{2\pi \cdot \left[1 + e^{\left[2\pi \frac{(V\_a - EII\_0)}{h\omega\_a}\right]}\right]}$$

$$\Gamma I\_f(E) := \sum_{i=0}^{79} DI \cdot \Gamma II\_c_i \cdot \frac{\Gamma II\_f_i}{2\pi \cdot \left[(EII\_0_i - E)^2 + \frac{(\Gamma II\_c_i + \Gamma II\_f_i)^2}{4}\right]}$$

$$\Gamma\_t(E) := \Gamma n + \Gamma I\_f(E) + 0.04 + 0.107$$

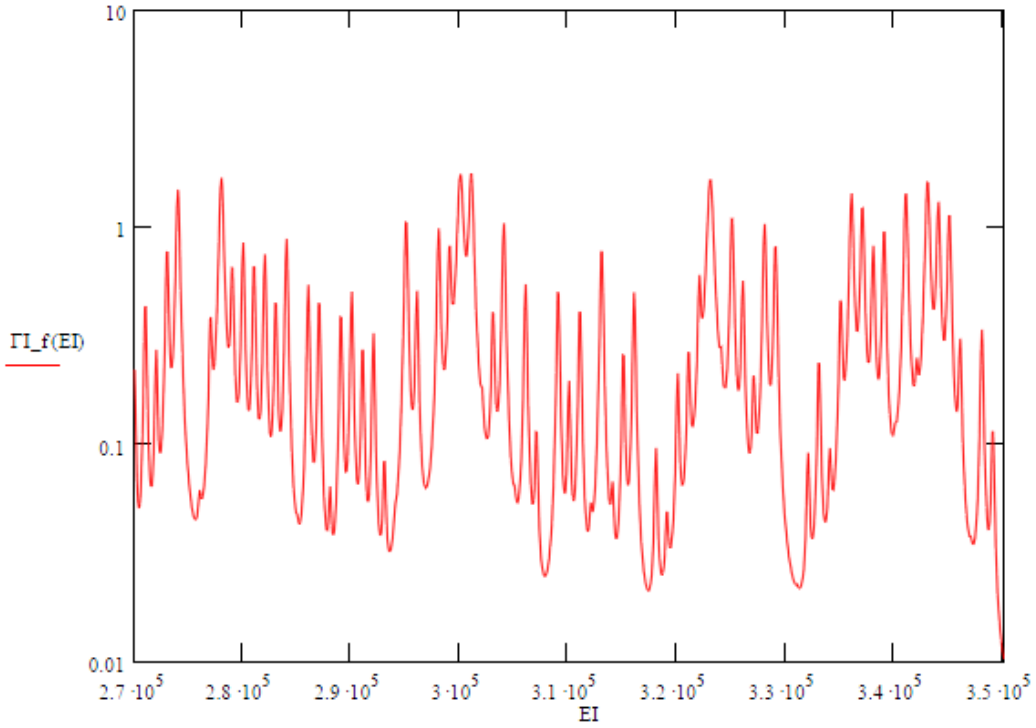

$F := 0.5$

$$\sigma(E) := \Lambda \cdot \Gamma n \cdot F \cdot \frac{\Gamma I\_f(E)}{E \cdot DI \cdot \Gamma\_t(E)}$$

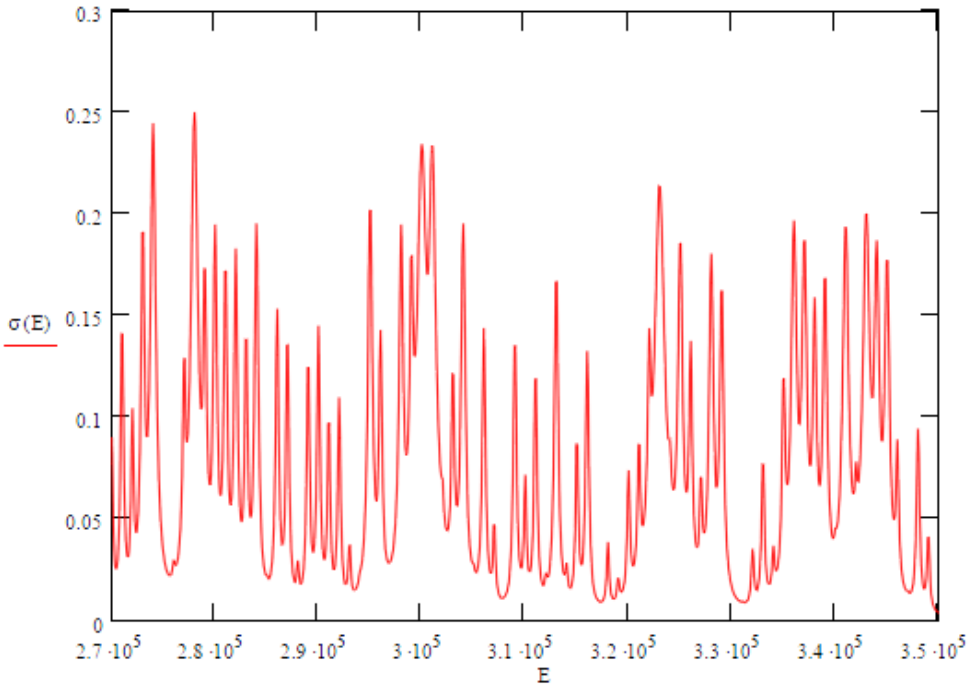

$$\sigma_{eff}(E) := \int_{E-4000}^{E+4000} \sigma(E1) \cdot dnorm(E1, E, 1000)\, dE1$$

$$\sigma\_ave := \frac{\left(\int_{270000}^{350000} \sigma(E)\, dE\right)}{350000 - 270000}$$

$\sigma\_ave = 0.075$

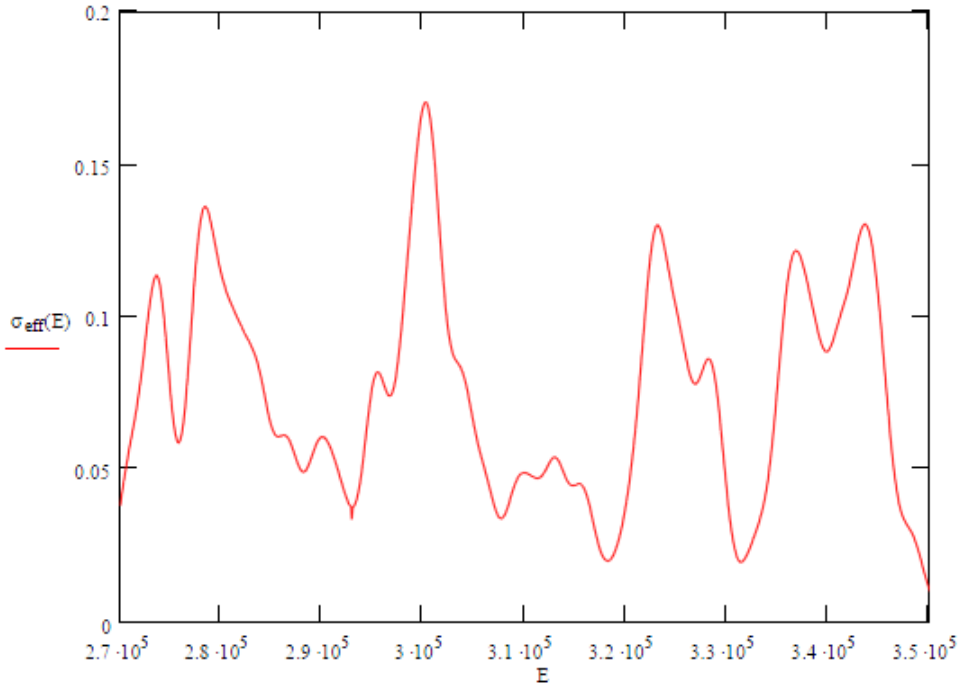

Acknowledgements

Author would like to express his deep appreciation to the International Science and Technical Center (Moscow, Russia) for financial support of the part of the work (ISTC project #471-97), Dr. W. I. Furman, councilor of the Directorate of the FLNP JINR (Dubna, Russia) for continuous interest and support of the work, n_TOF collaboration as a whole and personally Prof. C. Rubbia and P. Cennini for the atmosphere in the collaboration and Prof. H. Böck from Atominstitut Wien (Vienna, Austria) who help Author with his first steps at Vienna University of Techlology.

With deep sorrow Author would like to express his deep gratitude to his passed away Teachers, Acad. V. I. Mostovoy (1919-1996) and Prof. Yu. S. Zamyatnin (1921-2007).

Curriculum Vitæ

KONOVALOV Vitaly Yurievich

Employment record

July 2005 — May 2012:

Safeguards Inspector (P-3), Department of Safeguards,
International Atomic Energy Agency, A-1040, Wagramerstrasse, 5, Vienna, Austria

April 1994 — July 2005:

Researcher, Frank Laboratory of Neutron Physics,
Joint Institute for Nuclear Research, 141980, Joliot-Curie str., 6, Dubna Moscow reg., Russia

October 2001– December 2001:

Visiting scientist, PF1 beam,
Institute Laue-Langevin, 6, rue Jules Horowitz, 38042 Grenoble Cedex 9, France

August 2002 — February 2005

Project Associate (n_TOF project)
CERN, Geneva, Switzerland

Education

September 2007 up to now

Atominstitut, Technischen Universität Wien, Österreich

PhD candidate; dissertation title: 'Experimental Study of the Neutron Induced Fission Cross-Section of ^{234}U, ^{237}Np and ^{243}Am with Time-of-Flight Spectrometry Technics'.

February 1992 — February 1994

Training center of the Joint Institute for Nuclear Research, Dubna, Russia

Neutron Physics and Neutron Methods for Solid State Physics Specialization

September 1988 — February 1994

Ural State Technical University (Ural Polytechnic Institute), Ekaterinburg, Russia

Diploma of Physical Engineer in Experimental Nuclear Physics

Languages: Russian — mother tongue;
English — fluent;
French — fluently speak and read;

Honors and Awards:

Special JINR Prize 2001 for the work:
Yu.A.Alexandrov, Yu.S.Zamyatnin, A.V.Ignatyuk, M.V.Kazarnovsky, V.Yu.Konovalov, N.V.Kornilov, L.B.Pikelner, V.I.Plyaskin, Yu.P.Popov, W.I.Furman. "Low-Energy Neutrons and their Interaction with Nuclei and Matter".